Quantitative Characterization of Aluminum in Non-hydrated Zeolite Catalysts by Multi-nuclear Solid-state NMR Spectroscopy

Present by
Jian JIAO

Quantitative Characterization of Aluminum in Non-hydrated Zeolite Catalysts by Multi-nuclear Solid-state NMR Spectroscopy

vorgelegt von
Jian JIAO
aus V.R. China

Contents

Abbreviations and Symbols

Abbreviations

1 D	One-Dimensional
2 D	Two-Dimensional
AES-ICP	Inductively Coupled Plasma Atomic Emission Spectroscopy
Al^{IV}	Tetrahedrally Coordinated Aluminum Atom
Al^{V}	Five-fold Coordinated Aluminum Atom
Al^{VI}	Octahedrally Coordinated Aluminum Atom
DAS	Dynamic Angle Spinning
DFS	Double-Frequency Sweep
DOR	Double-Oriented Rotation
F1	Isotropic Dimension in MQMAS NMR Spectra
F2	Anisotropic Dimension in MQMAS NMR Spectra
FCC	Fluid Catalytic Cracking
HF	High Frequency
IR	Infrared
IUPAC	International Union of Pure and Applied Chemistry
IZA	International Zeolite Association
LF	Low Frequency
MAS	Magic Angle Spinning
MQ	Multiple-Quantum
NMR	Nuclear Magnetic Resonance
PAS	Principle Axis System
rf	Radio Frequency
SBU	Secondary Building Units
TPD	Temperature-Programmed Desorption
USY	Ultra-Stable Y Zeolite
u.c.	Unit Cell

XANES   X-Ray Absorption Near-Edge Spectroscopy

XRD   X-Ray Diffraction

Symbols

A	$m^{-2} \cdot g^{-1}$	Specific Surface Area
B	T	Magnetic Field Strength
C_{QCC}	MHz	Quadrupolar Coupling Constants
E	J	Energy
eQ	$C \cdot m^2$	Electric Quadrupolar Movement
eq	$C \cdot V \cdot m^{-2}$	z-component of Electric Field Gradient
I	-	Nuclear Quantum Number
h	$6.62 \times 10^{-34} J \cdot s$	Planck's Constant
$\hat{H}$	-	Hamilton Operator
m	-	Magnetic Quantum Number
p	Pa	Pressure
PA	$kJ \cdot mol^{-1}$	Proton Affinity
r	m	Internuclear Vector
$SOQE$	MHz	Second-Order Quadrupolar Effect Parameter
T_1	s	Longitudinal Relaxation Time
α, β	°	Euler Angles
δ	ppm	Chemical Shift
γ	$s^{-1} \cdot A^{-1} \cdot m$	Gyromagnetic Ratio
η	-	Asymmetry Parameter
μ	$J \cdot m \cdot A^{-1}$	Magnetic Momentum
σ	-	Shielding Constant
ν	Hz	Frequency

1. Zusammenfassung

Die Festkörper-NMR-Spektroskopie ist eine sehr empfindliche Methode für die Untersuchung der lokalen Struktur von kristallinen Alumosilicaten, wie z. B. von mikroporösen Zeolithen, die sowohl in der heterogenen Katalyse, als auch und in Adsorptionsprozessen breite Anwendungen finden. Daher wird die Festkörper-NMR-Spektroskopie der atomaren Bausteine der Zeolithe, wie z. B. von ^{1}H, ^{23}Na, ^{29}Si, ^{27}Al und ^{17}O, häufig für die Charakterisierung des Gerüstes und der Oberflächenzentren dieser Materialien verwendet [1-8]. Außerdem können durch Festkörper-NMR-Spektroskopie, neben der chemischen Natur von Adsorbaten, auch Wechselwirkungen dieser Moleküle mit Gerüstatomen und aktiven Zentren aufgeklärt werden [9-11].

Aluminiumatome in dealuminierten Zeolithen können in verschiedenen chemischen Umgebungen vorliegen, u. a. als tetraedrisch koordinierte Gerüstaluminiumatome, als verzerrt tetraedrisch koordiniertes Gerüst- oder Extragerüstaluminium, als fünffach koordinierte Extragerüstaluminiumspezies und als oktaedrisch koordinierte Aluminiumatome außerhalb des Gerüstes oder als flexibel koordinierte Gerüstaluminiumatome an Defektstellen. Bis jetzt wurden die meisten Festkörper-NMR-Untersuchungen von Zeolithen an hydratisierten Proben durchgeführt [11-16]. Die Charakterisierung fester Katalysatoren in einem Zustand, der mit ihrer Anwendung in katalytischen Prozessen vergleichbar ist, erfordert jedoch die Untersuchung calcinierter und nicht hydratisierter Materialien. ^{27}Al-Spin-Echo-NMR-Untersuchungen an dehydratisierten Zeolithen mit FAU- und MFI-Struktur lieferten Quadrupolkopplungskonstanten C_{QCC} der Gerüstaluminiumatome von bis zu 16 MHz [1]. Diese hohen C_{QCC}-Werte resultieren aus einer Abnahme der lokalen Symmetrie der AlO$_4$-Tetraeder aufgrund unterschiedlicher A-O-Bindungsabstände. Bei mittleren magnetischen Feldstärken, z.B. von $B_0 = 9,4$ T, können die ^{27}Al-NMR-Signale der oben erwähnten Gerüstaluminiumatome wegen ihrer starken Verbreiterung nicht mit der MAS-Technik detektiert werden. In der vorliegenden Arbeit wurden die Möglichkeiten und Grenzen der Festkörper-NMR-Spektroskopie für die Charakterisierung dealuminierter Zeolithe im dehydratisierten Zustand untersucht und diskutiert. In einem ersten Schritt

wurden die Zeolithe zunächst auf klassische Weise, d. h. im hydratisierten Zustand charakterisiert. In einem zweiten Schritt wurden anschließend NMR-Experimente an dehydratisierten Proben mit verschiedenen Festkörper-NMR-Techniken und bei unterschiedlichen NMR-Feldstärken durchgeführt.

Zur Untersuchung der Aluminiumspezies in Zeolithen wurde eine Reihe von dealuminierten Y-Zeolithen mit $2,8 \leq n_{Si}/n_{Al} \leq 60$ durch Behandlung mit Wasserdampf präpariert. Dazu wurde der Zeolith H,Na-Y mit Wasserdampfpartialdrücken zwischen 3,4 und 81,5 kPa bei einer Temperatur von 748 K behandelt. Durch Röntgenpulverdiffraktometrie (XRD) wurde festgestellt, dass die Kristallinität der Materialien unter den oben erwähnten Bedingungen erhalten bleibt.

i)   Charakterisierung von Aluminiumspezies auf Gerüst- und Extragerüstpositionen in hydratisiertem Zeolith Y durch Festkörper-NMR-Spektroskopie

Die hydratisierten Materialien wurden durch ^{29}Si-MAS-NMR-, ^{27}Al-MAS-NMR-, Hochfeld-^{27}Al-MQMAS- und ^{1}H-MAS-NMR-Spektroskopie charakterisiert. Nach Adsorption von Ammoniak wurde an dem dealuminierten Zeolith in der H-Form ein Koordinationswechsel von oktaedrisch zu tetraedrisch koordinierten Aluminiumatomen gefunden. Quantitative ^{29}Si-, ^{27}Al- und ^{1}H-MAS-NMR-Untersuchungen zeigten, dass dieser Koordinationswechsel mit der Bildung Brønsted-saurer Zentren (SiOHAl-Gruppen) in den dehydratisierten Materialien gekoppelt ist, während nur eine geringe Abnahme der Anzahl der Silanolgruppen (SiOH) und keine systematische Änderung der Anzahl der AlOH-Gruppen beobachtet wurde. Anhand dieser Resultate wurde ein Modell für den Koordinationswechsel von Gerüstaluminiumatomen in dealuminierten Zeolithen H-Y vorgeschlagen, nach dem dreifach koordinierte Gerüstaluminiumatome in der Nähe von Si-O-Defektstellen auftreten. Diese Aluminiumatome liegen in der hydratisierten Form in einer oktaedrischen Koordination vor. Nach Adsorption von Ammoniak auf dem dehydratisierten Material kommt es zur Ausbildung von Si-O-Al-Brücken unter Ausheilung der vorherigen Si-O-Defektstellen. Dreifach koordinierte Gerüstaluminiumatome vollziehen hierbei einen Koordinationswechsel

zu vierfach koordinierten Gerüstaluminiumatomen und liegen in dieser Form auch nach der Hydratisierung vor. Nach der thermischen Zersetzung der an den Si-O-Al-Brücken vorhandenen Ammoniumionen wurde die Bildung zusätzlicher Brønsted-Säurezentren festgestellt. Weiterhin ergaben die NMR-Untersuchungen der Säurezentren in dealuminierten Zeolithen, dass eine Rehydratisierung des Probenmaterials direkt nach der Dealuminierung zu einer starken Veränderung der Hydroxylbedeckung führt, evtl. gekoppelt mit einer Veränderung der Natur der Extragerüstaluminiumspezies. Daher waren Untersuchungen an dehydratisierten Zeolithen wünschenswert. Dieser Zustand der Proben entspricht auch eher dem Zustand von Zeolithkatalysatoren in ihrem industriellen Einsatz.

ii) Untersuchung der Ladungsbilanz zwischen Gerüst- und Extragerüstaluminiumspezies im dehydratisierten Zeolith Y durch Festkörper-NMR-Spektroskopie

Um die dealuminierten Zeolithe im dehydratisierten Zustand charakterisieren zu können, wurden die Proben sofort nach der Dealuminierung unter trockenem Stickstoff luftdicht abgefüllt. Hierzu wurde die Dealuminierungsapparatur mit einer Luftschleuse verbunden. Durch ^{29}Si-MAS-NMR-Spektroskopie wurde in den Spektren der dehydratisierten Proben im Vergleich zu denen der hydratisierten Materialien eine starke Hochfeldverschiebung der Si(3Al)- und Si(2Al)-Signale beobachtet. Als Erklärung dafür kommt Folgendes in Betracht: i) Eine durch die Dehydratisierung verursachte Veränderung der Nahstruktur der Gerüst-AlO$_4$-Tetraeder oder ii) der Einfluss hochgeladener Extragerüstkationen. Für die eindeutige Zuordnung der Signalverschiebungen zu einer dieser Erklärungen wurde Zeolith Y mit unterschiedlichen H$^+$- bzw. Al^{3+}-Austauschgraden mit der Festkörper-NMR-Spektroskopie untersucht. Die experimentellen Daten wiesen eindeutig darauf hin, dass der Hauptgrund für die Hochfeldverschiebungen der ^{29}Si-MAS-NMR-Signale der dehydratisierten Proben die Veränderung der Nahstruktur der Gerüst-AlO$_4$-Tetrader aufgrund von Veränderungen der Al-O-Bindungslängen während der Dehydratisierung ist. Im Gegensatz dazu resultieren aus der Anwesenheit von Extragerüstaluminiumkationen lediglich eine geringe Hochfeldverschiebung von ca. 1 ppm sowie eine Verbreiterung der Si(nAl)-Signale, wahrscheinlich aufgrund von ^{29}Si-^{27}Al-Kopplungen.

Mit der ^{29}Si-MAS-NMR-Spektroskopie wurde für dealuminierte Zeolithe, die mit zunehmend höheren Wasserdampfpartialdrücken behandelt worden waren, eine systematische Abnahme der Anzahl der Gerüstaluminiumatome in den dehydratisierten Materialien beobachtet. Die Anzahl der dreifach koordinierten Gerüstaluminiumatome in den dehydratisierten Zeolithen wurde anhand der Zunahme der Konzentration an Si-O-Al-Brücken nach Adsorption von Ammoniak per ^{1}H-MAS-NMR-Spektroskopie bestimmt. Durch einen quantitativen Vergleich der Anzahl an tetraedrisch koordinierten Gerüstaluminiumatomen, aufgrund derer die Gerüstladung zustande kommt, mit der Anzahl an ladungskompensierenden Natriumkationen und SiOHAl-Gruppen wurde die durchschnittliche Ladung der Extragerüstaluminiumkationen berechnet. Dieser durchschnittliche Wert pro Extragerüstaluminiumatom variierte zwischen ca. +2 für schwach dealuminierte Zeolithe und ca. +0,5 für stark dealuminierte Proben.

iii) Bestimmung der Anzahl und Natur von Gerüstaluminiumatomen in dehydratisiertem Zeolith Y durch Adsorption von Sondenmolekülen

Die Charakterisierung von Zeolithkatalysatoren durch Festkörper-NMR-Spektroskopie an Proben im hydratisierten Zustand ist oft von einer unkontrollierten Hydrolyse des Zeolithgerüsts sowie einer Veränderung der Natur von Extragerüstaluminiumspezies verbunden. In der vorliegenden Arbeit wird gezeigt, dass die Limitierungen der ^{29}Si- und ^{27}Al-MAS-NMR-Spektroskopie an dehydratisierten Zeolithen mit FAU-Struktur, wie z. B. eine deutlich schlechtere Auflösung und eine signifikante Verbreiterung von Signalen, durch Adsorption von Ammoniak überwunden werden können. Die ^{29}Si-MAS-NMR-Spektren von dehydratisierten und mit Ammoniak beladenen Zeolithen weisen keine durch die Dehydratisierung verursachten Hochfeldverschiebungen der Si(nAl)-Signale (mit n = 3, 2, 1) auf, die im Allgemeinen für eine Verschlechterung der Auflösung der Spektren im dehydratisierten Zustand verantwortlich sind. Die ^{27}Al-MAS-NMR-Spektren von dehydratisierten und mit Ammoniak beladenen Zeolithen bestehen ausschließlich aus Signalen, die tetraedrisch koordinierten Gerüstaluminiumatomen zuzuordnen sind. Diese

Signale weisen spektroskopische Parameter auf, die denen von hydratisierten Proben entsprechen. Die Gerüstaluminiumgehalte, die durch die quantitative Auswertung der ^{29}Si- und ^{27}Al-MAS-NMR-Spektren dehydratisierter Proben erhalten wurden, stimmen gut überein.

Neben der Adsorption von Ammoniak wurde auch die Adsorption von Pyridin, Aceton und Acetonitril an dehydratisierten Zeolithen mittels Festkörper-NMR-Spektroskopie untersucht. Interessanterweise spiegelt sich dabei die Protonenaffinität der Sondenmoleküle in einer Veränderung der Quadrupolkopplungskonstante der Gerüstaluminiumatome in den dehydratisierten Proben wider. Um Gerüstaluminiumatome mit Hilfe der ^{27}Al-MAS-NMR-Spektroskopie bei mittleren magnetischen Feldstärken (z.B. B_0 = 9,4 T) detektieren zu können, muss ein Protonentransfer von den Brücken-OH-Gruppen zu den Sondenmolekülen erfolgen. Weiterhin kann die Größe der Sondenmoleküle die Beobachtbarkeit von Gerüstaluminiumatomen in den ^{27}Al-MAS-NMR-Spektren beeinflussen. Quantitative Auswertungen zeigten, dass aufgrund der begrenzten Adsorptionskapazität der starken Base Pyridin nicht alle Gerüstaluminiumatome in den bei mittleren magnetischen Feldstärken aufgenommenen ^{29}Si- und ^{27}Al-MAS-NMR-Spektren beobachtet werden können. Aus dem Einfluss der verschiedenen Sondenmoleküle auf die Quadrupolkopplungskonstanten der Gerüstaluminiumatome im dehydratisierten Zeolith Y konnte abgeleitet werden, dass eine Protonenaffinität der Sondenmoleküle von ca. 850 kJ/mol notwendig ist, um den o.g. Protonentransfer von den Brücken-OH-Gruppen zu den Sondenmolekülen zu bewirken.

iv) Untersuchung der Extragerüstaluminiumspezies im dehydratisierten Zeolith Y mittels ^{27}Al-Spin-Echo-NMR-Spektroskopie, ^{27}Al-MAS-NMR-Spektroskopie mit schneller Probenrotation und ^{27}Al-MQMAS-NMR-Spektroskopie bei magnetischen Flussdichten von 9,4 bis 17,6 T

Für diese erstmalig durchgeführten Untersuchungen an deluminierten Zeolithen im dehydratisierten Zustand wurden dehydratisiertes γ-Al$_2$O$_3$ sowie ein mit Aluminiumkationen ausgetauschter Zeolith Al,Na-Y und ein Zeolith H,Na-Y als Referenzmaterialien verwendet. Die Festkörper-^{27}Al-NMR-Spektren des dealuminierten Zeoliths deH,Na-Y/81,5 wiesen vier

verschiedene Signale auf. Ein breites Signal bei niedrigem Feld (δ_{iso} = 70±10 ppm, C_{QCC} = 15.0±1.0 MHz) wird durch eine Überlagerung der Signale von Gerüstaluminiumatomen in der Nahstruktur von Brücken-OH-Gruppen und von Gerüstaluminiumatomen verursacht, deren negative Ladung durch Extragerüstaluminiumkationen kompensiert wird. Ein schmales Signal bei niederem Feld (δ_{iso} = 65±5 ppm, C_{QCC} = 8.0±0.5 MHz) kann Gerüstaluminiumatomen zugeordnet werden, deren Ladung von Natriumkationen kompensiert wird, als auch tetraedrisch koordinierten Aluminiumatomen in Extragerüstaluminiumoxidclustern. Weitere zwei Signale werden durch Aluminiumkationen (δ_{iso} = 35±5 ppm, C_{QCC} = 7.5±0.5 MHz) und oktaedrisch koordinierte Aluminiumatomen in Extragerüstaluminiumoxidclustern (δ_{iso} = 10±5 ppm, C_{QCC} = 5.0±0.5 MHz) erkärt. Durch Elementaranalyse und Auswertung der relativen Signalintensitäten der verschiedenen Aluminiumspezies in den ^{27}Al-Spin-Echo- und MAS-NMR-Spektren des dehydratisierten Zeoliths konnte die Aluminiumverteilung in dieser Probe bestimmt werden.

2.   Abstract

To study aluminum species in dealuminated zeolites, a series of dealuminated zeolites Y with framework n_{Si}/n_{Al} ratios of 2.8 to 6.0 was prepared by steaming. The steaming of zeolite H,Na-Y was performed under water vapor pressures of 3.4 to 81.5 kPa and at a temperature of 748 K. As determined by X-ray diffraction (XRD), the crystallinity of zeolites was well preserved after the above-mentioned treatments.

The hydrated materials were investigated by ^{29}Si MAS NMR, ^{27}Al MQMAS NMR, high-field ^{27}Al MAS NMR, and ^{1}H MAS NMR spectroscopy. Upon adsorption of ammonia on the steamed zeolites H,Na-Y, a reversible change of octahedrally coordinated to tetrahedrally coordinated aluminum atoms was found. Quantitative ^{29}Si, ^{27}Al, and ^{1}H MAS NMR measurements indicated that this coordination change is accompanied by the formation of bridging OH groups (SiOHAl) in the dehydrated materials, while only a weak decrease in the amount of silanol (SiOH) groups and no systematic change of AlOH groups occurred. Based on these results, a model for the reversible coordination change of aluminum atoms in the framework of hydrothermally treated zeolites H-Y is proposed assuming local structures consisting of threefold-coordinated framework aluminum atoms with SiO^{-} defect sites in their vicinity, which are coordinated to extra-framework aluminum species. After adsorption of ammonia at the threefold-coordinated framework aluminum atoms, the SiO^{-} defect sites are healed to Si-O-Al^{-} bridges leading to a transformation of the threefold-coordinated aluminum atoms to tetrahedrally coordinated atoms. Upon thermal decomposition of the ammonium ions formed at these Si-O-Al^{-} bridges, SiOHAl groups occur. It is also found that framework and extra-framework aluminum species in zeolite Y were strongly influenced upon rehydration. Therefore, the investigations of these materials in non-hydrated state, i.e., without hydration after the dealumination, are required.

To obtain dealuminated zeolites in non-hydrated state, these dealuminated materials were immediately filled into glass containers under dry nitrogen in an air-lock after steaming. By ^{29}Si MAS NMR spectroscopy, a strong high-field shift of the signals of Si(3Al) and Si(2Al)

sites in the spectra of non-hydrated zeolites Y in comparison with those of the hydrated samples was observed. These high-field shifts of the Si(nAl) signals of 2 to 5 ppm occurring in the ^{29}Si MAS NMR spectra of non-hydrated zeolites Y were discussed to be caused by i) a variation of the local structure of neighboring AlO$_4$ tetrahedra or ii) the presence of multivalent extra-framework aluminum cations. To clarify the reasons for these resonance shifts, zeolites Y with different H- and Al-exchange degrees were investigated by solid-state NMR spectroscopy. The experimental results indicate that the primary reason for the high-field shift of ^{29}Si MAS NMR signals of silicon atoms in non-hydrated state is the change of O-Al-O bond angles and Al-O bond lengths during the dehydration of AlO$_4$ tetrahedra in the framework. In contrast, the presence of extra-framework aluminum cations leads only to a strong broadening of the Si(nAl) signals, probably due to ^{29}Si-^{27}Al couplings, and a weak high-field shift of ca. 1 ppm.

With increasing water vapor pressure during the steaming of zeolite Y, a systematic decrease of the total amounts of framework aluminum atoms in the non-hydrated materials was found by ^{29}Si MAS NMR spectroscopy. The amounts of threefold coordinated framework aluminum atoms in non-hydrated zeolites Y were determined by the increase of the concentrations of bridging OH groups after an ammonia adsorption/desorption treatment and by application of ^{1}H MAS NMR spectroscopy. By a quantitative comparison of the amounts of tetrahedrally coordinated framework aluminum atoms, responsible for the occurrence of negative framework charges, and the amounts of charge-compensating residual sodium cations and bridging hydroxyl protons, the mean cationic charge of extra-framework aluminum atoms was calculated. This means that the cationic charge per extra-framework aluminum atom was found to vary from ca. +2 to ca. +0.5 for weakly and strongly dealuminated zeolites Y samples, respectively.

Solid-state NMR characterization of zeolite catalysts in the hydrated state is often accompanied by an uncontrolled hydrolysis of the framework and a variation in the coordination of aluminum species. It is demonstrated that the limitations occurring for ^{29}Si and ^{27}Al MAS NMR spectroscopy of non-hydrated zeolites Y, such as strong decrease of

resolution and significant line broadening, can be overcome by loading these materials with ammonia. In the ^{29}Si MAS NMR spectra of non-hydrated and ammonia-loaded zeolites Y, no dehydration-induced high-field shift of Si(nAl) signals (n = 3, 2, 1) occurs, which is generally responsible for the loss of resolution in the spectra of non-hydrated materials. The ^{27}Al MAS NMR spectra of the non-hydrated and ammonia-loaded zeolites Y consist exclusively of signals of the tetrahedrally coordinated framework aluminum atoms with spectroscopic parameters similar to those of framework aluminum atoms in hydrated samples. The framework n_{Si}/n_{Al} ratios obtained by quantitative evaluation of both ^{29}Si and ^{27}Al MAS NMR spectra of the non-hydrated and ammonia-loaded zeolites Y agree well with each other.

Beside adsorption of ammonia, the adsorption of other probe molecules, such as pyridine, acetone, and acetonitrile, was utilized to conquer the above-mentioned limitations occurring for ^{29}Si and ^{27}Al MAS NMR spectroscopy of non-hydrated zeolites Y. It is interestingly to note that the base strength of probe molecules is reflected by the variation of the second-order quadrupolar effect (*SOQE*) value of the framework aluminum atoms in the non-hydrated zeolites. The occurrence of a proton transfer from the catalyst to the probe molecules is necessary to detect the framework aluminum by ^{27}Al MAS NMR spectroscopy in moderate magnetic fields (ca. 9.4 T). It is demonstrated that a proton affinity (PA) of the adsorbate molecules of ca. 850 kJ/mol is required to induce a proton transfer from the zeolite framework to the adsorbate compounds. In addition, other effects could influence the observation of framework aluminum by ^{27}Al MAS NMR spectroscopy, such as, the size of probe molecules. The quantitative evaluation shows that the adsorption capacity of pyridine is hindering the detection of all framework aluminum atoms by both ^{29}Si and ^{27}Al MAS NMR spectroscopy in moderate magnetic fields.

^{27}Al spin-echo, high-speed MAS (ν_{rot} = 30 kHz), and MQMAS NMR spectroscopy in magnetic fields of B_0 = 9.4, 14.1, and 17.6 T were applied for the study of aluminum species at extra-framework positions in non-hydrated zeolites Y. Non-hydrated γ-Al$_2$O$_3$, aluminum-exchanged zeolite Y (Al,Na-Y) and parent zeolite H,Na-Y were utilized as reference materials. The solid-state ^{27}Al NMR spectra of steamed zeolite deH,Na-Y/81.5 were

found to consist of four signals. The broad low-field signal is caused by a superposition of the signals of tetrahedrally coordinated framework aluminum atoms in the vicinity of bridging hydroxyl protons and framework aluminum atoms compensated in their negative charge by aluminium cations (δ_{iso} = 70±10 ppm, C_{QCC} = 15.0±1.0 MHz). The second signal is due to a superposition of the signals of framework aluminum atoms compensated by sodium cations and tetrahedrally coordinated aluminum atoms in neutral extra-framework aluminum oxide clusters (δ_{iso} = 65±5 ppm, C_{QCC} = 8.0±0.5 MHz). The residual two signals were attributed to aluminum cations (δ_{iso} = 35±5 ppm, C_{QCC} = 7.5±0.5 MHz) and octahedrally coordinated aluminum atoms in neutral extra-framework aluminum oxide clusters (δ_{iso} = 10±5 ppm, C_{QCC} = 5.0±0.5 MHz). By chemical analysis and evaluating the relative solid-state ^{27}Al NMR intensities of the different signals of aluminum species occurring in non-hydrated zeolite deH,Na-Y/81.5, the aluminum distribution in this material could be determined.

3. Aims of the Work

Solid-state NMR spectroscopy is a very sensitive method for the investigation of the local structure of crystalline aluminosilicates, such as microporous zeolites applied in heterogeneous catalysis and adsorption processes. Therefore, e.g., solid-state ^{1}H, ^{23}Na, ^{29}Si, ^{27}Al, and ^{17}O NMR spectroscopy are utilized in a broad manner for the characterization of hydrogen, sodium, silicon, aluminum, and oxygen atoms, respectively, contributing to the lattice of these materials [1-8] (see Scheme 3.1) . In addition, the chemical nature of adsorbates and the effects of these molecules on the framework and surface sites of zeolites can be clarified by solid-state NMR spectroscopy [9-11].

Aluminum atoms in dealuminated zeolites can occur in various natures, i.e. as tetrahedrally coordinated framework aluminum, distorted tetrahedral framework or extra-framework aluminum, five-fold coordinated extra-framework aluminum, octahedrally coordinated extra-framework aluminum in alumina domains, and flexibly coordinated framework aluminum [11-16]. Until now, most of the solid-state NMR investigations of the framework of zeolites were performed on hydrated samples [11-16]. During industrial applications of zeolite catalysts and adsorbents, however, these materials are always in the calcined and non-hydrated state. Therefore, the characterization of the nature of aluminum

^{1}H and ^{27}Al NMR of probe molecules
adsorbed on surface sites

Al^{fr}: Framework aluminum atoms

Al^{ex}: Extra-framework aluminum atoms

^{29}Si NMR
^{1}H NMR
^{27}Al NMR

Al^{fr} | Al^{ex}

^{1}H NMR
^{27}Al NMR

dealuminated zeolites
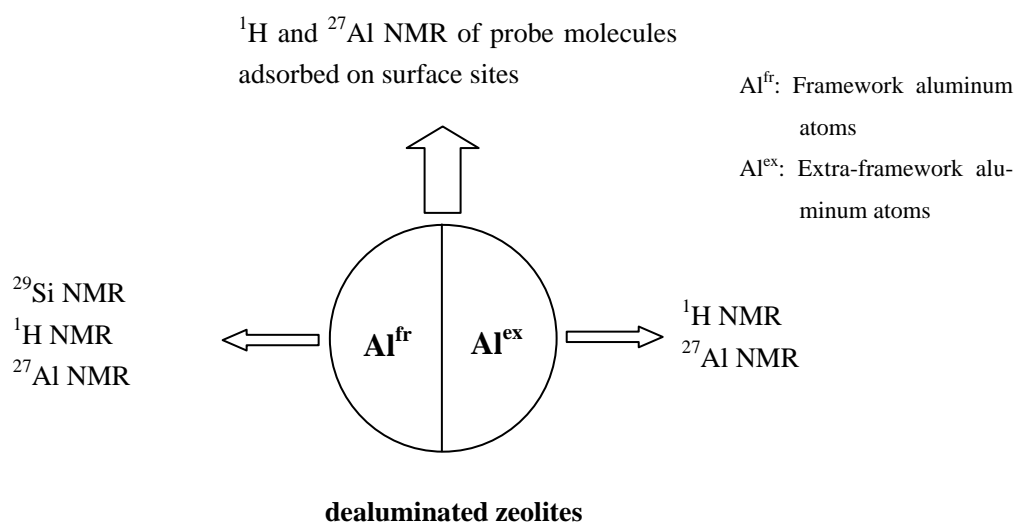
Scheme 3.1

species in zeolites being in the non-hydrated state is important for the improvement of our knowledge about the behavior in these materials. In the present work, the solid-state NMR investigation of a series of steamed zeolites Y is performed at first in a more classical way, i.e., using hydrated samples and, subsequently, in a new way, i.e. using samples, which were not rehydrated (denoted non-hydrated or dehydrated) upon the steaming. The general aims of the present work are summarized in the following:

a) It was planed to prepare a series of dealuminated zeolites Y by steaming at different water vapor pressures. In the first step, the aluminum content in the framework of these dealuminated zeolites Y as a function of the water vapor pressure is quantitatively studied by solid-state NMR spectroscopy of hydrated samples. The flexibility of the coordination of aluminum atoms at framework defects upon loading of ammonia and the effect of this coordination change on the hydroxyl coverage of the dehydrated zeolites should be studied.

b) The dealumination of zeolites is accompanied by the formation of cationic extra-framework aluminum species. The charge balance between extra-framework aluminum species and the framework of steamed and non-hydrated zeolites Y has to be investigated in an indirect manner by multinuclear solid-state NMR spectroscopy (see Scheme 3.1). Generally, it is accepted that the intensities of solid-state NMR signals are proportional to the populations of the respective species [17]. For quadrupolar nuclei, in some cases a correction of the obtained NMR intensities has to be performed [12, 13]. Therefore, the possibilities and limitations of solid-state NMR spectroscopy to obtain quantitative results about the dealuminated zeolites in the non-hydrated state are discussed.

c) Previous solid-state NMR studies have shown that the strength of the quadruploar interaction of aluminum atoms in non-hydrated zeolites and their NMR line broadening can be significantly influenced by the adsorption of probe molecules [11]. This effect is accompanied by a change of their local structure of the AlO_4 tetrahedra

and of neighboring SiO_4 tetrahedra. Therefore, it was planed to study the local structure of framework aluminum and silicon atoms and the hydroxyl coverage of dealuminated zeolites upon adsorption of different probe molecules. For these investigations, *ex situ* as well as *in situ* solid-state NMR spectroscopy should be utilized. A novel method for the quantitative characterization of the framework aluminum content in non-hydrated zeolites has to be developed.

d) The determination of the amount and nature of extra-framework aluminum species non-hydrated zeolites is important for the understanding of the catalytic and adsorption behavior of these materials [18, 19]. Different techniques of modern solid-state ^{27}Al NMR spectroscopy, such as ^{27}Al spin-echo NMR in magnetic fields of B_0 = 9.4 to 17.6 T, high-speed magic angle spinning (MAS) NMR, and multiple-quantum magic angle spinning (MQMAS) NMR were planed to apply for the determination of the spectroscopic parameters of the different extra-framework aluminum species in dealuminated and non-hydrated zeolites Y. Non-hydrated γ-Al_2O_3, aluminum-exchanged zeolite Y (Al,Na-Y), and the parent zeolite H,Na-Y have to be used as reference materials for the assignment of the ^{27}Al NMR signals of extra-framework aluminum species in dealuminated zeolites Y.

oxidation properties [38, 42, 47-51]. In addition, zeolite catalysts have an interesting shape selectivity, a high surface area, and a high thermal stability [47]. Concerning catalytic applications, more than 90% of zeolite catalysts are used in the fluid catalytic cracking (FCC) of vacuum distillates and residues into more valuable, olefines, as well as into high-octane gasoline and diesel-boiling-range products [39, 47]. This process takes place in a riser reactor at reaction temperatures of 753 - 823 K and at pressures of 2 - 3 bar [47].

Starting in the 1960s, zeolites H-Y were applied as catalysts in the FCC process because of their high intrinsic acidity, good selectivity towards gasoline compounds combined with low coke and gas formation, and good activity retention [47]. However, the high temperature treatment of zeolite H-Y with high framework aluminum content during the burning of coke in the regenerator leads to massive crystal destruction and, finally, to a collapse of the zeolite structure [47]. Dealumination of the framework is a suitable method to improve the stability of zeolite H-Y [47-49]. Due to the decrease of the framework aluminum content of zeolite H-Y, the number of Brønsted acid sites is strongly reduced. In result of this modification, only isolated acid sites exist and bimolecular hydrogen-transfer reactions are hindered. Hence, FCC products become more olefinic, and the quality of the gasoline is strongly improved [47-49].

4.1.2   Structure, Composition, and Nomenclature

Zeolites are crystalline substances with a three dimensional rigid structure characterized by a framework of linked tetrahedral, each consisting of four oxygen atoms surrounding a cation [21]. According to this definition of zeolites, TO_4 tetrahedra (T: Si or Al in most of cases) are the primary building blocks, which are organised in such a way that they form larger units, known as secondary building units (SBU). Under synthesis conditions, these secondary building units are combined to different structure types. The *Structure Commission* of the *International Zeolite Association* (IZA) assigned to every known structure a mnemonic three letter code, which represents the structure topology, such as FAU, LTA, etc. [38]. In addition, the *International Union of Pure and Applied Chemistry* (IUPAC) gave definitions of cages,

4. Introduction to Solid-state Nuclear Magnetic Resonance of Aluminum-containing Zeolites

4.1 Introduction to Zeolites

4.1.1 History and Applications of Zeolites

In 1756, a natural aluminosilicate mineral was discovered by Cronstedt [20]. This material started to bubble when heated. Derived from the Greek words "zeo" and "lithos", Cronstedt [20] named this material "zeolite", which means "boiling stone". In the following two centuries, a large amount of natural zeolite deposits were found [21]. In the beginning of the 20th century, the structures of most of the natural zeolites were determined by X-ray diffraction (XRD) [22]. At the same time, two pioneers, Barrer and Milton [23], found a suitable route for the preparation of aluminosilicate zeolites in the laboratory scale. In the 1980s, the synthesis of non-siliceous crystalline microporous solids (such as aluminophosphates) was achieved [24-27], and during the late 1980s and the 1990s, the range of chemical compositions was expanded by the incorporation of new metals into the framework, such as B, Fe, Ga, Ti, V, and Zn [28-33]. In addition, purely siliceous materials, such as silicalites and periodic mesoporous structures (MCM materials) [34-37] were prepared. Up till now, 161 structure types of zeolites have been discovered [38].

Zeolites are commercially applied in detergents (1.09×10^6 t per year), in separation processes (0.10×10^6 t per year), and most importantly, as catalysts (0.13×10^6 t per year) in heterogeneously catalyzed reactions [39]. These applications include the drying of refrigerants [40], the removal of atmospheric pollutants, such as sulphur dioxide [41], the separation of air components [23], the recovering of radioactive ions from waste solutions [42], the cracking and reformation of hydrocarbons [43], isomerization of light paraffin [44], and conversion of methanol to light gasoline [45, 46].

The most important application of zeolites is as catalysts with acidic, basic, redox, and

pores, and other parameters [52].

The chemical composition of zeolites can be described by the formula [23]

$$x_1 M_1{}^{n1+}; x_2 M_2{}^{n2+}; \ldots [(y_1 T_1; y_2 T_2 \ldots) O_{2(y1+y2+\ldots)}]^{x-} z_1 A_1 ; z_2 A_2 \ldots,$$
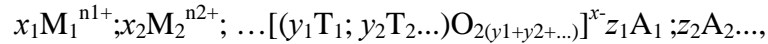
where the expression in the square brackets represents the framework composition. The other terms correspond to species located in the micropores:

- M_1, M_2 …: Cations with the charge of n1+, n2+, … , which compensate the negative charge of the framework (x_1n1 + x_2n2 + …= x),

- T_1, T_2 …: T atoms (Si, Al, ...) of the TO_4 tetrahedra,

- A_1, A_2 …: Water or template molecules.

The present work focuses on the study of zeolite Y, which belongs to the faujasite type zeolites (Figure 4.1) [53, 54]. The structure of faujasite type zeolites contains only one type of crystallographic T sites, but four crystallographically different oxygen sites (O1, O2, O3, and O4). All the T atoms are connected via three four-membered rings and one six-membered ring. These rings compose three different cages: Supercages, sodalite cages, and hexagonal prisms. The supercages have an inner diameter of 1.18 nm, and are connected each other via twelve-membered oxygen rings with a diameter of 0.74 nm [53, 54]. The supercages are surrounded by sodalite cages. The entrances to the sodalite cages are six-membered oxygen rings with a diameter of 0.24 nm. Each sodalite cage is connected with four hexagonal prisms [53, 54]. Extra-framework cations compensate the negative charges of the zeolite framework. Figure 4.1 shows the five extra-framework cation positions SI, SI', SII, SII', and SIII in faujasite type zeolites [8].

4.1.3   Dealumination of Zeolites

As-synthesized zeolites can not be utilized in experiments or industrial processes in a direct manner. According to the different applications, additional modifications of the as-synthesized materials are necessary to improve their properties. The detail description of post-synthesis modification methods is described References [23, 55-57]. Dealumination is one of the most

important modification procedures of zeolites. Since this work focuses on the dealumination of zeolite Y by steaming, this process is discussed in detail in the following section.

a)

Sodalite cage

Hexagonal prism

Supercage

SIII

O1

SI

O2

SII'

O3

SI'

O4

SII

○ Extra-framework cation

○ Oxygen atom

b)

0.74 nm

0.74 nm

0.74 nm

0.74 nm
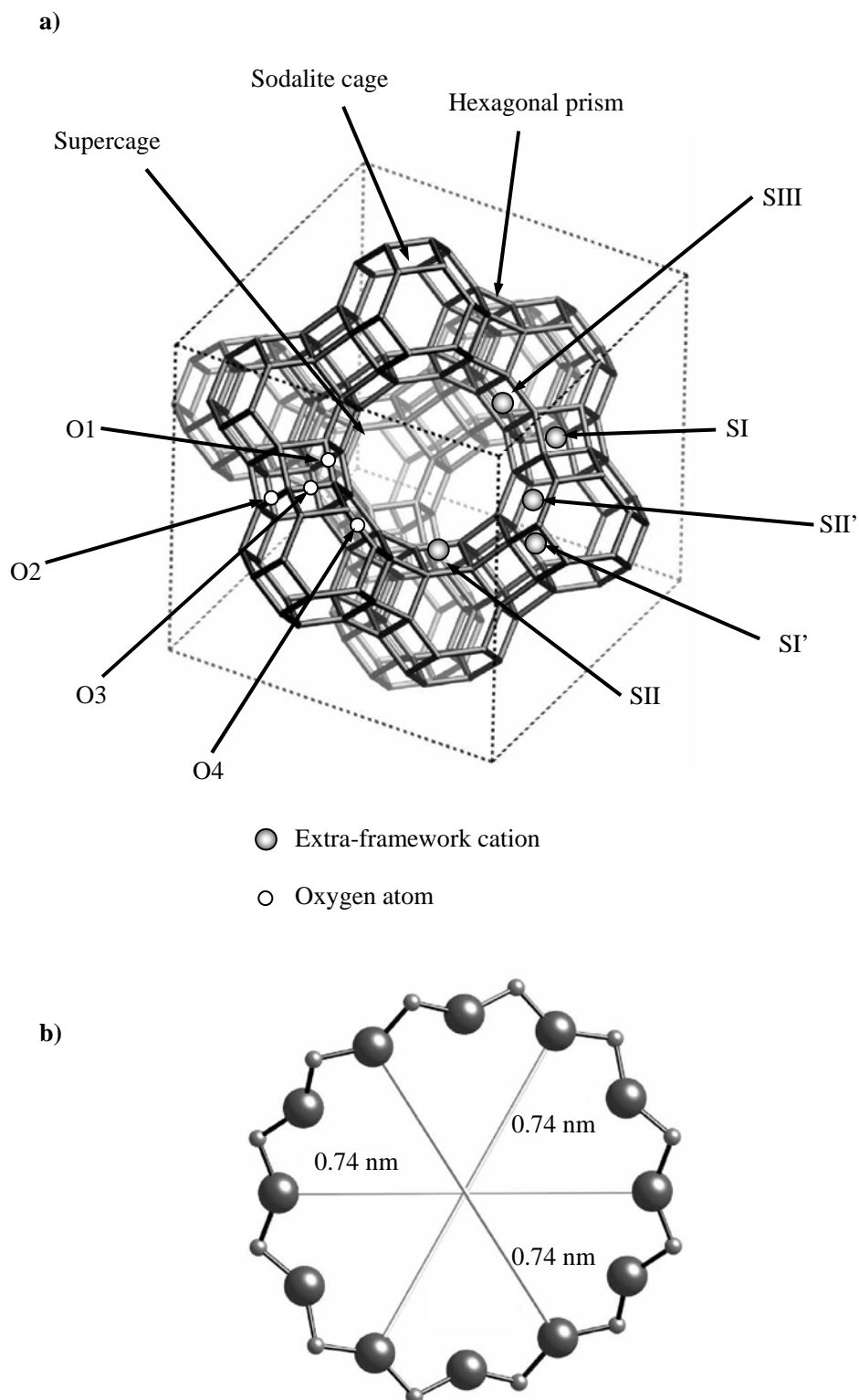
Figure 4.1 Framework of faujasite type zeolites (a). 12-ring viewed along <111> (b) [37].

The framework n_{Si}/n_{Al} ratio of zeolites is a very important parameter, which strongly influences the sorptive and catalytic properties of these materials [57, 58]. Generally, the range of n_{Si}/n_{Al} values of zeolites Y prepared by a hydrothermal synthesis is very narrow (1.5 to ca. 3.0) [59, 60]. Therefore, the improvement of techniques for the tuning of the framework aluminum content is of great importance for many technical applications. Possible treatments are extraction of framework aluminum by chemical agents, hydrothermal dealumination of the zeolites framework, isomorphous substitution of framework aluminum by silicon, and re-alumination of zeolites [55, 57]. In 1967, McDaniel and Maher [56] reported an ultrastabilization procedure to increase the thermal stability of zeolite Y. A few years later, Kerr [61, 62] evidenced that the -O-Al-O- bonds are cleaved by the water formed via the thermal dehydroxylation, which plays a decisive role in this process. Subsequently, the hydroxyaluminum species, for instance $Al(OH)_3$, are removed from the framework. In 1981, Lohse and Mildebrath [63] showed that silicon atoms refill the empty tetrahedral vacancies, which leads to a healing of the zeolite framework. It is concluded that a dealumination process can be described by three steps: 1) Cleavage of -O-Al-O- bonds in the framework, 2) removal of aluminum complexes, and 3) refilling of the empty sites by silicon atoms (Scheme 4.1) [64].
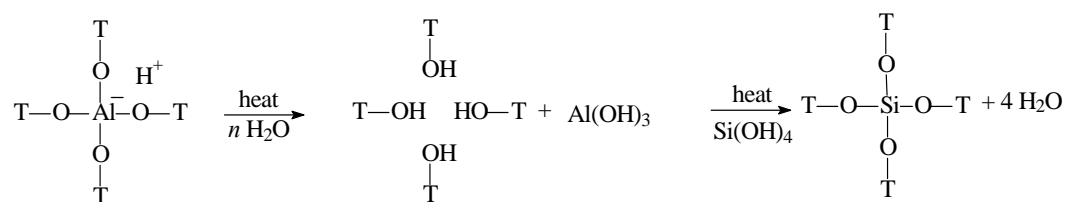

Scheme 4.1

Kuehl [65], suggested the dealumination mechanism shown in Scheme 4.2. In this mechanism, a framework silicon cation with one charge is formed after the dehydroxylation of two bridging OH groups at high temperatures. Simultaneously, an extra-framework aluminum complex (AlO^+) is formed. Subsequently, the zeolite framework is healed via formation of new -Si-O-Si- bonds.
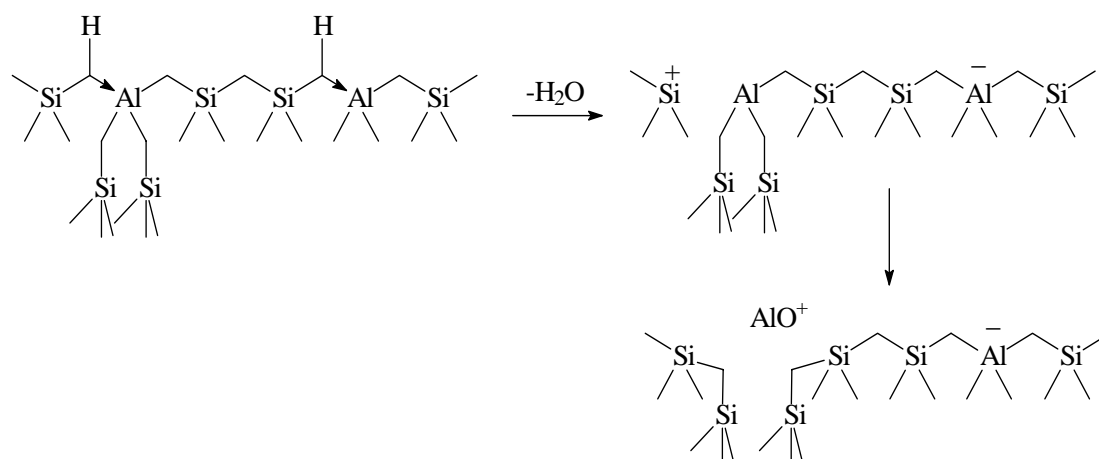
Scheme 4.2

The above-mentioned dealumination of the zeolite framework is accompanied by several changes in the local structure of zeolites. These structural rearrangements are accompanied by a silicon migration into vacancies created by dealumination and a decrease of the unit cell parameter a_0 from 24.78 (zeolite NH_4Y: ca. 54 Al atoms per unit cell) to ca. 24.24 Å (dealuminated zeolite Y: ca. 4 Al atoms per unit cell) [54, 66]. During the dealumination, the aluminum atoms released from the zeolite framework are transformed into a variety of extra-framework aluminum species. These species are mainly classified as condensed and non-condensed extra-framework aluminum species. The condensed extra-framework aluminum species occur in Al_2O_3 or silica-alumina phases. In addition, non-condensed extra-framework aluminum cations (Al^{3+}) or oxyaluminum species (e.g. AlO^+, $Al(OH)^{2+}$) are assumed [67-71]. By X-ray diffraction and Rietveld analysis of dealuminated zeolite Y, Gola *et.al.* [71] found three cation positions occupied by extra-framework aluminum atoms (Figures 4.1 and 4.2): Position 1 (the site $SI^{'}$) located at a distance of 0.225 nm from three framework O3 oxygen atoms; position 2 at the centre of the sodalite cage; position 3 between position 1 and 2. The distance between O3 oxygen atoms and the extra-framework aluminum atoms at position 1 indicates that this site is occupied by Al^{3+} cations. Another type of extra-framework aluminum atoms, e.g. $Al(OH)_2^+$, occupies the positions 2 and 3 [71]. The structures of different extra-framework aluminum species were studied by computational approaches [72-75]. Al^{3+}, $Al(OH)^{2+}$, AlO^+, $AlO(OH)$, and $Al(OH)_3$ were chosen as models of

the extra-framework aluminum species. The theoretical results indicate that the monovalent cations, AlO^+ and $Al(OH)_2^+$, prefer to attain two bondings to with the framework AlO_4^- moiety and show threefold and tetrahedral coordinations, respectively [72]. Di- and trivalent cations, i.e. $Al(OH)^{2+}$ and Al^{3+}, usually have four bondings to framework oxygen atoms and show five-fold and tetrahedral coordinations, respectively [72]. These extra-framework aluminum species coordinate to the oxygen atoms nearest to the negatively charged framework aluminum atoms [72].
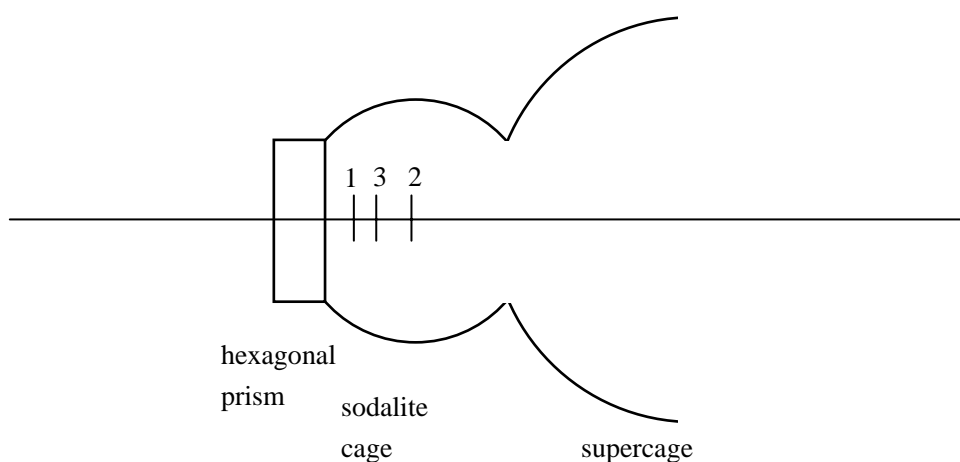
Figure 4.2 Positions of extra-framework aluminum species in dealuminated zeolites Y [71].

A further important result of dealumination is the increase of the acid strength of the Brønsted acid sites, which is correlated with the mean electronegativity of the zeolite framework [76, 77]. In addition, Lewis acid sites are formed at framework defect sites or extra-framework aluminum species [67, 76-80]. In the *n*-hexane cracking used as a catalytic test reaction, mildly dealuminated zeolite H-ZSM-5 catalysts show a higher catalytic activity than the parent and the strongly dealuminated materials [76]. It is proposed that these extra-framework aluminum species or Lewis acid sites interact with electron pairs of framework oxygen atoms near the Brønsted acid sites, which leads to a delocalization of the electron density. Therefore, the acid strength of Brønsted acid sites is increased (Scheme 4.3) [81]. These sites are sometimes referred to as superacid sites [81]. For the thiophene acylation by butyryl chloride, the initial reaction rate correlates with the number of Lewis acid sites [80].
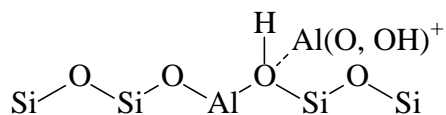
Scheme 4.3

4.1.4 Methods for the Characterization of Dealuminated Zeolites

Infrared (IR) spectroscopy is an extensively used method for the investigation of catalytically active surface sites and the framework of dealuminated zeolites [82-85]. IR spectroscopy is based on the interaction of electromagnetic radiation with species, which are characterized by a permanent or induced dipole moment [86].

An important advantage of IR spectroscopy for the investigation of zeolites is the high sensitivity of this method. The stretching vibration at ca. 3750 cm^{-1} is due to silanol groups on the external or internal (low frequency tail) surface [82, 85, 87]. The high-frequency (HF) band occurring at 3650 cm^{-1} is due to accessible bridging OH groups in the supercages, while the low-frequency (LF) band occurring at 3540 cm^{-1} is caused by bridging OH groups in the sodalite cages of zeolites Y [82, 85, 87]. Following characteristic lattice vibrations of the zeolitic structure can be distinguished: Asymmetric stretching vibrations (950-1025 cm^{-1} and 1050-1250 cm^{-1}), symmetric stretching vibrations (750-820 cm^{-1} and 650-750 cm^{-1}), double ring vibrations (500-650 cm^{-1}), T-O bending vibrations (420-500 cm^{-1}), and pore opening vibrations (300-420 cm^{-1}) [82, 83, 84]. For some of the structure sensitive bands, a linear relationship between the wave number and the number of lattice aluminum atoms was found [88]. According to the position of the structure sensitive asymmetric stretching band σ_1 (1050-1150 cm^{-1}), the number of the lattice aluminum atoms in dealuminated zeolites Y, n_{Al}, can be calculated by the equation [88]

$$n_{Al} = 0.960 \times (1068 - \sigma_1). \qquad (1)$$

In the spectral region below 250 cm^{-1}, IR spectra show the vibrations of extra-framework

cations [82]. However, a quantitative evaluation of the band intensities requires the knowledge of extinction coefficients, which are a function of the wavenumber. Therefore, this method is often limited in its application.

A very modern technique for the determination of the local structure of aluminum atoms in non-hydrated states is the X-ray absorption near-edge spectroscopy (XANES). If X-rays have enough energy to excite and eject electrons from the core orbits of the atoms under study, a sharp increase in the X-ray absorption is observed. This is the principle of the so called X-ray absorption spectroscopy [89]. With this method, the coordination of aluminum atoms and Al-O bond distances can be determined [18, 90, 91]. Van Bokhoven *et al*. [18] applied Al K-edge XANES for the characterization of the formation of threefold coordinated framework aluminum after steaming of zeolite H-Beta at temperatures above 675 K. The local structure of Brønsted acid sites was established to consist of three short Al-O bonds (0.168 nm) and one long Al-OH bond (0.183 nm) [18, 90]. In addition, the conversion of the coordination of aluminum atoms from an octahedral to a tetrahedral coordination under vacuum at 673 K in zeolites H-USY was observed [91].

Since the 1970s, Nuclear Magnetic Resonance (NMR) spectroscopy is an often applied method for the investigation of dealuminated zeolites [1-17, 92-94]. High-resolution ^{1}H magic angle spinning (MAS) NMR is a suitable method for the study of the hydroxyl coverage of zeolites. The spectroscopic parameters of metal OH groups (-0.5 to 0.5 ppm), silanol groups (1.3 to 2.2 ppm), AlOH groups (2.6 to 3.6 ppm), and bridging OH groups (3.8 to 7.0 ppm) were summarized in Reference [95]. A considerable advantage of ^{1}H MAS NMR spectroscopy in comparison with IR spectroscopy is the linear dependence of the signal intensities on the spin concentration, which permits a direct determination of the OH concentration.

The formation of aluminosilicate-type zeolites by TO_4 tetrahedra with silicon or aluminum atoms at the central T-position results in five different silicon environments denoted as Si(*n*Al) units (Figure 4.3). Here, *n* corresponds to the number of aluminum atoms

in the second coordination sphere of silicon atoms [96]. In the ^{29}Si MAS NMR spectra of zeolites, the chemical shifts of Si(4Al), Si(3Al), Si(2Al), Si(1Al), and Si(0Al) units are observed at -101 to -120, -97 to -108, -91 to -99, -85 to -94, and -81 to -91 ppm, respectively [96, 97]. Using the intensities $I_{Si(nAl)}$ of the Si(nAl) units, the framework n_{Si}/n_{Al} ratio can be calculated by the equation [3, 17, 97, 98]

$$n_{Si}/n_{Al} = \sum_{n=0}^{4} I_{Si(nAl)} / \sum_{n=0}^{4} 0.25 \times n \times I_{Si(nAl)} . \qquad (2)$$
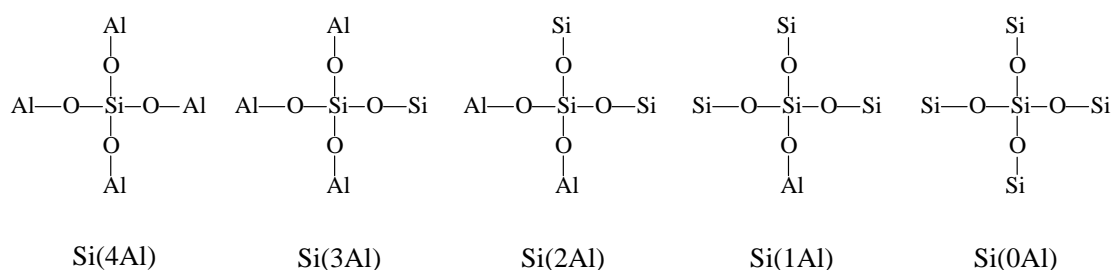
Figure 4.3 Different silicon environments in zeolite frameworks (Si(nAl) units, n = 4, 3, 2, 1, 0).

Solid-state ^{27}Al NMR spectroscopy allows a direct view on the aluminum atoms occurring in zeolites. In most of the solid-state ^{27}Al NMR studies of dealuminated zeolites published in the past decades, the nature of framework and extra-framework aluminum species was investigated in the hydrated state of the samples [16, 67, 101, 102]. By this approach, tetrahedrally coordinated framework aluminum atoms, distorted tetrahedrally coordinated aluminum atoms at framework position, five-fold coordinated extra-framework aluminum species, octahedrally coordinated aluminum in alumina domains, and flexibly coordinated aluminum atoms at framework defects were observed [12-16, 99, 100]. The spectroscopic parameters of the above-mentioned aluminum species are summarized in Table 4.1. In the ^{27}Al MAS NMR spectra of hydrated zeolites NH$_4$Y, a narrow signal of tetrahedrally coordinated framework aluminum atoms (Al^{IV}) is observed at ca. 60 ppm [12-16, 99, 100]. The ^{27}Al MAS NMR spectra of hydrated dealuminated zeolites consist of a broad signal at ca. 60 ppm and various signals of octahedrally coordinated aluminum species at ca. 0

ppm [12-16, 99, 100]. The polarization effect of extra-framework aluminum cations on the zeolite framework leads to the broadening observed for the signal at ca. 60 ppm [99]. Upon ammonia adsorption, parts of the octahedrally coordinated aluminum atoms (broad signal at 0 ppm) are transformed into tetrahedrally coordinated atoms [16]. These flexibly coordinated aluminum atoms are either associated with framework related aluminum species or with aluminum atoms belonging to amorphous silica-alumina phases [16]. The residual octahedrally coordinated aluminum atoms (i.e. no change of coordination upon ammonia) may occur in amorphous γ-Al_2O_3 phases [16].

Table 4.1 Isotropic chemical shifts δ_{iso}, quadrupolar coupling constants (see Section 4.2) C_{QCC}, and assignments of the different ^{27}Al MAS NMR signals of dealuminated zeolites in the hydrated state.

δ_{iso} /ppm	C_{QCC} /MHz	Coordination	Location
ca. 60	2.2-3.1	Al^{IV}	Framework [12, 13, 16, 99, 100]
ca. 60	6.4-7.1	Al^{IV}(distorted)	Framework [12, 13, 16, 99, 100]
ca. 30	4.4-4.6	Al^{V}	Extra-framework [12, 13, 16, 99, 100]
0-10	1.8-3.0	Al^{VI}(flexible)	Framework related [16, 100] or extra-framework [12, 13, 16, 99]
0-10	3.2-5.0	Al^{VI}	Extra-framework [12, 13, 16, 99, 100]

Since the nature of framework and extra-framework aluminum species is strongly influenced by the presence of water [16, 18, 90], the characterization of zeolite catalysts under conditions similar to their industrial application, i.e. in the non-hydrated state, is required. As a consequence, the quadrupolar interactions of ^{27}Al nuclear are strongly increased and the solid-state ^{27}Al NMR signals become significantly broader in comparison with signals of hydrated zeolites [94, 103-105]. In 1994, Freude *et.al.* [93, 104] found broad and characteristic quadrupolar patterns in the static (without MAS) ^{27}Al spin-echo NMR spectra of non-hydrated zeolites H-Y and H-ZSM-5. These patterns are due to framework aluminum atoms in the vicinity of bridging hydroxyl protons. The application of the static spin-echo method, however, is limited because of low resolution. In 2001, an improvement of the resolution of the solid-state ^{27}Al NMR spectra of non-hydrated zeolites H-ZSM-5 was

achieved by the development of the double-frequency sweep (DFS) enhanced multiple-quantum magic angle spinning MQMAS technique [94]. In the present work, methods suitable for the characterization of the various aluminum species in non-hydrated zeolites Y by solid-state NMR spectroscopy were explored in detail.

4.2 NMR Spectroscopy of Quadrupolar Nuclei

Solid-state NMR spectroscopy is a powerful technique for the characterization of aluminum atoms in zeolites [95, 96, 106]. Aluminum nuclei are characterized by a nuclear spin $I = 5/2$ leading to an electric quadrupole moment. An important prerequisite for the success of solid-state NMR spectroscopy of aluminum atoms in zeolites was the development of effective line narrowing techniques and two-dimensional experiments that make the detection of highly resolved solid-state NMR spectra and the determination of different spectral parameters possible. In this section, the basic principles of solid-state NMR spectroscopy of quadrupolar nuclei are briefly described.

For nuclear spins in solid materials, the dominating line broadening interactions are described by the total Hamiltonian

$$\hat{\boldsymbol{H}} = \hat{\boldsymbol{H}}_0 + \hat{\boldsymbol{H}}_{\mathrm{II}} + \hat{\boldsymbol{H}}_{\mathrm{IS}} + \hat{\boldsymbol{H}}_{\mathrm{CSA}} + \hat{\boldsymbol{H}}_{\mathrm{Q}}, \qquad (3)$$

where $\hat{H}_0$, $\hat{H}_{\mathrm{II}}$, $\hat{H}_{\mathrm{IS}}$, $\hat{H}_{\mathrm{CSA}}$, and $\hat{H}_{\mathrm{Q}}$ are the Hamiltonians of the Zeemann interaction, the homonuclear and heternuclear magnetic dipole-dipole interaction, the chemical shifts anisotropy, and the quadrupolar interaction, respectively [106]. In the case of spin $I = 1/2$ nuclei, the chemical shift anisotropy and dipole-dipole coupling can be averaged by the magic angle spinning (MAS) technique leading to highly resolved spectra. The MAS technique is described in Chapter 5.

For nuclei with nuclear spin $I > 1/2$, such as for aluminum nuclei with spin $I = 5/2$, an electric quadrupole moment, eQ, occurs due to the non-spherical electric charge distribution

ρ(r) in the nucleus. The orientation energy E_Q of the electric quadrupole in the electric crystal field V(r) is given by [103, 107]

$$E_Q = \int \rho(r)V(r)dv .$$ (4)

The Hamiltonian $\hat{H}_Q$ of the quadrupolar interaction is [103, 107]

$$\hat{H}_Q = \frac{e^2qQ}{4I(2I-1)}[3I_z - I(I+1)](\frac{3\cos^2\beta - 1}{2} + \frac{\eta}{2}\sin^2\beta\cos 2\alpha),$$ (5)

with z-component $V_{zz} = eq$ of the electric field gradient, the asymmetry parameter

$$\eta = \frac{V_{xx} - V_{yy}}{V_{zz}},$$ (6)

and the Euler angles α and β [103, 107]. The quadrupole coupling constant C_{qcc} is given by

$$C_{qcc} = \frac{e^2qQ}{h},$$ (7)

and the quadrupole frequency is defined by

$$v_Q = \frac{3e^2qQ}{2I(2I-1)h} = \frac{3C_{qcc}}{2I(2I-1)}.$$ (8)

If $\hat{H}_Q \ll \hat{H}_0$, the quadrupolar interaction can be treated as a perturbation. The first-order perturbation energy E_m^1 is described by [103, 107]

$$E_m^1 = \frac{\pi}{3} v_Q (3\cos^2 \beta - 1)[3m^2 - I(I+1)]. \tag{9}$$

The energy difference between the states m-1 and m is given by [103, 107]

$$\Delta E = E_0 + \pi v_Q (3\cos^2 \beta - 1)(1 - 2m). \tag{10}$$

Therefore, the line broadening caused by first-order quadrupolar interaction can be eliminated, if the MAS technique is applied $((3\cos^2\beta - 1) = 0)$.

In the laboratory frame and in the case of the central transition (m = -1/2 to +1/2), the second-order frequency function is given by [107]

$$v_{-1/2,1/2}^2 = -\frac{v_Q^2}{6v_0}[I(I+1) - \frac{3}{4}](A\cos^4 \beta + B\cos^2 \beta + C) \tag{11}$$

with

$$A = -\frac{27}{8} - \frac{9}{4}\eta\cos 2\alpha - \frac{3}{8}\eta^2 \cos^2 2\alpha ,$$

$$B = +\frac{15}{4} - \frac{1}{2}\eta^2 + 2\eta\cos 2\alpha + \frac{3}{4}\eta^2 \cos^2 2\alpha ,$$

$$C = -\frac{3}{8} + \frac{1}{3}\eta^2 + \frac{1}{4}\eta\cos 2\alpha - \frac{3}{8}\eta^2 \cos^2 2\alpha .$$

If $\eta = 0$, this equation leads to

$$v_{-1/2,1/2}^2 = -\frac{v_Q^2}{16v_0}[I(I+1) - \frac{3}{4}](-9\cos^4 \beta + 10\cos^2 \beta - 1). \tag{12}$$

Equation (11) allows the calculation of the field-dependent second-order quadrupolar frequency shift, v_{qs}, of the center of gravity, v_{cg}, of the central transition in comparison with the resonance position observed without quadrupolar interaction [106]

$$v_{qs} = v_{cg} - v_0(1-\sigma) = -\left[\frac{I(I+1) - 3/4}{30}\right]\frac{v_Q^2}{v_0}(1 + \frac{1}{3}\eta^2). \tag{13}$$

The complete suppression of the influence of the second-order quadrupole broadening requires the application of the double-oriented rotation (DOR) [108-110] or the dynamic angle spinning (DAS) technique [111, 112]. In 1995, a two-dimensional NMR technique, the multiple-quantum magic angle spinning (MQMAS) NMR, was introduced to record high-resolution solid-state NMR spectra of nuclei with nuclear spin $I > 1/2$. This technique is introduced in Chapter 5.

5.   Experimental Part

5.1   Preparation of Zeolite H,Na-Y

An amount of 100 g zeolite Na-Y (n_{Si}/n_{Al} = 2.7) delivered by Degussa AG, Hanau, Germany, was six-fold exchanged in an 1.0 M aqueous solution of NH_4NO_3 at 353 K for 12 h. The obtained zeolite NH_4-Y was washed by demineralized water until no nitrate ions were detected any more. Subsequently, the powder material was dried in air at 353 K for 12 h. After this treatment, a cation-exchange degree of 93.3 % was reached as determined by inductively coupled plasma atomic emission spectroscopy (AES-ICP, Perkin Elmer Plasma 400). X-ray diffraction (Siemens D5000, CuK$_\alpha$ radiation) was applied to exclude framework defects and extra-framework aluminum in the obtained zeolite NH_4,Na-Y. It is clear from Figure 5.1 that the crystallinity is well persevered after the ion-exchange treatment.
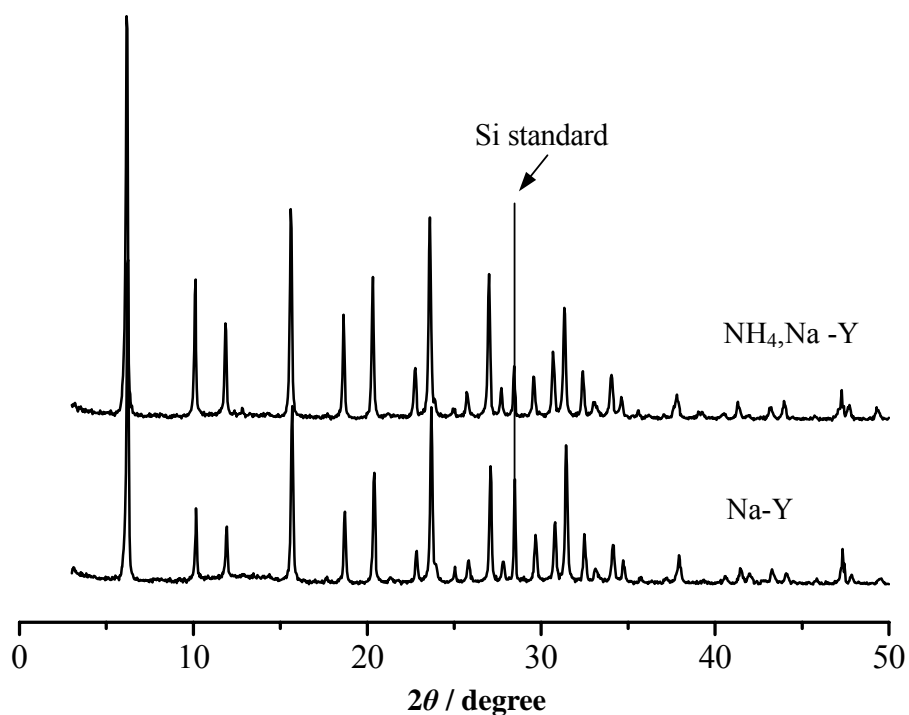
Figure 5.1 XRD patterns of zeolites Na-Y and NH_4,Na-Y acquired on a Siemens D5000 equipment using CuK$_\alpha$ radiation.

5.2   Steaming of Zeolite H,Na-Y

5.2.1   Steaming Technique

The dealumination set-up is shown in Figure 5.2. This set-up can be separated into three parts: the water vapor generator, the dealumination reactor, and the air-lock. The water vapor generator mainly consists of a water bath. A flow of dry nitrogen (200 cm^3/min) passes through the water bath and, subsequently, the nitrogen loaded with water vapor is collected by a funnel. The water vapor pressure of the nitrogen is controlled by the temperature of the water bath. The relationship between the vapor pressure and the water temperature is given in Table 5.1. The dealumination takes place in the dealumination reactor, which is connected to the water vapor generator by a valve. This valve is used to switch between dry nitrogen and nitrogen loaded with water vapor. The dealumination reactor is made of quartz glass and can be heated up to 1100 K by an oven. In order to eliminate the effect of hydration of the dealuminated sample, the dealumination reactor connected to an air-lock. Using this design, the non-hydrated samples can be transferred into gas-tight glass containers under dry nitrogen without contacting to air.

Table 5.1 The water vapor pressure $p_{water\ vapor}$ as a function of the temperature of the water bath $T_{water\ bath}$.

$T_{water\ bath}$ / K	299	313	323	333	343	353	363	367
$p_{water\ vapor}$ / kPa	3.4	7.4	12.4	19.9	31.1	47.4	70.1	81.5

5.2.2   Steaming Procedure

In order to study the influence of the temperature and vapor pressure on the dealumination, two series of dealuminated zeolites H,Na-Y under water vapor pressures between 3.4 to 81.5 kPa were prepared at 748 and 813 K. To perform the hydrothermal treatment, ca. 2 g zeolite NH_4,Na-Y (93.3%) are placed in a ship-like crucible in the reactor. Subsequently, the flow of
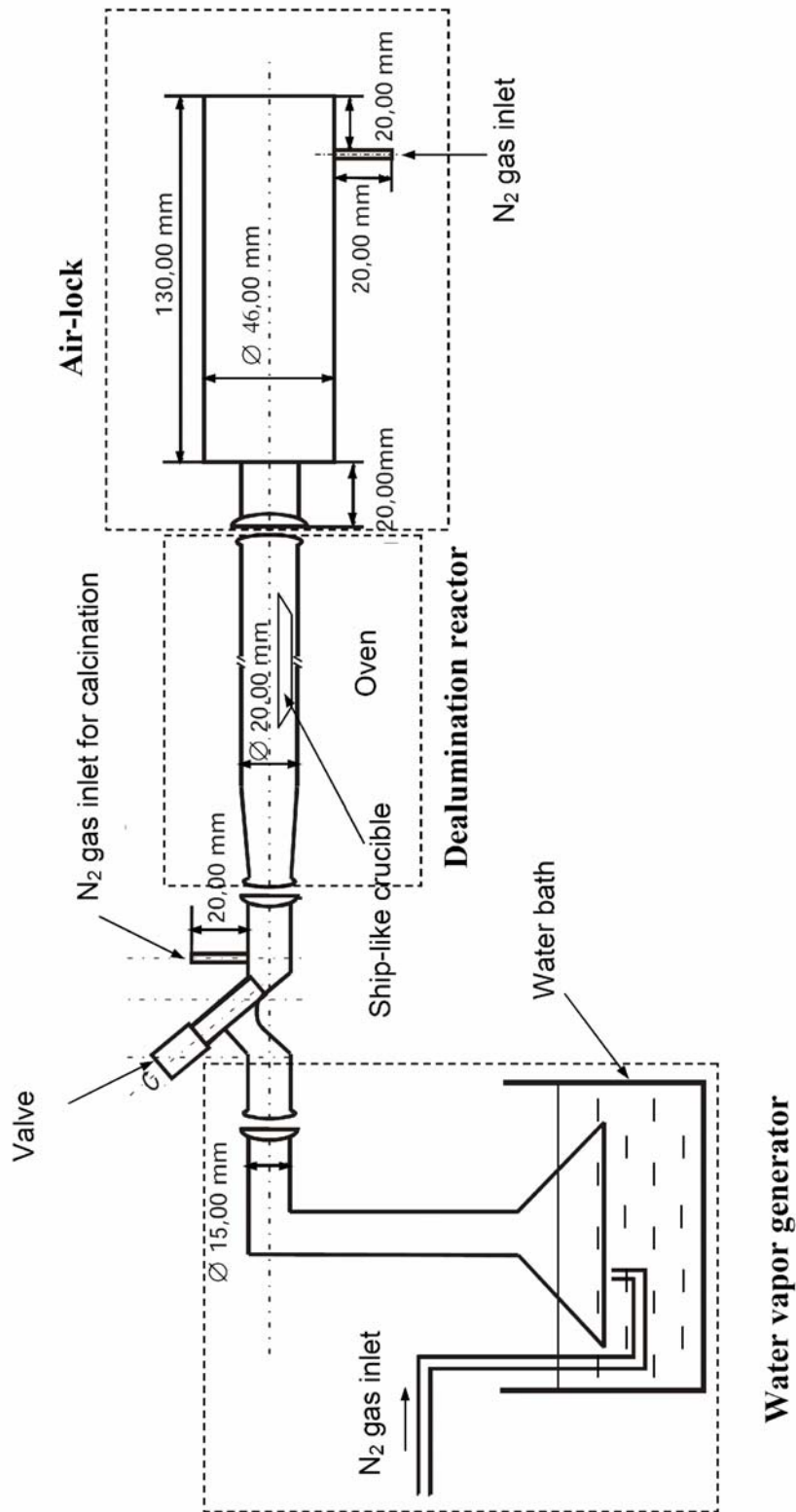
Figure 5.2 Scheme of dealumination set-up.

dry nitrogen (200 cm^3/min) is started, and, the material is heated with a rate of 1.6 K/min up to the dealumination temperature. At this temperature, the calcination is performed for 10 hours. In the present work, the steaming of the zeolite materials was carried out at 748 or 813 K for 2.5 hours after switching from the flow of dry nitrogen to the flow of nitrogen loaded with water vapor. The water vapor pressures of 3.4 to 81.5 kPa can be adjusted via the temperature of water bath according to Table 5.1. After the dealumination, the samples are cooled down to room temperature under dry nitrogen. Subsequently, these materials are filled into the gas-tight glass containers in the air-lock.

Before further investigations, the two series of dealuminated samples were quantitatively evaluated by ^{1}H MAS NMR spectroscopy. The results showed that a weak dealumination of zeolite H,Na-Y already took place during the calcination at 813 K. In addition, a strong dealumination occurred at 813 K even under a very low water vapor pressure. However, ^{1}H MAS NMR spectra of the series of samples dealuminated at 748 K showed a gentle decrease of bridging OH groups with the vapor pressure. This variation is helpful to understand the dealumination procedure. Therefore, in the present work, the series of samples dealuminated at 748 K were investigated in detail. These dealuminated zeolites H,Na-Y are denoted as deH,Na-Y/p, where p is the water vapor pressure.

5.3   NMR Experiments

5.3.1   Magic Angle Spinning Experiments

In Section 4.2, the line broadening interactions in solid materials were introduced. The Hamiltonians of the homonuclear ($\hat{H}_{II}$) and heternuclear ($\hat{H}_{IS}$) magnetic dipole-dipole interaction are described by [45]

$$\hat{H}_{II} = \frac{\mu_0}{4\pi}\sum_{i \neq k}\frac{\gamma_I^2\hbar^2}{r_{ik}^3}(\frac{1-3\cos^2\theta_{i,k}}{2})(3I_{z,i}I_{z,k}-I_iI_k) \tag{14}$$

and

$$\hat{H}_{IS} = \frac{\mu_0}{4\pi} \sum_k \frac{\gamma_I \gamma_S \hbar^2}{r_{ik}^3} \left(\frac{1 - 3\cos^2 \theta_{i,k}}{2}\right)(2I_{z,i} I_{z,k}) \tag{15}$$

respectively, where μ_0 is the permeability of vacuum, r_{ik} is the distance between two nuclei, and $\theta_{i,k}$ is the angle between $\boldsymbol{r}_{ik}$ and the direction of the external magnetic field $\boldsymbol{B}_0$. In liquids, the dipolar interaction is averaged by the isotropic reorientation of molecules [113].

If the sample rotates around an axis inclined by an angle χ to the external magnetic field $\boldsymbol{B}_0$, the angle θ varies periodically (shown Figure 5.3). The running angle of rotation is denoted by φ. The relationship between $\cos\theta$ and φ can be obtained from a spherical triangle formed by the directions of $\boldsymbol{B}_0$, the spin-spin vector $\boldsymbol{r}$, and the axis of rotation (Figure 5.3). Application of the 'cosine theorem' of spherical trigonometry gives [113]

$$\cos \theta = \cos \phi \cos \chi + \sin \chi \sin \varphi \tag{16}$$

According to Equation (16), the term $(3\cos^2\theta - 1)$ can be expressed by [113]

$$3\cos^2 \theta - 1 = \frac{1}{2}(3\cos^2 \chi - 1)(3\cos^2 \phi - 1) + \frac{3}{2}\sin^2 \chi \sin^2 \phi \cos 2\varphi \tag{17}$$

The angles α and β are constant and only the angle φ is time depended. The mean value of the functions of φ is zero ($\overline{\cos 2\varphi} = 0$ and $\overline{\cos\varphi} = 0$). Therefore, Equation (17) leads to [113]

$$\overline{3\cos^2 \theta - 1} = \frac{1}{2}(3\cos^2 \chi - 1)(3\cos^2 \phi - 1). \tag{18}$$

If the angle χ between the axis of rotation and the direction of the magnetic field is equal to 54°44′ (the magic angle), Equation (18) vanishes independently of the value of ϕ.
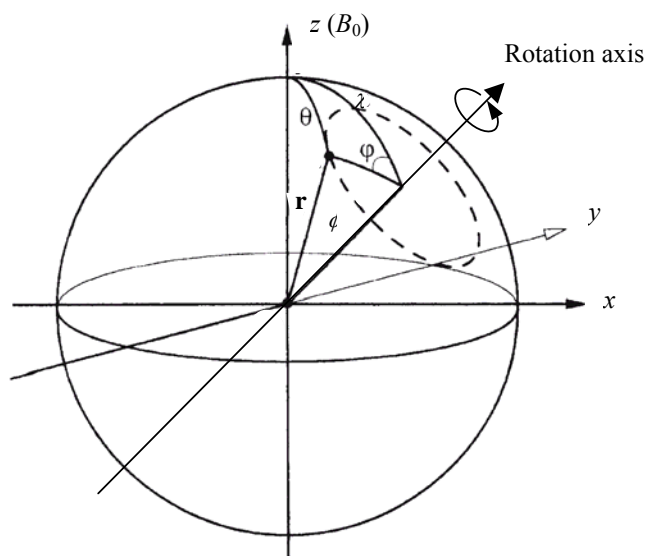
Figure 5.3 Scheme of sample rotation under the magic angle. Explanation of the parameters sees the text [113].

Magic angle spinning (MAS) leads to a MAS NMR spectrum consisting of a narrow central line at the center of gravity, ν_{cg}, and spinning sidebands at the frequencies $\nu_k = \nu_{cg} + k\nu_{rot}$, where $k = \pm1, \pm2,\ldots$ denotes the order of the spinning sideband and ν_{rot} is the sample spinning rate [106]. The influence of the magic angle spinning technique on a typical solid-state NMR signal of a spin $I = 1/2$ nucleus is demonstrated in Figure 5.4. In some cases, the evaluation of the spinning sidebands may be useful since their intensities contain information about the chemical shift anisotropy [114].

5.3.2   Spin-echo Experiments

The spin-echo technique is suitable to investigate non-integer spins $I > 1/2$ with strong quadrupolar interactions [103, 115-117]. The quadrupolar interaction strongly influences the formation of an echo, due to an incomplete refocusing and limited excitation [103]. The Hamiltonian of a radio frequency (rf) pulse along the x axis (a x pulse) can be described by [103]

$$\hat{H}_{rf} = \hbar\omega_1 \cos(\omega t)I_x \tag{19}$$
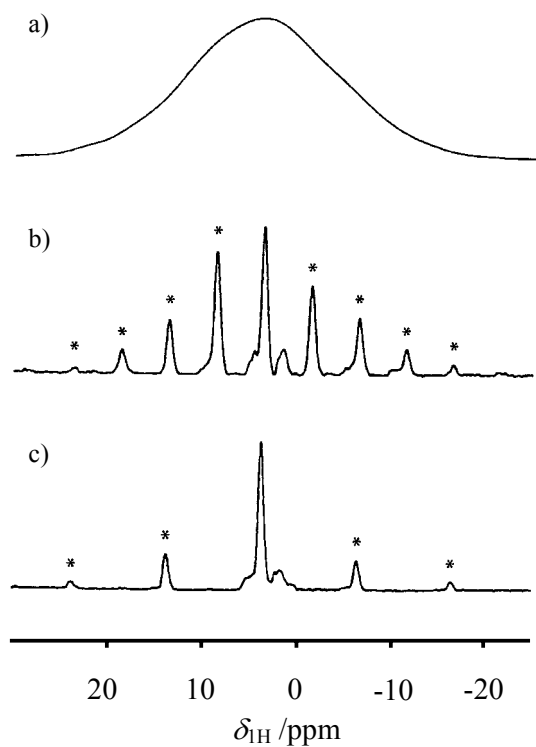
Figure 5.4 The influence of the magic angle spinning technique on the ^{1}H NMR spectrum of non-hydrated zeolite H,Na-Y recorded at a resonance frequency of 500 MHz [106]. Spectrum (a) is measured without spinning. Spectra (b) and (c) are recorded at spinning rates of 2.5 kHz, and 5.0 kHz, respectively.

with the nutation frequency $\omega_1 = \gamma B_1$. Generally, the pulse length t_p is given by

$$t_p = \frac{\alpha}{\omega_1} = \frac{\alpha}{\gamma B_1} \tag{20}$$

with the nutation angle α. The frequency range Δv, which is excited by a pulse with the length t_p, amounts to

$$\Delta v \approx 1/(\pi \times t_p). \tag{21}$$

According to Equation (21), the pulse length can be estimated if the Δv is known. For the

quadrupolar interaction causing broad frequency distribution functions, following cases have to be distinguished

$$\omega_1 \gg \omega_Q, \tag{22}$$

and

$$\omega_1 \ll \omega_Q, \tag{23}$$

where ω_Q is the quadrupolar frequency. A so-called hard pulse (short duration, high power) leads to a nonselective excitation of whole quadrupolar spectrum if the rf field strength meets the condition of Equation (22). Under the condition of Equation (23), a soft pulse (long duration, low power) causes a selective excitation of single transitions ($m = -I, -I + 1, \ldots, I - 1$) such as the central transition ($m = -1/2$ to $+1/2$) [106]. If the rf pulse fulfilled the condition $\omega_1 \approx \omega_Q$, the degree of excitation depends on ω_1 and ω_Q and the molecular orientation in external magnetic field. In a powder sample, nuclei in equivalent sites may be excited differently in different crystallites. This leads to distorted powder patterns and intensities that are not proportional to the number of nuclear spins corresponding to the different sites.

Haase and Oldfield [115] compared the spin-echo behaviors of quadrupolar nuclei after nonselective and selective excitation. They found that nonselective excitation is difficult to achieve in real systems [115]. They claimed that a selective excitation of the central ($m = -1/2$ to $+1/2$) transition is important for a quantitative experiment and low power levels are required in this case [115].

In the present work, the echo-sequence $(t_{p1})\phi_1$-τ_1- $(t_{p2})\phi_2$-τ_2-$(AQ)\phi_3$ with a 16-step phase cycling was used [117, 118]. The phases of the pulses and receiver were [117]

$$\phi_1 = \quad xxxx \quad yyyy \quad \overline{xxxx} \quad \overline{yyyy}$$

$$\phi_2 = \quad xy\overline{x}\overline{y} \quad xy\overline{x}\overline{y} \quad xy\overline{x}\overline{y} \quad xy\overline{x}\overline{y}$$

$$\phi_3 = \quad \overline{y}\overline{y}yy \quad \overline{x}\overline{x}xx \quad \overline{y}\overline{y}yy \quad \overline{x}\overline{x}xx.$$

$x, y, \bar{x}$, and $\bar{y}$ represent 0°, 90°, 180°, and 270° phase shifts, respectively. The pulse lengths are t_{p1} and t_{p2}. The t_{p1} pulse was typically a $\pi/4$ or $\pi/2$ pulse, and t_{p2} was twice the length of t_{p1}. In the present case, a t_{p1} pulse length of 0.61 μs ($< \pi/12$) and t_{p2} pulse length of 1.22 μs were utilized in ^{27}Al spin-echo NMR experiments, because the broadening of the ^{27}Al NMR signal of non-hydrated zeolites is up to 2.4 MHz [93, 104]. The intervals τ_1 and τ_2 are the delays between the two pulses and the echo. Delays of $\tau_1 = 10$ μs, and $\tau_2 = 9$ μs and a repetition time of 2 s were applied in a typical experiment. It should be noticed that a power of 120 W was used in all spin-echo studies in order to obtain quantitative results [115].

5.3.3 Multiple Quantum Magic Angle Spinning Experiments

The multiple quantum magic angle spinning (MQMAS) technique is a two-dimensional solid-state NMR experiment [12-16, 94, 119-123]. This technique affords high resolution central transition spectra of half-integer quadrupolar nuclei by using both spin and spatial manipulations of the broadening interactions. In Section 5.3.1, it is shown that the MAS technique can average the chemical shift anisotropy and the dipolar interactions. Actually, this technique also can be used to remove the second-rank Legèndre polynomials of the quadrupolar interaction because it includes the term $(3\cos^2\chi - 1)$. In MQMAS experiments, rf pulses are used to manipulate the spin part and average the fourth-rank elements of the second-order quadrupolar Hamiltonian [119].

Under rotation around an axis in angle χ to the direction of the external magnetic field B_0, the evolution phase for symmetric transitions ($p/2 \rightarrow -p/2$, $p = 2m$) can be expressed by [119, 120]

$$\phi_{p/2,-p/2} = v^{CS}pt + v_0^Q C_0(I,m)t + v_2^Q(\alpha,\beta)C_2(I,m)P_2(\cos\chi)t + v_4^Q(\alpha,\beta)C_4(I,m)P_4(\cos\chi)t \tag{24}$$

v^{CS} is the isotropic chemical shift, while v_0^Q, v_2^Q, and v_4^Q are the isotropic (or zero rank),

second-rank, and fourth-rank quadrupolar shift, respectively. It should be noted that v_2^Q and

v_4^Q depend on the Euler angles α and β and are responsible for the line broadening. $C_0(I, m)$,

$C_2(I, m)$, and $C_4(I, m)$ are zero-, second- and fourth-rank spin coefficients

$$C_0(I,m) = 2m[I(I+1) - 3m^2], \tag{25a}$$

$$C_2(I,m) = 2m[8I(I+1) - 12m^2 - 3], \tag{25b}$$

$$C_4(I,m) = 2m[18I(I+1) - 34m^2 - 5]. \tag{25c}$$

which depend on the spin and magnetic quantum numbers [119, 120]. $P_2(\cos\chi)$ and $P_4(\cos\chi)$

are the second- and fourth-order Legèndre polynomials of $\cos\alpha$. These are given by [120]

$$P_2(\cos\chi) = (3\cos^2\chi - 1)/2, \tag{26a}$$
$$P_4(\cos\chi) = (35\cos^4\chi - 30\cos^2\chi + 3)/8. \tag{26b}$$

Under MAS condition ($3\cos^2\chi - 1 = 0$), Equation (24) leads to

$$\phi_{p/2,-p/2} = v^{CS}pt + v_0^Q C_0(I,m)t + v_4^Q(\alpha,\beta)C_4(I,m)P_4(\cos\chi)t. \tag{27}$$

In order to obtain an isotropic spectrum, the second-order quadrupolar broadening

induced by the fourth-rank quadrupolar shift should be averaged to zero. In the MQMAS

experiments shown in Figure 5.5, this is achieved by two different evolution phases,

$\phi_1(m_1,\chi,t_1)$ and $\phi_2(m_2,\chi,t_2)$ under the condition of $C_4(I,m_1)t_1 + C_4(I,m_2)t_2 = 0$. With $p_2 = -1$

(the coherence evolving during t_2 is the observable single-quantum coherence), the

anisotropic second-order quadrupolar broadening is averaged when the ratio of the times t_1

and t_2 spent on quantum levels pQ and -1Q, respectively, fulfils the condition [119]

$$t_2 = -\frac{C_4(I,p)}{C_4(I,-1)}t_1 = p\frac{36I(I+1)-17p^2-10}{36I(I+1)-27}t_1 = R(I,p)t_1. \tag{28}$$

After a two fold Fourier transformation regarding to t_1 and t_2, a two-dimensional spectrum along anisotropic and isotropic axis is obtained.
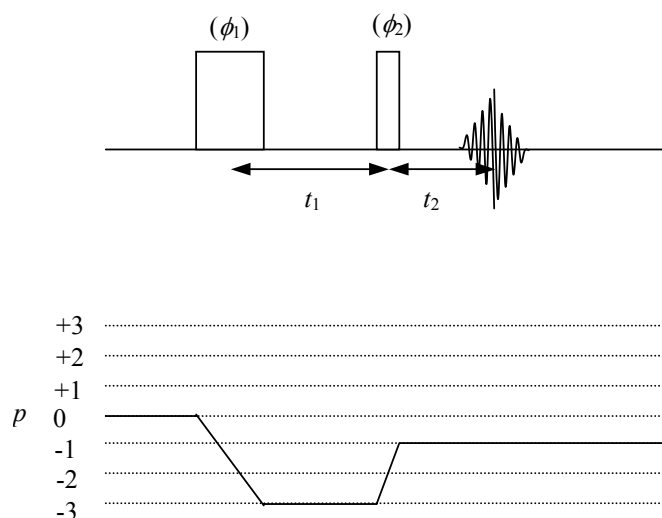
Figure 5.5 Scheme of two-pulse MQMAS NMR experiments (top) and coherence pathways (bottom) [120]. ϕ_1 and ϕ_2 are the phases of the two pulses. The relationship between time of t_1 and t_2 are exhibited in Equation (27).

After the first MQMAS experiments by Harwood *et al.* [123] in 1995, several modifications and improvements of this technique have been performed [121, 122, 124-127]. Fernandez and Amoureux [121, 122, 125] found that the pure adsorption-mode lineshapes are obtained by combining echo and antiecho coherence-transfer pathways. Later on, the MQMAS split-t_1 whole-echo method was adopted by Brown *et al.* [124, 126]. In this method, a split multiple-quantum/single-quantum evolution (t_1) period was used to obtain the complete refocusing of the second-order quadrupolar broadening [124, 126]. Kentgens *et al.* [128, 129] proved that the double frequency sweep (DFS) can be utilized to increase the efficiencies in population and coherence transfer in half-integer quadrupolar spins. The first two-dimension spectrum of non-hydrated zeolite H-ZSM-5 was recorded by DFS-enhanced ^{27}Al MQMAS NMR spectroscopy [94].

In the present work, the split-t_1 whole-echo 3QMAS sequence [126] with DFS was applied (shown in Figure 5.6). Two hard pulses of 3.3 and 13.7 μs (125 kHz) and one soft pulse of 47 μs (10 kHz) were used. The times t_1 and t_2 are the multiple-quantum/single-quantum evolution period and the acquisition period, respectively. t_1 was split into $\dfrac{b}{a+b} t_1$ and $\dfrac{a}{a+b} t_1$, where a and b are constants. For spin $I = 5/2$, $a = 19$ and $b = 12$ should be used [126]. According to investigations performed by Massiot *et al.* [127], the length of τ is a multiple of the rotor period. In comparison with the MQMAS technique introduced by Harwood *et al.* [123], the above-mentioned technique has the advantage that no shearing of 2D spectrum is required. In addition, the DFS technique made the investigation of non-hydrated zeolites with large C_{QCC} values possible. The calculation of isotropic chemical shifts δ_{iso} and *SOQE* values was performed as given Reference [119].
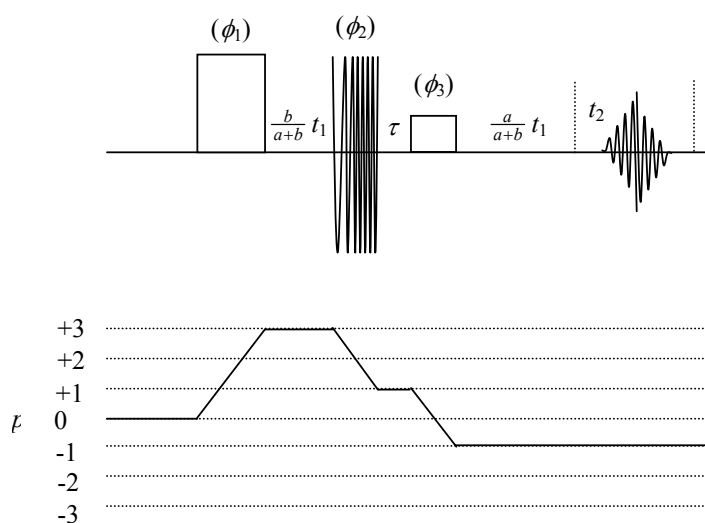
Figure 5.6 Scheme of split-t_1 whole-echo 3QMAS NMR experiments with DFS (top) and coherence pathways (bottom) [126]. Two hard pulses and one soft pulse are applied. t_1 and t_2 are the multiple-quantum/single-quantum evolution period and the acquisition period, respectively. The length of τ should be the multiple of the rotor period. ϕ_1, ϕ_2 and ϕ_3 are the phases of the three pulses given in Reference [127]. For spin $I = 5/2$, the constants a and b are equal to 19 and 12, respectively [126].

5.3.4 *In situ* and *ex situ* **Magic Angle Spinning Experiments**

To characterize the influence of probe molecules on framework and extra-framework

aluminum atoms in dealuminated zeolites, *in situ* and *ex situ* MAS NMR experiments of the adsorption of probe molecules were carried out. Prior to the NMR experiments, the non-hydrated materials were prepared in the following way. The dealuminated samples, storaged in gas-tight glass containers, were transferred into glass tubes under dry nitrogen gas in a glove box. An additional evacuation is performed at a pressure of $p \leq 1.5$ Pa for 12 h at 723 K. For *ex situ* NMR experiments, these materials were loaded with probe molecules using a vacuum line until the saturation was reached. Subsequently, these glass tubes were sealed. Before the NMR measurements, the non-hydrated powder materials loaded with probe molecules were filled into MAS NMR rotors under dry nitrogen in a glove box.

The *in situ* MAS NMR probe was built using a commercial Bruker double-bearing 4 mm MAS probe (Figure 5.7) [130]. A saturator, which is cooled to 285 K by a cryostat, is used to load the carrier gas with the adsorbate (Figure 5.7a). The flow of carrier gas is adjusted by the mass flow controller. The carrier gas loaded with adsorbate molecules is injected into the rotor via an injection tube (Figure 5.7b). This injection tube is fixed on the top of the turbine and is inserted into the rotor through a hole in the cap as shown in Figure 5.7b. An additional tube is used to purge the top of the turbine to avoid a rehydration of the non-hydrated sample (Figure 5.7b). The carrier gas loaded with adsorbate molecules flows inside the rotor from the bottom to the top of catalyst bed and leaves the rotor via an annular gap in the cap (Figure 5.7c).

Before the *in situ* NMR investigations, the non-hydrated catalyst is filled into a 4 mm rotor under the dry nitrogen in a glove box and is carefully shaped to a cylindrical catalyst bed by a special tool. The rotor is closed by a cap with hole, which is blocked by a plug. Subsequently, this rotor with cap is transferred into the turbine. At the same time, the purging gas on the top of turbine is started. The plug on the cap is removed and the injection tube is quickly inserted into the rotor. Afterwards, the regular MAS NMR experiment can be performed.

For quantitative ^{1}H MAS NMR measurements, a non-hydrated zeolite H,Na-Y with an

ammonium exchange degree of 35 % was used as an external intensity standard. A fully hydrated zeolite NH_4-Y was used as the external intensity standard for all quantitative ^{27}Al MAS NMR investigations. The repetition times of the experiments were chosen in such a way that all nuclei (^{1}H, ^{27}Al, and ^{29}Si) under study could be detected with the correct intensities. Table 5.2 gives a summery of longitudinal relaxation times, which were determined for characteristic samples with different pretreatments. Comparison of the total intensities of the standard sample and the samples under study ensured that no invisible ^{27}Al nuclei effected the quantitative evaluation.

Table 5.2 The longitudinal relaxation times T_1 of ^{1}H, ^{27}Al, and ^{29}Si nuclei in characteristic non-hydrated samples.

Nuclei	Samples or species	Longitudinal Relaxation Time T_1
^{1}H	Bridging OH groups	6.5 s
	SiOH groups	2 s
^{27}Al	Non-hydrated H,Na-Y	0.6 s
	Non-hydrated deH,Na-Y/7.4	0.5 s
	Non-hydrated deH,Na-Y/47.4	0.2 s
	Non-hydrated deH,Na-Y/81.5	0.1 s
	Non-hydrated Al,Na-Y/723	0.15 s
	Non-hydrated Na-Y	0.06 s
^{29}Si	Non-hydrated H,Na-Y	188 s
	Non-hydrated H,Na-Y loaded with oxygen (0.2 bar)	16 s

In Reference [134], it is shown that the intensities of ^{27}Al MAS NMR signals depend on the quadrupole frequency ν_Q (Section 4.2), the resonance frequency ν_0, the sample spinning frequency ν_{rot}, and the asymmetry parameter η. For aluminum species with similar ν_Q and η values, the same intensities of the isotropic line in different ^{27}Al MAS NMR spectra are achieved if the same resonance frequency ν_0 and spinning frequency ν_{rot} were used [134]. This approves the feasibility of quantitative evaluations of *in situ* ^{27}Al MAS NMR experiments in the moderate magnetic field of $B_0 = 9.4$ T. However, to perform reasonable quantitative ^{27}Al MAS NMR studies of nuclei with different ν_Q and η values, a high sample spinning frequency ν_{rot} and a high resonance frequency ν_0 are required [134]. Hence, a sample

spinning frequency of 30 kHz and a magnetic field of $B_0 = 17.6$ T were used in our quantitative investigations of both framework and extra-framework aluminum species by ^{27}Al NMR MAS spectroscopy.
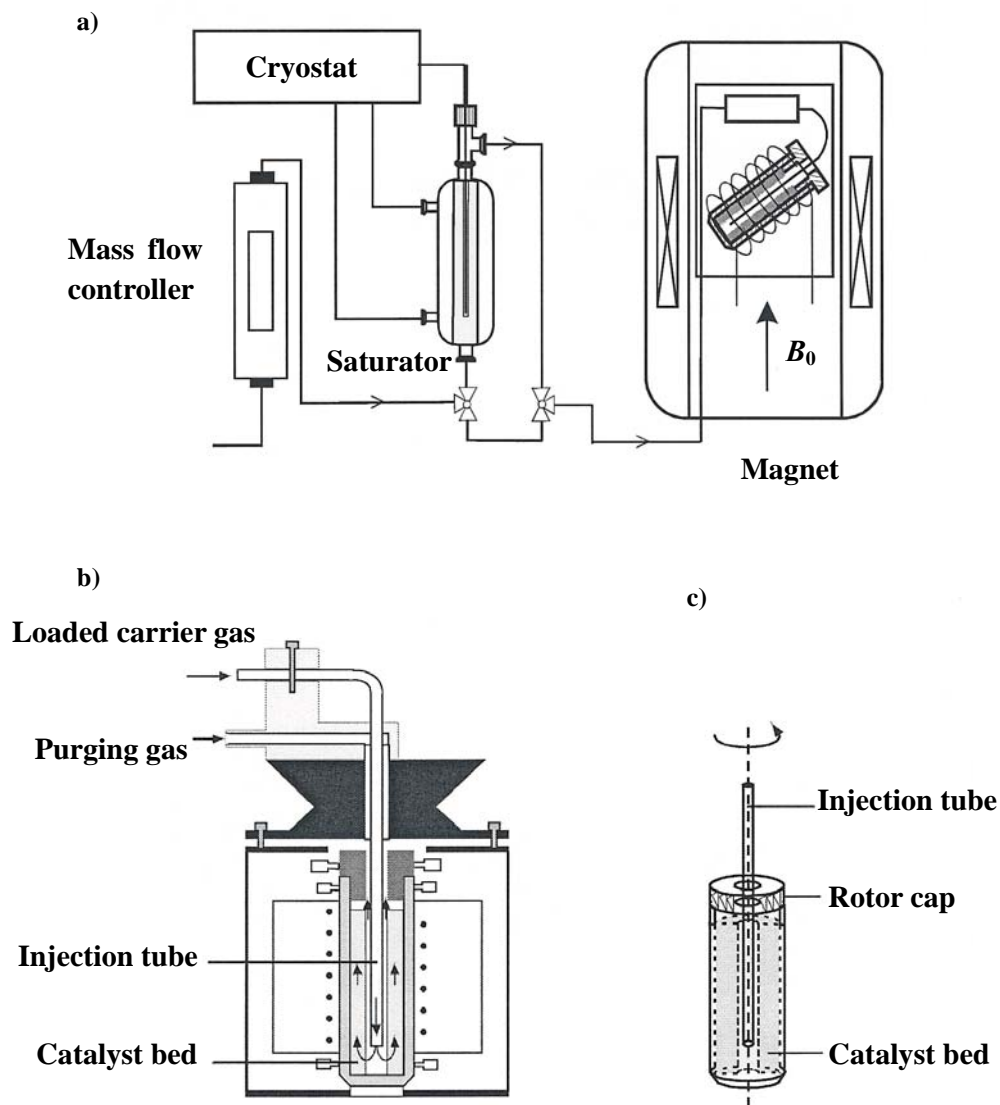
Figure 5.7 *In situ* MAS NMR probe (a) for investigations of non-hydrated solid-state catalyst [130]. The designs of the turbine and the MAS rotor are shown in (b) and (c), respectively.

6.   Characterization of Framework and Extra-framework Aluminum in Hydrated Zeolites Y by Solid-state NMR Spectroscopy

6.1   Introduction

Recent solid-state NMR investigations of acidic zeolites pretreated by steaming indicated that a coordination change of aluminum atoms from a tetrahedral (Al^{IV}) to an octahedral (Al^{VI}) coordination is not always accompanied by a dealumination of the framework [14, 131]. While the ^{27}Al MAS NMR spectra of dealuminated zeolites consist of signals at ca. 0 ppm due to octahedrally coordinated aluminum atoms, which were often assigned to extra-framework aluminum species, an adsorption of a strong base (ammonia, pyridine) leads to a partial transformation of Al^{VI} to Al^{IV} species [14, 131]. In the work of Wouters *et al.* [14], it was found an agreement between the framework n_{Si}/n_{Al} ratios of dealuminated zeolites H,Na-Y determined by ^{27}Al MAS NMR and ^{29}Si MAS NMR spectroscopy only upon adsorption of ammonia. This indicates that octahedrally coordinated aluminum species may be formed in the zeolite framework, which is caused by an additional coordination of water molecules or an additional bonding of OH groups. In this case, most of the Al-O-Si bonds in the local structure of the octahedrally coordinated aluminum atoms remain unchanged. Therefore, ^{29}Si MAS NMR spectroscopy detects these aluminum species as framework atoms, while in the ^{27}Al MAS NMR spectra of hydrated samples a signal of octahedrally coordinated aluminum atoms occurs.

By Woolery and coworkers [132], it was assumed a calcination-induced transformation of SiOHAl groups to threefold-coordinated, Lewis acidic framework aluminum atoms (Al^{III}) with neighboring silanol groups (SiOH). Upon hydration of the zeolite, the above-mentioned threefold-coordinated aluminum atoms are transformed to octahedrally coordinated framework species causing a ^{27}Al MAS NMR signal at ca. 0 ppm. Moreover, the adsorption of ammonia on the calcined material leads to a coordination of this strong base at the Al^{III} atoms resulting in a healing of the Si-O-Al bridges and the formation of ammonium ions. The transformation of the framework Al^{III} atoms to Al^{IV} atoms and a subsequent

hydration of the material cause an increase of the ^{27}Al NMR signal at ca. 60 ppm. At variance to Woolery *et al.* [132], Wouters *et al.* [14, 15] proposed a partial hydrolysis of framework Al-O bonds and a generation of framework-connected AlOH groups. In a second step, these framework AlOH groups host water molecules giving rise to octahedrally coordinated framework aluminum species. A subsequent adsorption of ammonia on the material converts these Al^{VI} atoms back to Al^{IV} atoms.

It was the aim of the present work to investigate the influence of water on the framework and extra-framework aluminum species in dealuminated zeolites H,Na-Y and to reconsider the above-mentioned models of a reversible coordination change of framework aluminum atoms. In addition, the limitation of hydrated sample for the investigation of the dealumination mechanism and the nature of framework and extra-framework aluminum species should be clarified. For these purposes, a homologous series of dealuminated zeolites deH,Na-Y/p was prepared under different vapor pressures (p) as described in Section 5.2.2. Before the investigations by ^{29}Si and ^{27}Al NMR spectroscopy, a total rehydration (R) was performed and these samples were denoted H,Na-Y(R) or deH,Na-Y/p(R). Before recording of ^{1}H MAS NMR spectra, a dehydration of the samples was carried out in vacuum ($p \leq 1.5$ Pa) at 723 K for 12 h. Ammonia was absorbed on the dehydrated materials at a partial pressure of 5 kPa at room temperature for 1.5 h.

Modern techniques of solid-state NMR spectroscopy, such as ^{27}Al MQMAS NMR [133, 134] and high-field ^{27}Al MAS NMR spectroscopy, were applied to study the aluminum distribution. ^{27}Al MQMAS NMR experiments were performed on a Bruker Avance 500WB spectrometer at a resonance frequency of 130.32 MHz using the three-pulse z-filter pulse sequence introduced by Amoureux *et al.* [133]. Pulse lengths of 3.9, 1.3, and 20.0 μs, a repetition time of 300 ms, and a 4 mm MAS NMR rotor with a sample spinning rate of 12.5 kHz were used. High-field ^{27}Al MAS NMR spectra were recorded on a Bruker Avance 750WB spectrometer at a resonance frequency of 195.43 MHz after a single-pulse excitation of 1.4 μs, a repetition time of 0.5 s, and using a 4 mm MAS NMR rotor with a sample spinning rate of 12 kHz.

The ^{29}Si and ^{1}H MAS NMR measurements were performed on a Bruker MSL 400 spectrometer at resonance frequencies of 79.46 and 400.13 MHz, respectively. ^{29}Si MAS NMR spectra were recorded after a single-pulse excitation of 3.5 μs, high-power proton decoupling, a repetition time of 10 s, and using a 7 mm MAS NMR rotor with a sample spinning rate of 3.5 kHz. The ^{1}H MAS NMR spectra were obtained after a single-pulse excitation of 2.1 μs, a repetition time of 30 s, and using a 4 mm MAS NMR rotor with a sample spinning rate of 10 kHz.

## 6.2   Investigation of the Framework of Dealuminated Zeolites H,Na-Y

For the determination of the framework compositions of zeolites deH,Na-Y/p, ^{29}Si MAS NMR spectroscopy was applied. In Table 6.1, a survey on some of the most characteristic samples of the above-mentioned series of zeolites deH,Na-Y is given. The ^{29}Si MAS NMR spectra (not shown) of the hydrated zeolites deH,Na-Y/p under study consist of well resolved signals of Si(nAl) species with $n = 0$ to 4, which allow the calculation of the framework n_{Si}/n_{Al} ratios given in column 2. According to these values, the dealumination of zeolite Y caused an increase in the framework n_{Si}/n_{Al} ratio from 2.7 to 5.2.

Since the steaming procedure applied in the present work does not change the total aluminum content in the zeolite materials, which is evidenced by atomic emission spectroscopy (AES-ICP, Perkin Elmer Plasma 400), the difference between the amounts of framework aluminum atoms in the parent sample and in the dealuminated samples gives the amount of extra-framework aluminum atoms in the steamed materials. A direct investigation of the distribution of aluminum atoms in the dealuminated and rehydrated samples was performed by two-dimensional (2D) ^{27}Al MQMAS NMR and one-dimensional (1D) high-field ^{27}Al MAS NMR spectroscopy. As an example, Figure 6.1 shows the 2D ^{27}Al MQMAS NMR spectra of rehydrated zeolites deH-Y/47.4(R) (a) and deH-Y/94.3(R) (b). Two signals Al^{IVa} and Al^{IVb} of tetrahedrally coordinated aluminum species and up to three different signals Al^{VIa}, Al^{VIb}, and Al^{VIc} of octahedrally coordinated aluminum species can be observed.

The isotropic chemical shifts, δ_{iso}, and the second-order quadrupolar effect parameters, *SOQE*, of these signals are given in Table 6.2. The parameter *SOQE* depends on the quadrupolar coupling constant, C_{QCC}, in the following manner: $SOQE = C_{QCC} \cdot (1 + \eta^2/3)^{-1/2}$, where η is the asymmetry parameter. Generally, the asymmetry parameter covers a range of $0 \leq \eta \leq 1$, but has often values of $\eta = 0.3$ to 0.6 in the case of framework aluminum atoms in zeolites [103]. Hence, the values of *SOQE* and C_{QCC} deviate by maximum 10 %, which is in the order of the experimental accuracy. The data given in Table 6.2 are an important prerequisite for the simulation of the 1D ^{27}Al MAS NMR spectra, which are often complicated by overlapping signals in the chemical shift range of signals due to Al^{IV} and Al^{VI} species. Since the 2D MQMAS NMR technique is limited in the quantitative evaluation of the signal intensities, the 1D MAS NMR technique is used for the quantitative determination of the aluminum distribution in the dealuminated and rehydrated zeolites deH,Na-Y(R).

Table 6.1 Framework n_{Si}/n_{Al} ratios of dealuminated and rehydrated zeolites deH,Na-Y(R) determined by ^{29}Si MAS NMR spectroscopy and high-field ^{27}Al MAS NMR spectroscopy (experimental accuracy of ± 5 %) [135].

| Sample	^{29}Si MAS NMR		^{27}Al MAS NMR
	n_{Si}/n_{Al}	n_{Al} / u.c.	n_{Al} / u.c.
NH$_4$,Na-Y	2.7	51.8	52.0
deH,Na-Y/7.4(R)	2.9	49.4	39.5
deH,Na-Y/47.4(R)	3.5	42.9	37.7
deH,Na-Y/94,3 (R)	5.2	31.0	27.3
deH,Na-Y/7.4 ammonia-treated	3.0	48.2	47.6
deH,Na-Y/47.4 ammonia-treated	3.6	41.9	44.1
deH,Na-Y/94,3 ammonia-treated	4.7	33.8	33.3
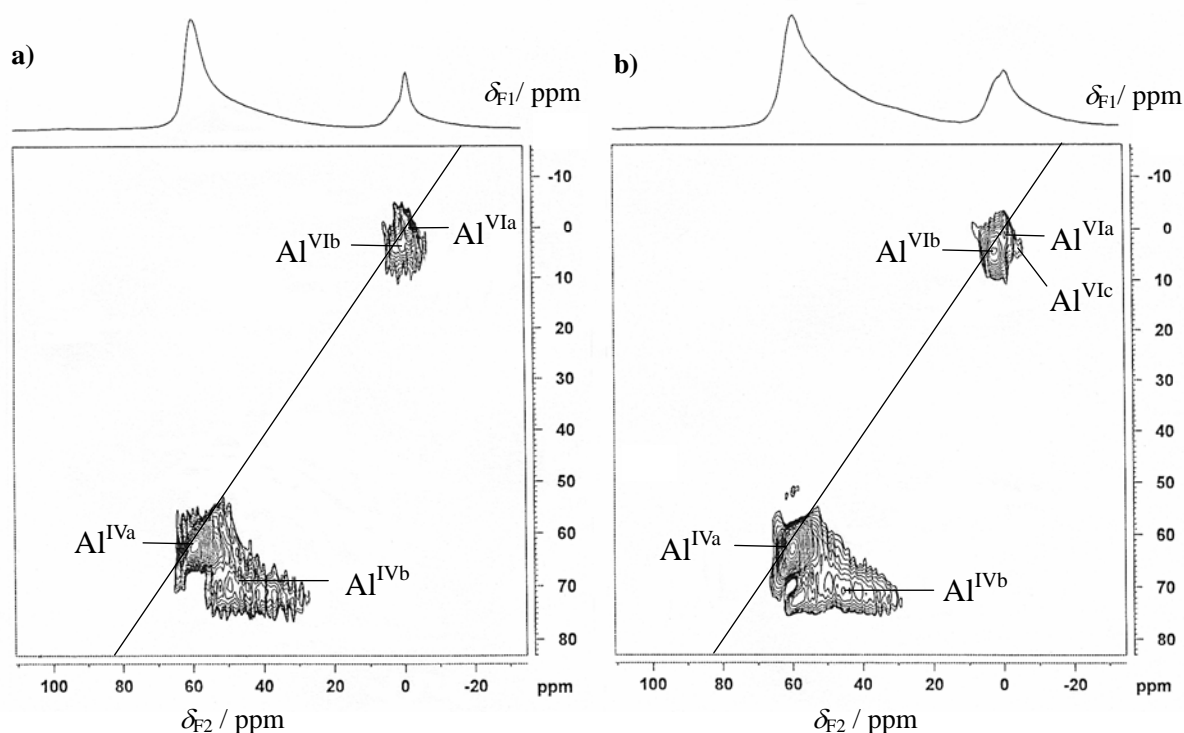
Figure 6.1 ^{27}Al MQMAS NMR spectra of the dealuminated and rehydrated zeolites deH-Y/47.4(R) (a) and deH-Y/94.3(R) (b) with framework n_{Si}/n_{Al} ratios of 3.5 and 5.2, respectively, recorded with a three-pulse z-filter pulse sequence at a resonance frequency of 130.3 MHz [135].

Table 6.2 Isotropic chemical shift δ_{iso} and second-order quadrupolar effect parameter *SOQE* of the ^{27}Al MQMAS NMR signals of dealuminated and rehydrated zeolites deH,Na-Y(R) [135]. The evaluation of the spectra was performed according to the method described in Reference [136].

Signal	Al^{VIa}	Al^{VIb}	Al^{VIc}	Al^{IVa}	Al^{IVb}
δ_{iso} / ppm	0	5	0	62	61
SOQE / MHz	<2.2	2.8	5.1	2.2	6.7

The 1D ^{27}Al MAS NMR spectra of zeolites deH,Na-Y(R) in Figure 6.2 are in good agreement with the signals and spectroscopic parameters found by the 2D ^{27}Al MQMAS NMR experiments. The signal Al^{IVa} corresponds to tetrahedrally coordinated framework aluminum atoms as occurring in the spectra of the parent zeolite Na-Y. The signal Al^{IVb} occurs with increasing dealumination of zeolite H,Na-Y, which indicates that these tetrahedrally coordinated aluminum species are located in the vicinity of framework defects or, as proposed

by van Bokhoven *et al.* [99], in the vicinity of highly charged extra-framework aluminum species. According to these authors, these highly charged extra-framework aluminum atoms correspond to Al^{VI} species characterized by a quadrupolar coupling constant, C_{QCC}, of 2-3 MHz (signals Al^{VIa} and Al^{VIb}). In addition, van Bokhoven *et al.* [99] found that Al^{VI} species characterized by a quadrupolar coupling constant of $C_{QCC} \approx 5$ MHz (signal Al^{VIc}) can be washed out.
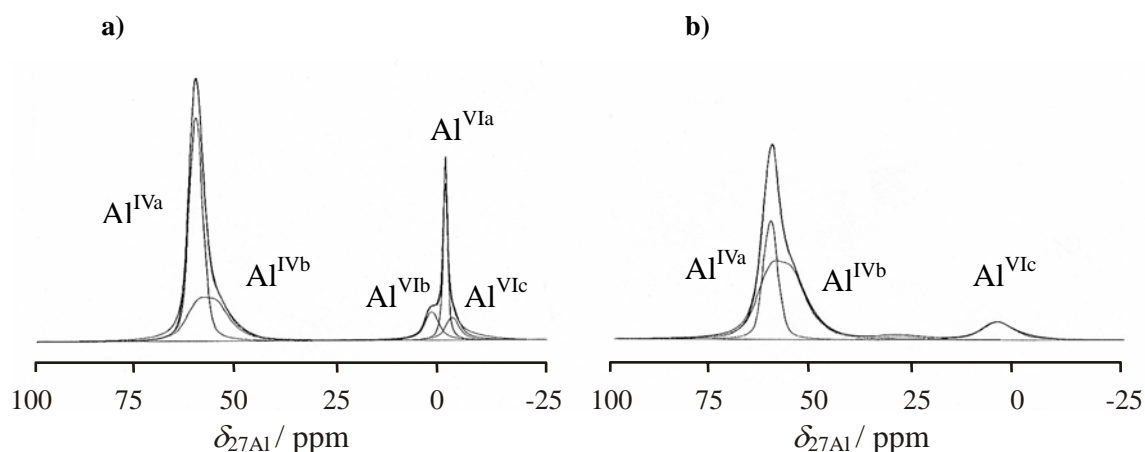
Figure 6.2 ^{27}Al MAS NMR spectra of the dealuminated and rehydrated zeolites deH,Na-Y/47.4(R) recorded before (a) and after (b) ammonia treatment [168]. The spectra were obtained at a resonance frequency of 195.4 MHz.

The quantitative evaluation of the 1D ^{27}Al MAS NMR spectra yielded the amount of framework aluminum atoms (signals Al^{IVa} and Al^{IVb}) per unit cell given in column 4 of Table 6.1. A comparison of these values with the amount of framework aluminum atoms obtained by ^{29}Si MAS NMR spectroscopy (column 3 in Table 6.1) shows a systematic difference. In agreement with the studies of Wouters *et al.* [14, 15], an ammoniation of the dealuminated zeolites deH,Na-Y, before the 1D ^{27}Al MAS NMR measurements are preformed, leads to amounts of tetrahedrally coordinated framework aluminum atoms equal to those determined by ^{29}Si MAS NMR spectroscopy (compare columns 3 and 5 in Table 6.1). Up to ca. 10 aluminum atoms per unit cell changed their coordination from an octahedral to a tetrahedral one as result of adsorption of ammonia. Interestingly, no significant change of the amount of framework aluminum atoms, as obtained by ^{29}Si MAS NMR spectroscopy, occurred after the ammoniation of zeolites deH,Na-Y. This finding indicates that the Al^{VI} species involved in the coordination change were at least partially bound via oxygen bridges to framework silicon

atoms before being transformed to Al^{IV} species. This observation supports the presence of octahedrally coordinated aluminum atoms in the framework of the dealuminated and rehydrated zeolites deH,Na-Y.
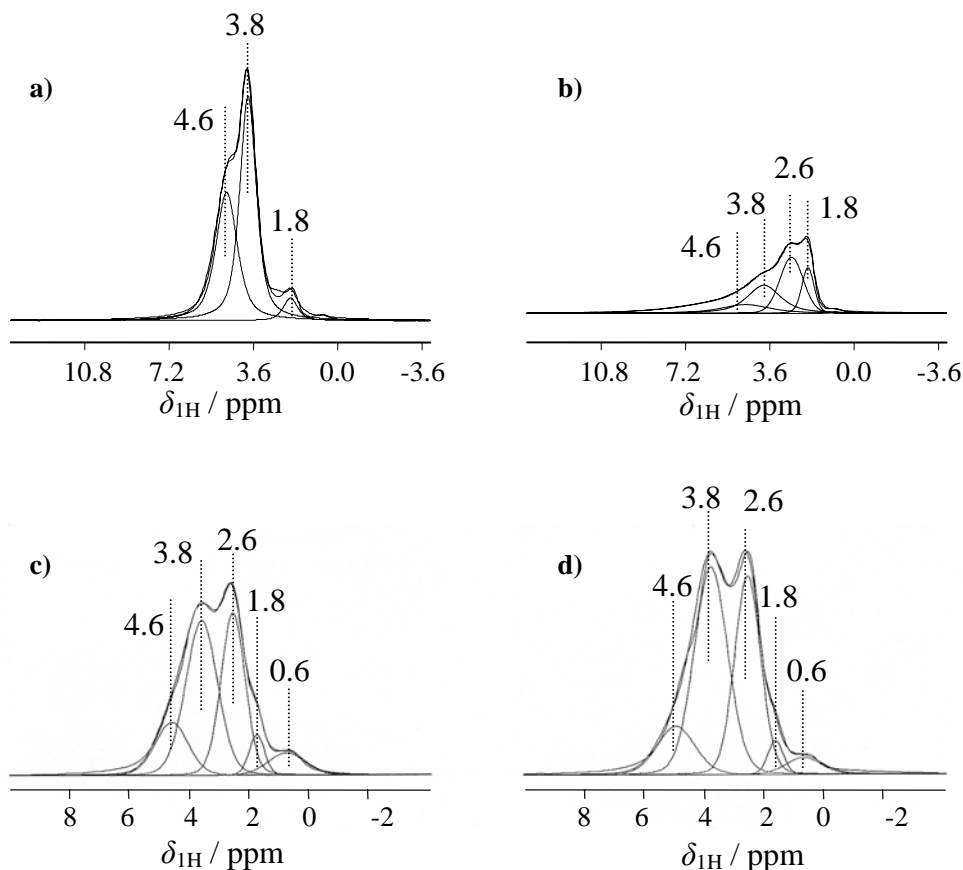
Figure 6.3 ^{1}H MAS NMR spectra of non-hydrated zeolite H,Na-Y (a), zeolites H,Na-Y(R) (b), deH,Na-Y/47.4(R) (c) upon dehydration, and zeolite deH,Na-Y/47.4(R) upon loading with ammonia and thermal deammoniation (d). All spectra were obtained at a resonance frequency of 400.1 MHz.

6.3 Hydroxyl Coverage of Dealuminated Zeolites H,Na-Y

The catalytic activity of zeolites H,Na-Y is caused by bridging hydroxyl protons (SiOHAl) in the vicinity of tetrahedrally coordinated framework aluminum atoms. These bridging OH groups are directly influenced by a coordination change of the neighboring framework aluminum atoms. A suitable method for quantitative investigations of the amount of bridging OH groups is ^{1}H MAS NMR spectroscopy of dehydrated samples. In Figure 6.3a, the ^{1}H MAS NMR spectrum of zeolite H,Na-Y is shown, which was not rehydrated after

dealumination. This spectrum consists of signals due to silanol groups (SiOH) at 1.8 ppm and bridging OH groups in the supercages and sodalite cages at 3.8 and 4.6 ppm, respectively. A quantitative evaluation using an external intensity standard indicates that ca. 46 bridging OH groups per unit cell occur, which agrees with the result of AES-ICP. Figure 6.3b shows the ^{1}H MAS NMR spectrum of dehydrated zeolite H,Na-Y(R), which was rehydrated after dealumination. Five ^{1}H MAS NMR signals appear at 0.6, 1.8, 2.6, 3.8, and 4.6 ppm, which are assigned to isolated AlOH groups, silanol groups, hydrogen-bonded AlOH groups, and bridging OH groups in the supercages and sodalite cages, respectively. After deconvolution, ca. 5 bridging OH groups per unit cell, 2 silanol groups per unit cell, and 5 AlOH groups per unit cell were found. Further XRD and ^{29}Si MAS NMR investigations proved that the framework of this zeolite H,Na-Y was collapsed.

Figure 6.3c and 6.3d shows the ^{1}H MAS NMR spectra of zeolite deH,NaY/47.4(R) in the dehydrated state recorded without and with adsorption of ammonia. The spectra consist of signals at 1.8 ppm, 0.6, 2.6, 3.8 and 4.6 ppm with the above-mentioned assignments. A quantitative evaluation of the spectra yielded the amounts of bridging OH, AlOH, and SiOH groups summarized in columns 2, 3, and 4 of Table 6.3. Interestingly, the adsorption of ammonia on the rehydrated dealuminated materials is accompanied by a significant increase in the amount of bridging OH groups of up to ca. 10 OH/u.c. On the other hand, no systematic change was found for the amount of AlOH groups. In addition, only a weak ammonia-induced decrease of the SiOH groups was observed, which is not in the order of the increase of bridging OH groups.

6.4 Coordination Changes of Aluminum Atoms at Framework Defects in Zeolites H,Na-Y upon Ammonia Adsorption

In the first studies of the reversible coordination change of aluminum atoms in zeolites H-Y, a mechanism according to pathway I in Scheme 6.1 was proposed [132]. A steaming treatment of zeolite H,Na-Y leads to a break of framework Si-O-Al$^-$ bridges and the formation of threefold-coordinated, Lewis acidic framework aluminum atoms with neighboring silanol

groups (structure I_a). Hydration of these Lewis sites results in the formation of octahedrally coordinated aluminum species observed as a ^{27}Al MAS NMR signal at ca. 0 ppm. Adsorption of ammonia on the dehydrated structure I_a causes a coordination of this strong base at the threefold-coordinated aluminum atoms and a subsequent healing of the framework Si-O-Al[-] bridges (structure I_b) [132]. In the hydrated state, the aluminum atoms of the former Lewis sites would now occur as tetrahedrally coordinated aluminum species at a ^{27}Al NMR shift of ca. 60 ppm. Furthermore, after the thermal decomposition of the ammonium ions in structure I_b, bridging OH groups are formed. The mechanism according to pathway I in Scheme 6.1 explains most of the spectroscopically observed effects accompanied by the reversible coordination change of aluminum atoms in zeolites H,Na-Y. However, the model requires a simultaneous change of the amount of silanol groups, which is not supported by the present results.

Table 6.3 Amounts of bridging OH (SiOHAl), aluminum OH (AlOH), and silanol (SiOH) groups in dehydrated zeolites deH,Na-Y(D) as determined by ^{1}H MAS NMR spectroscopy (columns 2, 3 and 4, experimental accuracy of $\pm$ 10 %) [135]. In columns 5 and 6, the amounts of tetrahedrally (Al^{IV}) and octahedrally coordinated (Al^{VI}) aluminum atoms are given, as obtained by high-field ^{27}Al MAS NMR spectroscopy of the hydrated samples [135].

Material	SiOHAl n_{OH} / u.c	AlOH n_{OH} / u.c.	SiOH n_{OH} / u.c.	Al^{IV} n_{Al} / u.c.	Al^{VI} n_{Al} / u.c.
deH,Na-Y/47.4	14.4	12.1	1.5	37.7	14.3
deH,Na-Y/47.4 ammonia-treated	22.8	11.4	1.1	44.1	7.9
deH,Na-Y/94.3	22.5	15.6	2.0	27.3	24.7
deH,Na-Y/94.3 ammonia-treated	33.6	18.4	1.7	33.3	18.7

According to mechanism II of Scheme 6.1, which is proposed in Reference [135] and the present work as an additionally occurring pathway, again a break of the framework Si-O-Al[-] bridges is induced by the steaming treatment. In contrast to structure I_a, however, extra-framework aluminum species coordinate at the SiO[-] defect sites in the vicinity of the threefold-coordinated aluminum atom (structure II_a). After a hydration, structure II_a causes more than one ^{27}Al MAS NMR signal of octahedrally coordinated aluminum atoms, since

also the coordinated extra-framework aluminum species are hydrated. Due to the coordination of extra-framework aluminum species at the SiO⁻ defect sites, these silicon atoms are Q^4 species, which is in agreement with the results of ^1H (no SiOH formation) and ^{29}Si MAS NMR spectroscopy. As discussed for mechanism I, adsorption of ammonia on structure II_a leads to a coordination of this strong base at the threefold-coordinated, Lewis acidic aluminum atoms and healing of the Si-O-Al⁻ bridges (structure II_b). After the thermal decomposition of the ammonium ions, bridging OH groups are formed. Hydration of the extra-framework aluminum species in structure II_b may be accompanied by the formation of further AlOH groups.
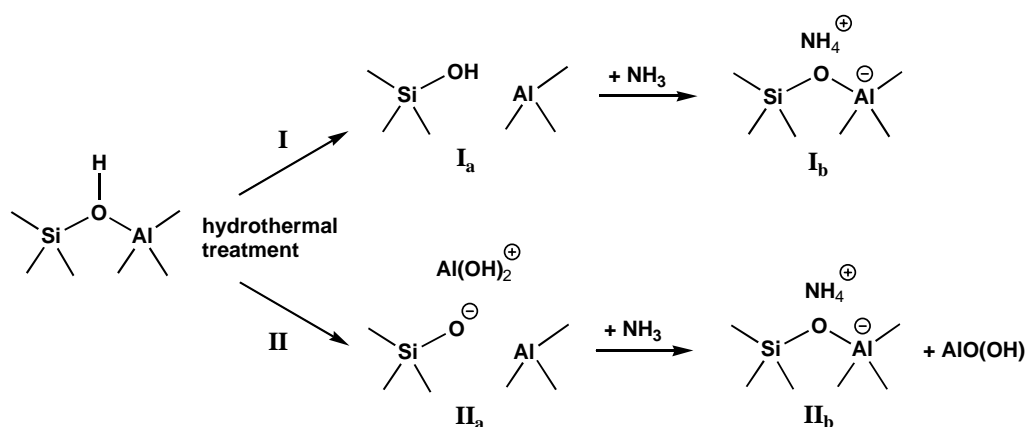
Scheme 6.1

6.5   Conclusions

In this Chapter, a reversible coordination change of aluminum atoms in dealuminated and rehydrated zeolites H,Na-Y from an octahedral (Al^{VI}) to a tetrahedral coordination (Al^{IV}) upon adsorption of ammonia, was found to be accompanied by the formation of bridging OH groups (SiOHAl). On the other hand, only a weak decrease in the amount of SiOH groups and no systematic change of AlOH groups occurred. Based on these experimental results obtained for a series of dealuminated zeolites H,Na-Y, a new mechanism with extra-framework aluminum species coordinated to SiO⁻ defect sites instead of hydroxyl protons is proposed. Upon adsorption of ammonia, the SiO⁻ defect sites are converted to Si-O-Al⁻ bridges leading to a transformation of the threefold-coordinated aluminum atoms to tetrahedrally coordinated

atoms. After the thermal decomposition of the ammonium ions located at these Si-O-Al⁻
bridges, additional bridging OH groups are formed.

Upon the rehydration of calcined zeolites, the additional water molecules could
coordinate to aluminum atoms at the above-mentioned framework defects, which leads to a
variation of their coordination from Al^{III} to Al^{IV}. By application of X-ray absorption
near-edge spectroscopy, e.g., van Bokhoven *et al.* [18] also observed changes in coordination
of aluminium atoms from a disturbed tetragonal to a nearly ideal tetragonal one upon
rehydration. Furthermore, the extra-framework aluminum species may be influenced upon
rehydration. These findings remind that the rehydration may induce changes in the nature of
framework and extra-framework aluminum species.

In addition, it was shown by ^{1}H MAS NMR spectroscopy that rehydrated H-form
zeolites are not suitable for the investigation of the hydroxyl coverage (see Figures 6.3a and
6.3b). If a rehydration of calcined H-form zeolites is carried out, the zeolite framework may
collapse, which strongly influences the hydroxyl coverage. In order to obtain more reasonable
information of different aluminum species and hydroxyl protons in dealuminated zeolites, the
investigation of non-hydrated samples is required.

7.   Investigation of the Charge Balance between the Framework and Extra-framework Species in Non-hydrated Zeolites Y by Multi-nuclear Solid-state MAS NMR Spectroscopy

7.1   Introduction

In most of the solid-state NMR studies of dealuminated zeolites published in the past decades, the nature of framework and extra-framework aluminum species was investigated in the hydrated state of the samples. Recently introduced techniques, however, have shown that strong changes of aluminum species occur upon hydration of zeolites, which is also discussed in Chapter 6 and Reference [14, 15, 18, 91, 135]. According to Scherzer [70], extra-framework aluminum species in steamed zeolites can be cationic compounds, such as Al^{3+}, AlO^+, $Al(OH)^{2+}$, and $Al(OH)_2^+$, or neutral and polymerized compounds, such as $AlO(OH)$, $Al(OH)_3$, and Al_2O_3. Since the nature of extra-framework aluminum species is strongly influenced by the presence of water, a first NMR investigation of the non-hydrated state of these aluminum species is performed in the current work using samples, which were not rehydrated after the dealumination by steaming. For this purpose, the equipment used for the steaming of zeolites H,Na-Y was combined with an air-lock allowing to fill the non-hydrated samples without contacting to air into gas-tight glass containers as described in Section 5.2.

Generally, solid-state ^{27}Al NMR spectroscopy can be directly used to investigate aluminum species in zeolites. However, the application of this spectroscopic method is limited by the strong line broadening due to quadrupolar interactions of aluminum atoms in the non-hydrated state. As shown by Kentgens *et al.* [94], ^{27}Al DFS enhanced 3QMAS spectroscopy (DFS: double frequency sweep) allows the separation of signals caused by different aluminum species in dehydrated zeolite H-ZSM-5. Another most widely applied technique for investigating aluminum atoms in non-hydrated zeolites is the application of an ^{27}Al spin-echo NMR experiment, which allows the determination of the quadrupole coupling constants and the relative amounts of the corresponding species [104, 130]. By application of

the above-mentioned techniques, quadrupole coupling constants of C_{QCC} = 13 to 16 MHz were obtained for tetrahedrally coordinated framework aluminum atoms in the local structure of bridging OH groups (SiOHAl) in non-hydrated zeolites H,Na-Y and H-ZSM-5 [94, 104, 130].

A further approach to study the state of aluminum atoms in non-hydrated zeolites is the NMR spectroscopic investigation of ^{1}H and [29]Si nuclei contributing to the local structure of these species. ^{29}Si MAS NMR spectroscopy, e.g., allows the determination of the relative amounts of framework silicon atoms bound to 0 to 4 framework aluminum atoms in the first coordination sphere of T atoms (Si(0Al) to Si(4Al)) and the calculation of the framework n_{Si}/n_{Al} ratio [96]. Via quantitative ^{1}H MAS NMR spectroscopy, the coverage of non-hydrated zeolites by bridging OH groups, defect SiOH groups, and AlOH groups is obtained [92]. Hence, the latter technique gives the amount of framework aluminum atoms, which are compensated in their framework charges by bridging hydroxyl protons. In present work, a series of non-hydrated zeolites deH,Na-Y/*p* is prepared and quantitatively investigated by ^{1}H and ^{29}Si NMR spectroscopy. These materials and the charge balance were used to clarify the state of extra-framework aluminum atoms in these materials. Further more detailed studies of the framework and extra-framework aluminum atoms in non-hydrated zeolites deH,Na-Y/*p* by DFS enhanced ^{27}Al 3QMAS and spin-echo NMR spectroscopy are described in Chapter 8 and 9.

^{1}H and ^{29}Si MAS NMR studies were carried out on a Bruker MSL 400 spectrometer at resonance frequencies of 400.13 and 79.49 MHz, respectively. ^{29}Si MAS NMR spectra were recorded with a 7 mm MAS NMR probe, a sample spinning rate of 3.5 kHz, and after a $\pi/2$ single-pulse excitation of 6.0 μs. Repetition times of 50 s for non-hydrated samples and 10 s for rehydrated samples were used. To decrease the longitudinal relaxation time of silicon atoms in non-hydrated zeolites deH,Na-Y/*p*, these samples were loaded with synthetic air (*p* = 100 kPa) consisting of 20 vol. % oxygen and 80 vol. % nitrogen. By comparison of the ^{29}Si MAS NMR spectra of loaded and unloaded samples it was ensured that the gaseous oxygen has no influence on the shapes of spectra at room temperature, which is also convinced by

Fyfe *et al.* [137]. To explain the ^{29}Si MAS NMR spectra of non-hydrated zeolites deH,Na-Y/*p*, Al-exchanged zeolites Al,Na-Y (69 % of the sodium cations were replaced by aluminum cations in zeolite Al,Na-Y) and zeolites H,Na-Y with cation exchange degrees of 46 %, 69 %, 77 % and 93 % were used as reference materials [138]. ^{1}H MAS NMR spectra were recorded with a 4 mm MAS NMR probe, a sample spinning rate of 10.0 kHz, after a $\pi/2$ single-pulse excitation of 2.1 μs, and with a repetition time of 30 s.

7.2 ^{1}H and ^{29}Si MAS NMR Investigations of Non-hydrated Zeolites deH,Na-Y

The ^{29}Si MAS NMR spectroscopy of non-hydrated zeolites H,Na-Y and deH,Na-Y/*p* was performed to determine the framework aluminum content in these materials [96]. The results are shown in Figure 7.1, top. The spectrum of non-hydrated zeolite H,Na-Y (Figure 7.1a, top), i.e., of zeolite NH$_4$-Y after calcination in the dealumination equipment without subsequent rehydration and steaming, consists of a dominating signal at –102 ppm with a low-field shoulder at –97 ppm and a high-field shoulder at –107 ppm. No signals occur at –90 and –95 ppm, which are indicative for Si(3Al) and Si(2Al) sites in zeolites Y [96]. After hydration of the non-hydrated zeolite H,Na-Y, well-separated Si(*n*Al) signals in the ^{29}Si MAS NMR spectrum are observed (Figure 7.1a, bottom). By simulation, a framework n_{Si}/n_{Al} ratio of 2.7 is obtained. The agreement between the framework n_{Si}/n_{Al} ratio determined by ^{29}Si MAS NMR spectroscopy and the bulk n_{Si}/n_{Al} ratio obtained by AES-ICP indicates that hydration of the non-hydrated zeolite H,Na-Y is not accompanied by a strong dealumination of the framework. However, the formation of octahedrally coordinated framework aluminum species, as described by Wouters *et al.* [14, 15], and a corresponding change of the hydroxyl coverage (Chapter 6) cannot be excluded.

It is important to note, that the total intensities of the ^{29}Si MAS NMR spectra of the non-hydrated zeolites (Figure 7.1, top spectra) are equal to those of the hydrated materials (Figure 7.1, bottom spectra). This indicates a high-field shift up to 5 ppm of the ^{29}Si MAS NMR signals of Si(*n*Al) sites with large numbers *n* in the spectra of non-hydrated zeolites H,Na-Y. The comparison of the ^{29}Si MAS NMR spectra of strongly dealuminated zeolites

deH,Na-Y/*p* in the non-hydrated and hydrated states (Figures 7.1c and 7.1d) shows that the above-mentioned high-field shift is only 1 to 2 ppm for the signals due to Si(1Al) and Si(0Al) sites.
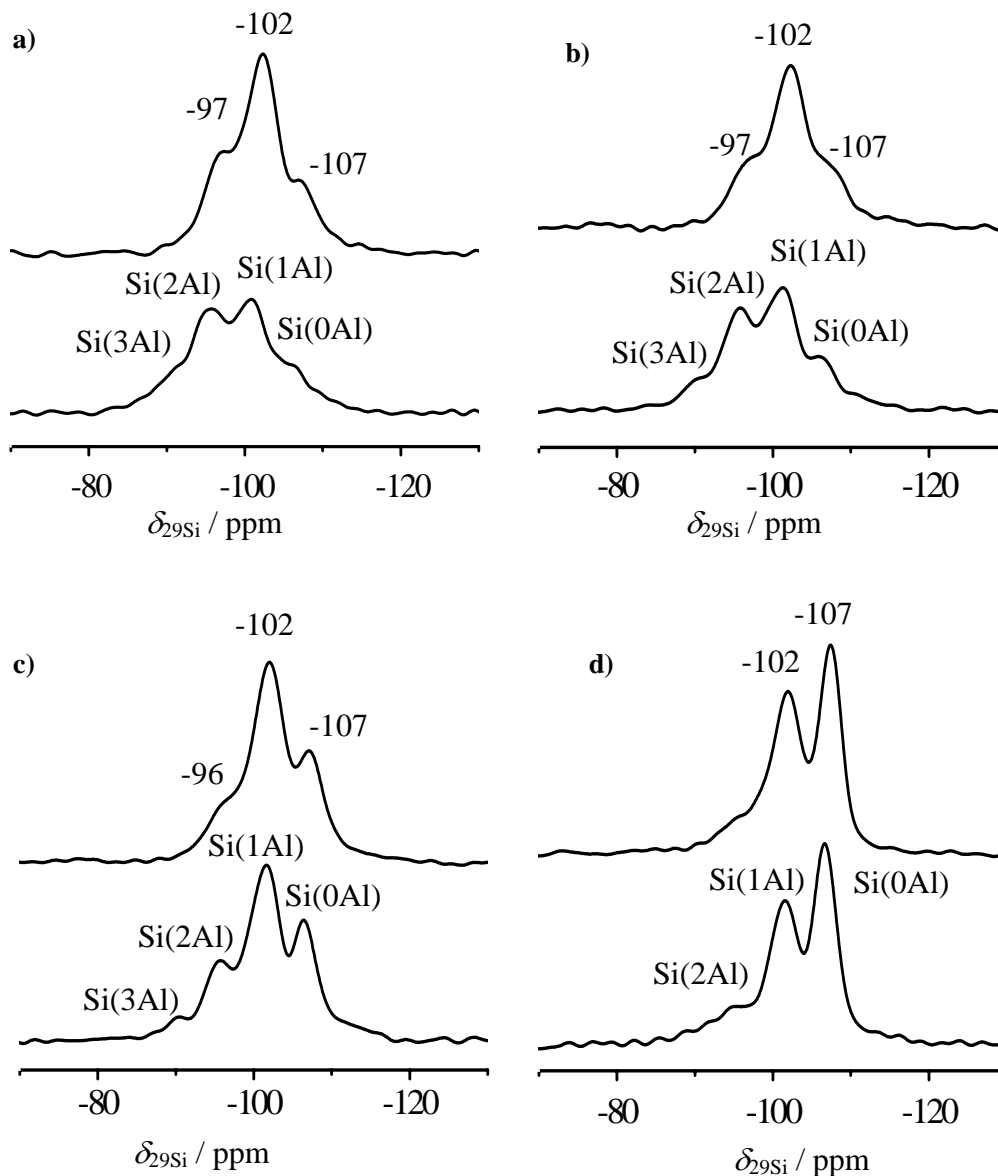
Figure 7.1 ^{29}Si MAS NMR spectra of non-hydrated (top spectra) and rehydrated (bottom spectra) zeolites H,Na-Y (a), deH,Na-Y/7.4 (b), deH,Na-Y/31.1 (c), and deH,Na-Y/81.5 (d).

There are various reasons for a resonance shift of ^{29}Si MAS NMR signals of Si(*n*Al) sites. As proposed by van Bokhoven *et al.* [99], the presence of large cations, such as lanthanum cations or charged extra-framework aluminum species, can lead to a local

framework strain accompanied by a distortion of the Si-O-T bond angles in their vicinity. The above-mentioned cationic species would be preferentially located in the neighbourhood of negative framework charges, i.e., of Si(nAl) sites with a large number n of aluminum atoms in the first coordination sphere of T atoms. According to the well-known relationship between the mean Si-O-T bond angle and the ^{29}Si NMR shift, therefore, a cation-induced local framework distortion would lead to a resonance shift preferentially of the signals of Si(3Al) and Si(2Al) sites in zeolites Y [99].

On the other hand, already the ^{29}Si MAS NMR spectrum of non-hydrated zeolite H,Na-Y shows a significant high-field shift of the signals of Si(3Al) and Si(2Al) sites (Figure 7.1a). Since there is no extra-framework aluminum in this material, only the dehydration of the framework may be a reason for the distortion of Si-O-Al bond angles. The experimentally observed broadening of the solid-state ^{27}Al NMR signals of framework aluminum atoms in non-hydrated zeolite Y indicates a strong strain of AlO$_4$ tetrahedra. This strain of AlO$_4$ tetrahedra is caused by changes in the O-Al-O bond angles and Al-O bond lengths due to dehydration [139, 140]. In EXAFS investigations of dehydrated zeolite H,Na-Y [140], an Al-O bond length of 1.87 Å and three Al-O bond lengths of 1.68 Å were observed, while the hydrated material has the equal Al-O bond lengths. Therefore, also the Si-O-Al bond angles of neighbouring silicon atoms must be influenced by a dehydration of AlO$_4$ tetrahedra. To clarify the reasons for the high-field shift, zeolites Y with different H- and Al-exchange degrees were investigated by solid-state NMR spectroscopy, which is discussed in Sections 7.4 and 7.5.

The strong overlap of the ^{29}Si MAS NMR signals of different Si(nAl) sites in the spectra of non-hydrated zeolites H,Na-Y makes a quantitative evaluation complicated. Therefore, ^{29}Si MAS NMR spectra of hydrated samples (Figure 7.1, bottom spectra) were used to determine the relative intensities $I_{Si(n Al)}$ of Si(nAl) sites and to calculate the framework n_{Si}/n_{Al} ratios and amounts of framework aluminum atoms summarized in Table 7.1, columns 2 and 3, respectively. The amounts of framework aluminum atoms given in Table 7.1, column 3, also contain threefold coordinated framework species existing in the non-hydrated samples.

Table 7.1 Framework n_{Si}/n_{Al} ratios (column 2) and numbers of framework aluminum atoms per unit cell (column 3) in zeolites H,Na-Y and deH,Na-Y (^{29}Si MAS NMR spectroscopy), numbers of extra-framework aluminum species per unit cell (column 4) calculated from the total amount of aluminum (AES-ICP) and the values in column 3, total amounts of bridging OH groups before (column 5) and after (column 6) an ammonia adsorption/desorption treatment (^{1}H MAS NMR spectroscopy), and amounts of tetrahedrally coordinated framework aluminum atoms (column 7) calculated by the values in column 3 minus the difference between the values in columns 5 and 6.

Sample	n_{Si}/n_{Al} [*)	$n_{fr.\,Al}$ [*) / u.c.	$n_{ex.\,Al}$ [*) / u.c.	n_{SiOHAl} [**) / u.c.	n_{SiOHAl}^{NH3} [**) / u.c.	n_{Al}^{IV} / u.c.
H,Na-Y	2.7	51.7	-	46.5	-	-
deH,Na-Y/3.4	2.8	50.1	1.9	41.4	43.0	48.5
deH,Na-Y/7.4	2.9	48.6	3.4	38.9	39.2	48.3
deH,Na-Y/12.4	3.0	48.4	3.6	38.3	38.8	47.9
deH,Na-Y/19.9	3.3	45.0	7.0	31.3	34.4	41.9
deH,Na-Y/31.1	4.0	38.2	13.8	23.8	25.7	36.3
deH,Na-Y/47.4	4.8	33.0	19.0	14.2	20.4	26.8
deH,Na-Y/70.1	5.4	30.0	22.0	10.9	17.4	23.5
deH,Na-Y/81.5	6.0	27.6	24.4	10.5	17.3	20.8

*) accuracy of $\pm$ 2 %

**) accuracy of $\pm$ 5 %

The ^{1}H MAS NMR spectra of non-hydrated zeolites H,Na-Y and deH,Na-Y/p shown in Figure 7.2, consist of signals of AlOH groups at 0.6 and 2.6 ppm, SiOH groups at 1.8 ppm, and bridging OH groups in supercages and sodalite cages at 3.8 and 4.7 ppm, respectively. The amounts of different hydroxyl groups as a function of the water vapor pressure during the steaming are given in Figure 7.3. It is interesting to note, that dealumination of the zeolite framework is not accompanied by a strong increase of defect SiOH groups, but rather with an increase of AlOH groups occurring at 2.6 ppm. Simultaneously, the amounts of bridging OH groups decrease, and this effect is more pronounced for SiOHAl groups located in the sodalite cages than for SiOHAl groups located in the supercages.
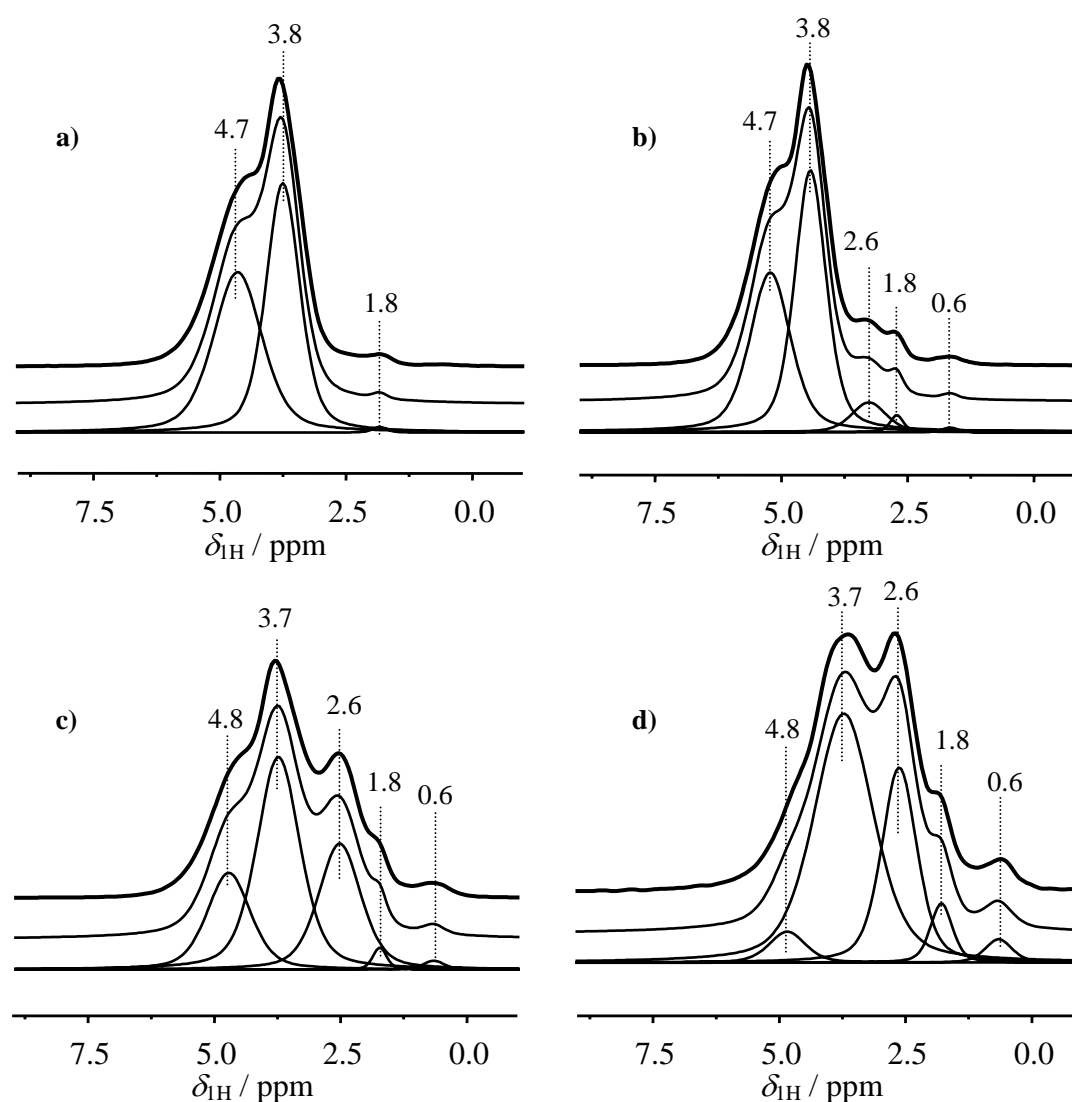
Figure 7.2 ^{1}H MAS NMR spectra of non-hydrated zeolites H,Na-Y (a), deH,Na-Y/7.4 (b), deH,Na-Y/31.1 (c), and deH,Na-Y/81.5 (d). Experimental spectra (top) are compared with simulated spectra (bottom).

As found in previous investigations (Chapter 6 and Reference [135]), ammonia adsorption on non-hydrated zeolites Y leads to a conversion of disturbed framework aluminum atoms from a threefold coordinated state into tetrahedrally coordinated state. Upon desorption of ammonia, an increase in the amount of bridging OH groups occurs. In the present work, therefore, an ammonia adsorption/desorption treatment and ^{1}H MAS NMR spectroscopy were utilized to determine, in an indirect manner, the amounts of threefold coordinated framework aluminum atoms in dealuminated and non-hydrated zeolites H,Na-Y as a function of the water vapor pressure during the steaming. In Table 7.1, the total amounts

of bridging OH groups in non-hydrated zeolites H,Na-Y before (column 5) and after (column 6) the ammonia adsorption/desorption treatment are compared. These values show that, in non-hydrated zeolites H,Na-Y, which were steamed at low water vapor pressures, up to ca. 1 Al/u.c. are in a threefold coordination, while in samples treated at high vapor pressures up to 6.5 Al/u.c. are threefold coordinated. The qualitative behavior of the amount of threefold coordinated aluminum atoms in the framework of steamed and non-hydrated zeolites agrees with the finding of van Bokhoven *et al.* [18]. The amounts of threefold coordinated framework aluminum species determined by the ammonia adsorption/desorption treatment and ^{1}H MAS NMR spectroscopy were utilized to calculate the amounts of tetrahedrally coordinated framework aluminum atoms in non-hydrated zeolites Y (Table 7.1, column 7).
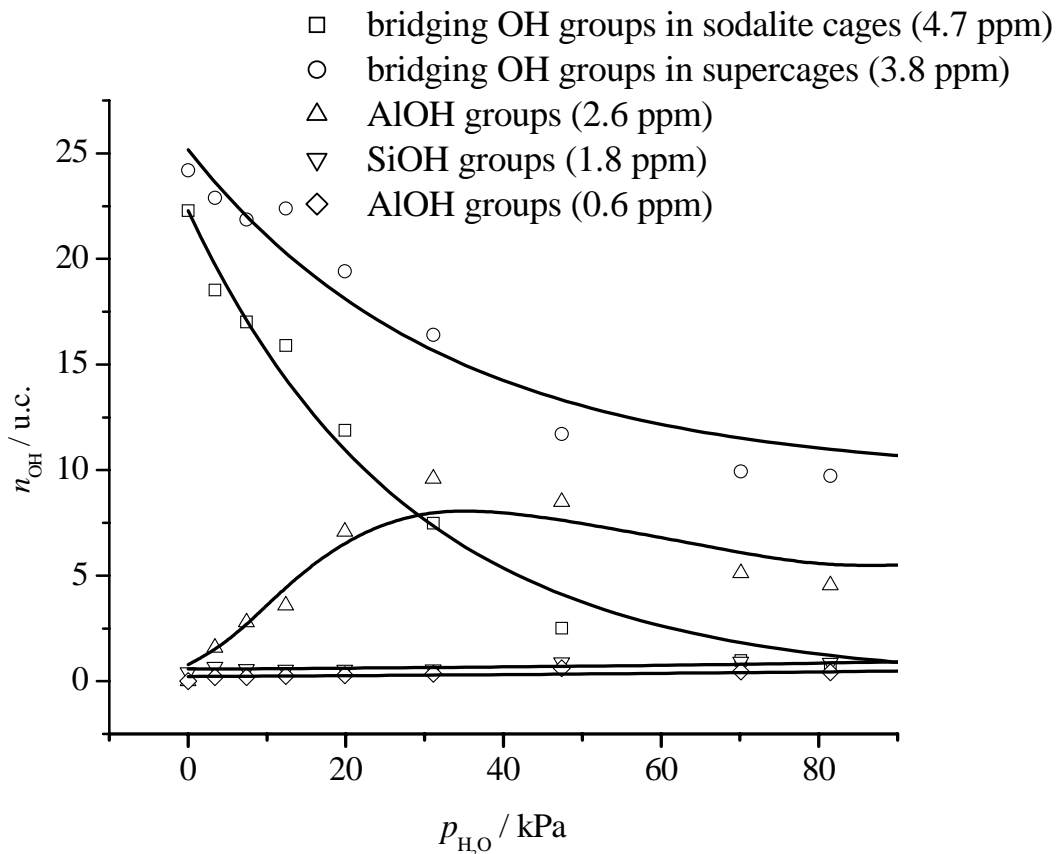
Figure 7.3 Amounts of hydroxyl groups in non-hydrated zeolites deH,Na-Y/*p* plotted as a function of the water vapor pressure p_{H2O} during the steaming.

### 7.3   State of Aluminum Species in Non-hydrated Zeolites deH,Na-Y

The solid-state ^{1}H and ^{29}Si NMR investigations described in Section 7.2 clearly evidence that tetrahedrally coordinated framework aluminum atoms in non-hydrated zeolites H,Na-Y exist as strained AlO_4 tetrahedra. The difference in the amounts of tetrahedrally coordinated aluminum atoms in non-hydrated zeolites Y (Table 7.1, column 7) and of bridging OH groups (Table 7.1, column 5) indicates the presence of cationic extra-framework species. It has to be mentioned that the above-mentioned difference is much larger than the number of residual sodium cations (3.5 Na^+/u.c.). In the case of strongly dealuminated zeolites H,Na-Y/81.5, the amount of cationic extra-framework charges necessary to compensate the negative framework charges increases up to ca. 12 per unit cell. This finding indicates the formation of cationic extra-framework aluminum species during the steaming.

By Equation (29) and using the corresponding values summarized in Table 7.1, the mean cationic charge x per extra-framework aluminum can be calculated

$$x = (n_{Al}^{IV} - n_{Na} - n_{SiOHAl}) / n_{ex.Al} \qquad (29)$$

The behavior of the mean cationic charge per extra-framework aluminum atom obtained in this way for non-hydrated zeolites Y dealuminated under water vapor pressures of 3.4 to 81.5 kPa is given in Figure 7.4. The mean cationic charge per extra-framework aluminum atom was found to decrease from ca. +2 to ca. +0.5 with increasing severity of the steaming. Performing a Rietveld refinement of the X-ray pattern of a weakly dealuminated zeolite Y in the dehydrated state, Gola *et al.* [71] found extra-framework aluminum atoms in the state of Al^{3+} cations on SI' positions in the sodalite cages. This indicates that a mean cationic charge of ca. +2 according to Figure 7.4 is not exclusively caused by $Al(OH)^{2+}$ species, but by a variety of highly charged cationic species. However, it can be generally stated that the probability of the occurrence of extra-framework aluminum species with a high cationic charge is significantly higher after a weak steaming of zeolite Y than after a strong steaming and *vice versa*.
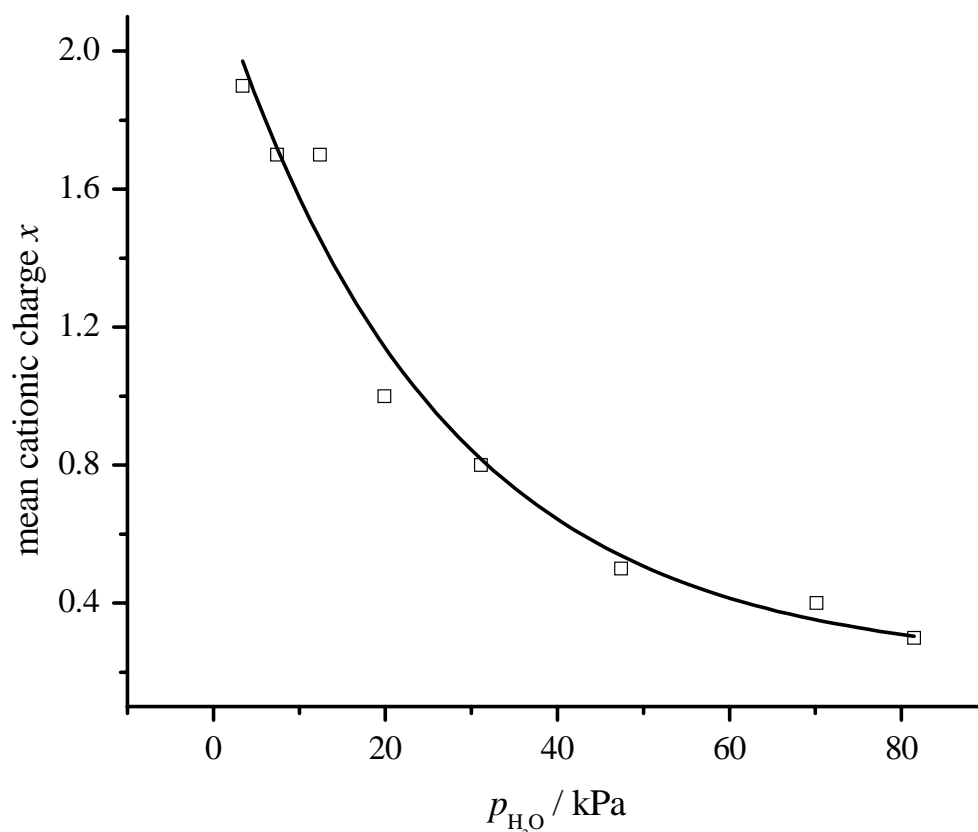
Figure 7.4 Behavior of the mean cationic charge *x* per extra-framework aluminum atom in non-hydrated zeolites Y calculated after Equation (29) and plotted as a function of the water vapor pressure p_{H2O} during the steaming.

7.4 ^{1}H and ^{29}Si MAS NMR Investigations of Non-hydrated Zeolites Al,Na-Y

In order to elucidate the effect of extra-framework aluminum species on neighboring framework silicon atoms, zeolites Al,Na-Y with a cation exchange degree of 69 % were investigated by ^{1}H and ^{29}Si MAS NMR spectroscopy (Figure 7.5). According to the amount of extra-framework aluminum species introduced by cation exchange, as determined by AES-ICP, the extra-framework aluminum cations preferentially existed as two-fold charged species, such as $Al(OH)^{2+}$. Prior to the NMR studies, the zeolites Al,Na-Y were evacuated at 433 or 723 K for 12 hours under vacuum and sealed in glass ampoules. The corresponding samples were denoted Al,Na-Y/433 and Al,Na-Y/723, respectively.
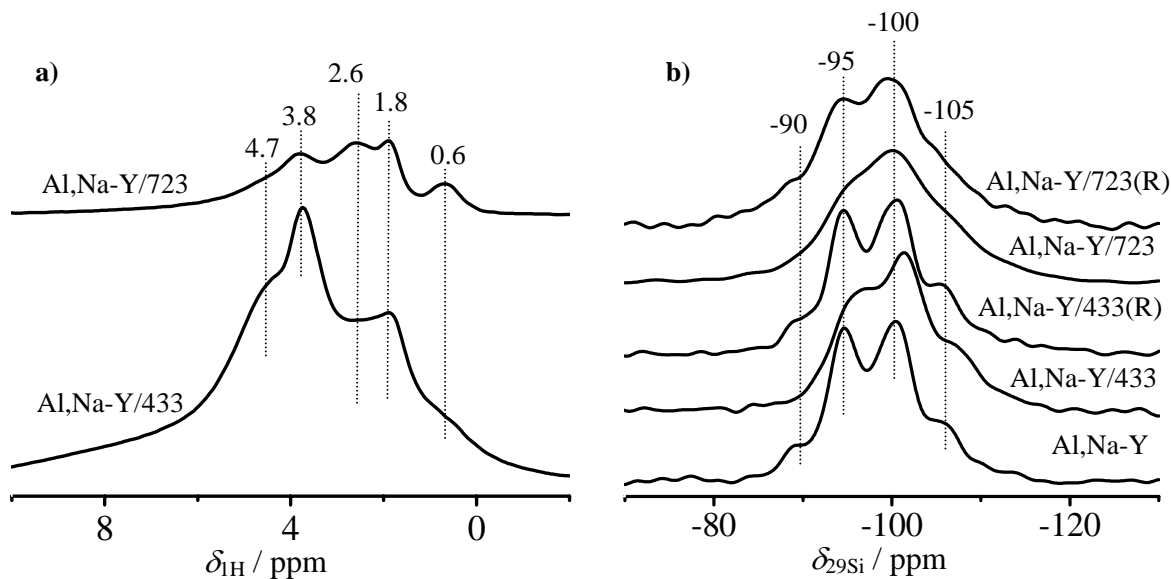
Figure 7.5 ^{1}H (a) and ^{29}Si MAS NMR spectra (b) of zeolites Al,Na-Y in different dehydration and rehydration states. Zeolites Al,Na-Y/433 and Al,Na-Y/723 were dehydrated at 433 and 723 K, respectively. Zeolites denoted by (R) were rehydrated after the thermal treatment.

The ^{1}H MAS NMR spectra of zeolites Al,Na-Y/433 and Al,Na-Y/723 (Figure 7.5a) consist of signals at 0.6, 1.8, 2.6, 3.8, and 4.7 ppm. The assignments of these signals are given in Section 7.2. Performing a quantitative evaluation of the ^{1}H MAS NMR intensities, concentrations of 29 SiOHAl/u.c. and 6.5 SiOHAl/u.c. were determined for zeolites Al,Na-Y/433 and Al,Na-Y/723, respectively. These bridging OH groups were formed via the mechanism of Hirschler and Plank [141, 142], i.e., by a dissociation of water molecules in the electrostatic field of multivalent extra-framework cations, as described for zeolites Mg,Na-Y and Ca,Na-Y in Reference [143]. In Scheme 7.1, the formation of SiOHAl and AlOH groups by this mechanism is explained. Hence, in zeolite Al,Na-Y/433, most of the negative framework charges are compensated by bridging hydroxyl protons (SiOHAl) instead of extra-framework cations. In zeolite Al,Na-Y/723 most of these hydroxyl groups are dehydroxylated again.

In Figure 7.5b, the ^{29}Si MAS NMR spectra of zeolite Al,Na-Y and of zeolites Al,Na-Y/433 and Al,Na-Y/723 before and after rehydration (R) are shown. The spectrum of the as-exchanged zeolite Al,Na-Y consists of well resolved signals of Si(0Al), Si(1Al), Si(2Al), and Si(3Al) silicon species at -105, -100, -95, and -90 ppm [96], respectively. In

contrast to this finding, the spectrum of zeolite Al,Na-Y/433 shows a broadening of all Si(nAl) signals, which is stronger for the Si(2Al) and Si(3Al) silicon species than for the Si(0Al) and Si(1Al) silicon species. A similar behavior was found for zeolite Al,Na-Y/723. It could be evidenced by X-ray diffraction that the zeolite framework was not damaged by the cation exchange and thermal treatment. Upon rehydration of the zeolite materials, the ^{29}Si MAS NMR spectrum of zeolite Al,Na-Y/433(R) is almost recovered and corresponds to the spectrum of the as-exchanged zeolite Al,Na-Y. In contrast, the signals in the spectrum of zeolite Al,Na-Y/723(R) are narrowed in comparison with those of zeolite Al,Na-Y/723, but do not reach the line widths of zeolite Al,Na-Y.

It is interesting to note, that the ^{29}Si MAS NMR signals in the spectrum of zeolite Al,Na-Y/433 are high-field shifted by up to 5 ppm in comparison with the spectrum of zeolite Al,Na-Y/433(R), while no or only weak high-field shifts (maximum 1 ppm) occurred in the spectrum of zeolite Al,Na-Y/723. This may be due to the presence of extra-framework aluminum cations in zeolite Al,Na-Y/723, while in zeolite Al,Na-Y/433 bridging OH groups are formed via the mechanism of Hirschler and Plank (see Scheme 7.1).

The strong broadening of the Si(nAl) signals in the spectra of non-hydrated zeolites Al,Na-Y might be caused by ^{29}Si-^{27}Al couplings, such as dipolar/quadrupolar couplings described for ^{13}C and ^{14}N nuclei [17, 144]. In this case, the ^{29}Si-^{27}Al couplings preferentially influence the line shapes of Si(nAl) signals with large n values, since the aluminum cations are located on cationic sites near the framework aluminum atoms responsible for negative framework charges.

In Figure 7.6, the simulations of the spectra of zeolite Al,Na-Y/723 before and after rehydration are depicted. The parameters used are summarized in Table 7.2. A comparison of these parameters gives a reasonable agreement of the relative intensities in the spectra of the non-hydrated (Al,Na-Y/723) and hydrated (Al,Na-Y/723(R)) material. In addition, these simulations support the above-mentioned statement that no or only a weak resonance shift, but a strong broadening of the Si(nAl) signals occur in the presence of cationic

extra-framework aluminum species. In contrast to this finding, the simulation of zeolite Al,Na-Y/433 requires to assume two sets of Si(nAl) signals: (i) one set, which corresponds to the Si(nAl) signals of zeolite Na-Y, and (ii) another set, which is high-field shifted by 2 to 5 ppm. This situation makes a quantitative simulation of the ^{29}Si MAS NMR spectrum of zeolite Al,Na-Y/433 very complicated (not shown).

Scheme 7.1
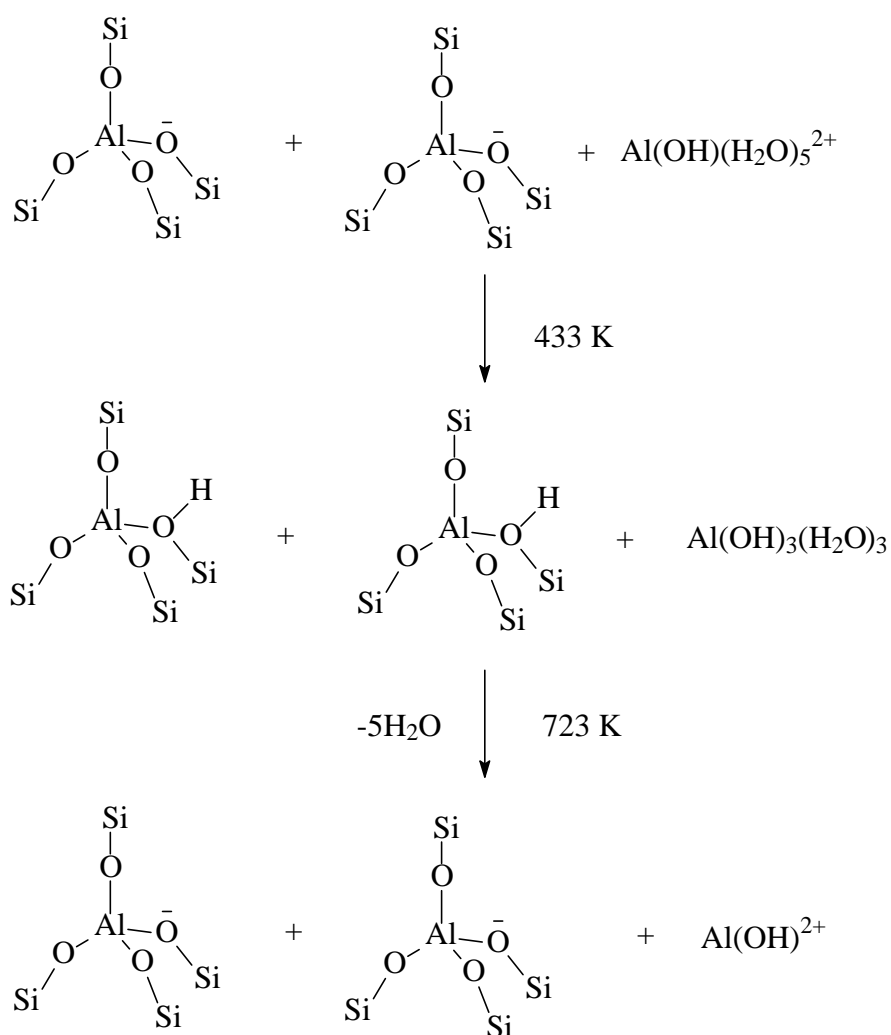
a) Al,Na-Y/723   **b)** Al,Na-Y/723(R)
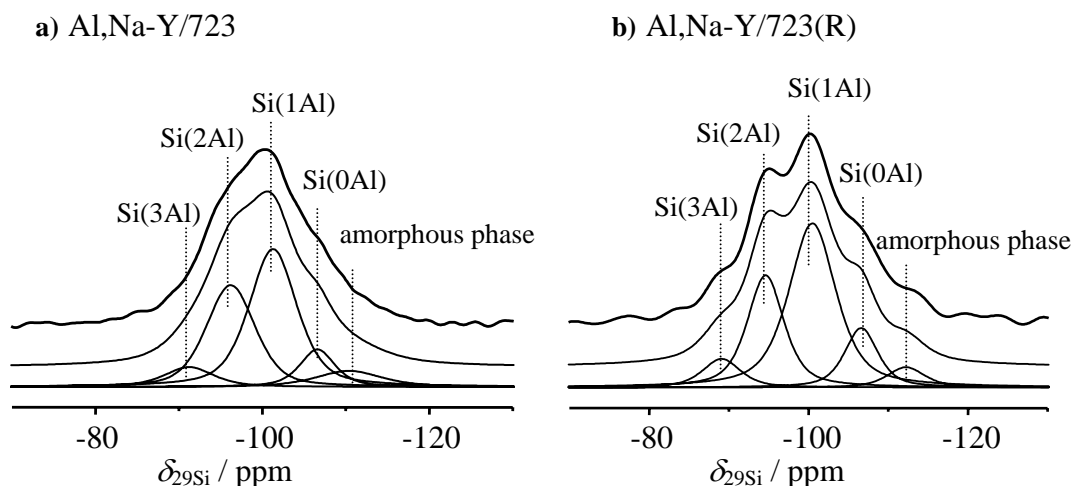
Figure 7.6 Simulation of the ^{29}Si MAS NMR spectra of zeolites Al,Na-Y/723 (a) and Al,Na-Y/723(R) (b). The simulation parameters are given in Table 7.2.

Table 7.2 Isotropic chemical shifts δ_{iso} and relative intensities I of the different Si(nAl) silicon species obtained by simulation of the ^{29}Si MAS NMR spectra of zeolites Al,Na-Y/723, Al,Na-Y/723(R), H(93),Na-Y, and H(46),Na-Y and calculated n_{Si}/n_{Al} ratios of the non-hydrated and rehydrated samples.

| Samples	Si(0Al)		Si(1Al)		Si(2Al)		Si(3Al)		n_{Si}/n_{Al}
	δ_{iso}/ppm	I/%	δ_{iso}/ppm	I/%	δ_{iso}/ppm	I/%	δ_{iso}/ppm	I/%	
Al,Na-Y/723	-106.4	9.9	-101.0	49.4	-95.9	28.1	-91.7	7.0	3.0
Al,Na-Y/723-R	-106.6	12.7	-100.4	49.0	-94.6	26.4	-89.1	7.0	3.1
H(93),Na-Y	-107.6	13.9	-102.8	34.6	-101.0[I]	27.8	-95.3	7.2	2.8
					-97.2[II]	16.6			
H(46),Na-Y	-105.3	5.8	-99.7	23.0	-94.8	22.0	-90.3	2.8	2.8
	-107.6	6.8	-102.0	13.8	-100.8[I]	14.6	-95.3	3.4	
					-97.1[II]	7.8			

I) and II) are the different Si(2Al)-I and Si(2Al)-II silicon species shown in Figure 7.8.

7.5 ^{1}H and ^{29}Si MAS NMR Investigations of Non-hydrated Zeolites H,Na-Y with Different Cation Exchange Degrees

The ^{1}H and ^{29}Si MAS NMR spectra of a series of non-hydrated zeolites H(x),Na-Y with different cation exchange degrees x are shown in Figure 7.7. The ^{1}H MAS NMR spectra

(Figure 7.7a) consist of signals of SiOH groups (1.8 ppm), bridging OH groups in the supercages (3.8 ppm), and bridging OH groups in the sodalite cages (4.7 ppm). A quantitative evaluation of the ^{1}H MAS NMR intensities gives a good agreement with the concentrations of SiOHAl groups calculated using the chemical compositions obtained by AES-ICP. This finding indicates that no damage of the zeolite framework occurred during the cation exchange and calcination of zeolites H(x),Na-Y.
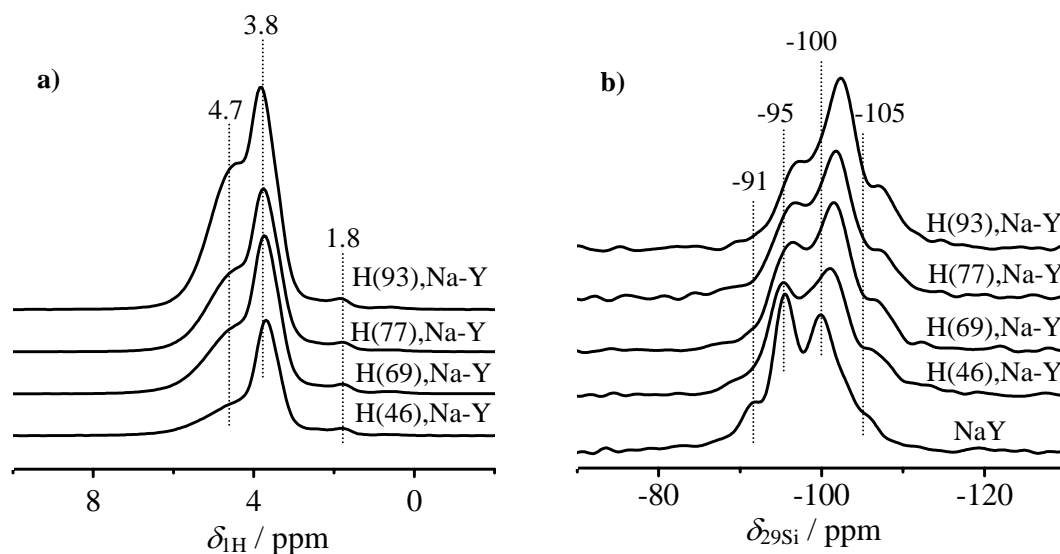
Figure 7.7 ^{1}H (a) and ^{29}Si MAS NMR spectra (b) of non-hydrated zeolite H(x),Na-Y with different cation exchange degrees x.

The ^{29}Si MAS NMR spectra of non-hydrated zeolites Na-Y and H(x),Na-Y are shown in Figure 7.7b. In the spectrum of the parent zeolite Na-Y, signals occur at -105, -100, -95, and -91 ppm, which are caused by Si(0Al), Si(1Al), Si(2Al) and Si(3Al) silicon species [96], respectively. It should be noted that the relative intensities and resonance positions of these signals do not depend on the hydration state of zeolite Na-Y. With increasing cation exchange degree x of zeolites H(x),Na-Y, all Si(nAl) signals are shifted to higher field and a change in line shape can be observed. In particular, the signals occurring at -95 and -91 ppm show a strong high-field shift. However, all signals can be completely recovered upon full rehydration or ammonia adsorption (Chapter 8).

A suitable simulation of the ^{29}Si MAS NMR spectrum of non-hydrated zeolite H(93),Na-Y (Figure 7.8a) can be reached by applying the parameters given in Table 7.2. For the Si(3Al) signal, a high-field shift of ca. 5 ppm was found in comparison with the same signal in the spectrum of the hydrated sample (or zeolite Na-Y, see Figure 7.7). For the Si(2Al), Si(1Al) and Si(0Al) signals, the high-field shift amounts to ca. 2 ppm. To reach a suitable simulation, a high-field shift of ca. 5 ppm has to be assumed also for more than 50 % of the Si(2Al) silicon atoms.
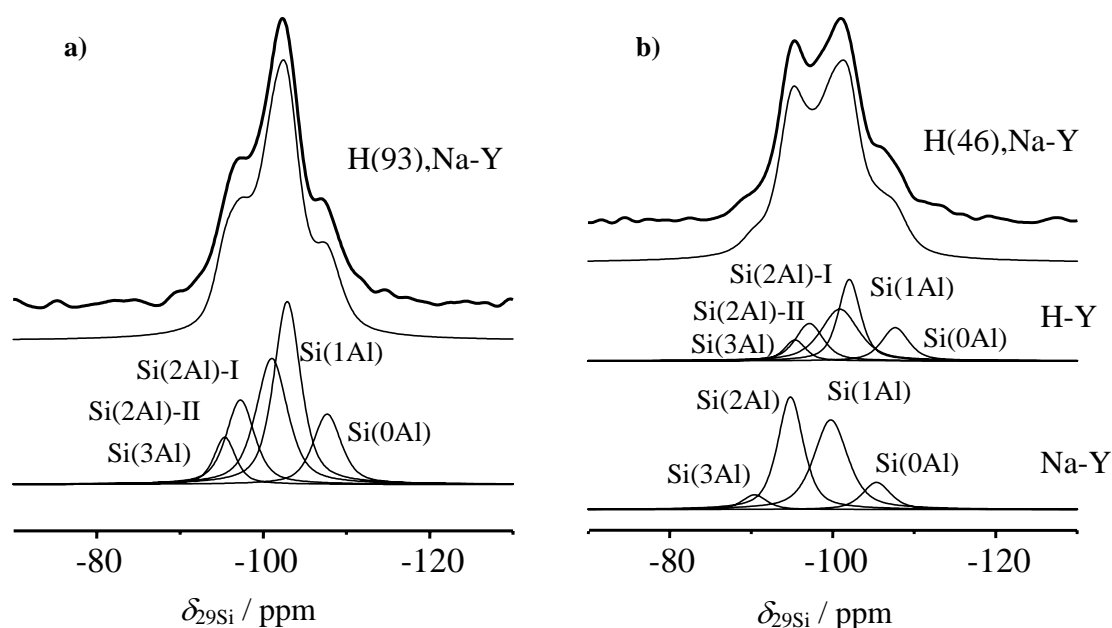
Figure 7.8 Simulation of the ^{29}Si MAS NMR spectra of zeolites H(93),Na-Y (a) and H(46),Na-Y (b). The simulation parameters are given in Table 7.2.

The ^{29}Si MAS NMR spectra of the non-hydrated H(x),Na-Y zeolites, e.g. of zeolite H(46)Na-Y, with lower cation exchange degrees x were simulated by a superposition of the Si(nAl) signals of the non-hydrated zeolite H-Y and zeolite Na-Y (Figure 7.8b). Also in this case, high-field shifts of the signals of Si(nAl) silicon atoms contributing to the local structure of the H-form of the zeolite occurred (upper trace of simulation in Figure 7.8b). The parameters used for the simulation of the spectrum of zeolite H(46),Na-Y are given in Table 7.2.

^{27}Al spin-echo NMR studies of non-hydrated zeolites H-Y demonstrated the strong influence of the adsorption of water or other adsorbate molecules on the quadrupolar parameters of framework aluminum atoms [93, 94, 145, 146]. Upon dehydration, the local structure of the framework AlO_4 tetrahedra is changed to strongly distorted tetrahedra with characteristics of a threefold oxygen coordination. The change from an M-form of a zeolite (M: Na^+, NH_4^+ or H_3O^+) to its H-form (Scheme 7.2) is accompanied by an increase in the quadrupole coupling constant of the framework aluminum atoms from ca. 6 MHz to ca. 16 MHz [93, 94, 145, 146], which corresponds to a decrease of the local symmetry.

M^+: Na^+ , NH_4^+ or H_3O^+

M-Y

H-Y
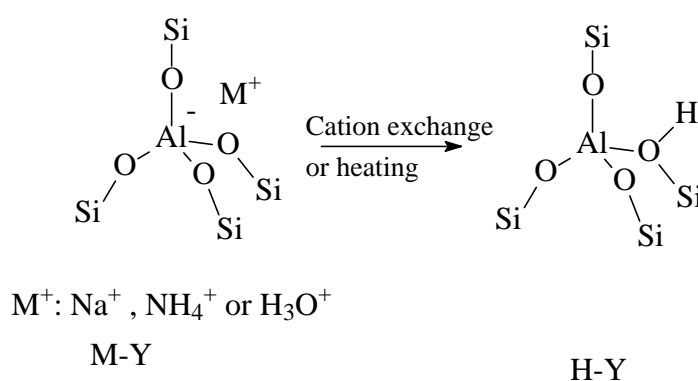
Scheme 7.2

As shown by theoretical studies [139], the dehydration of AlO_4 tetrahedra and the formation of bridging OH groups is accompanied by a strong increase of the Al-O bond in the Si-OH-Al bridge and significant changes of the O-Al-O bond angles. Upon rehydration, water molecules are adsorbed at the SiOHAl groups and H_3O^+ ions are formed, which compensate the negative framework charges instead of bridging hydroxyl protons in SiOHAl groups. This recovers the local symmetry of the AlO_4 tetrahedra and leads to a decrease of the electric field gradient at the aluminum site and, therefore, of the [27]Al quadrupole coupling constant. Changes in the local structure of AlO_4 tetrahedra certainly influence the chemical environment, i.e., the local structure of neighboring silicon atoms and induce variations of their ^{29}Si MAS NMR parameters. According to the well-known correlation of the ^{29}Si NMR shift and the mean Si-O-T bond angle α of framework silicon atoms [96, 147], a change of α, e.g., induced by the dehydration of neighboring AlO_4 tetrahedra, causes a shift of the [29]Si

MAS NMR signals. In addition, the number of different AlO_4 tetrahedra and different secondary building units in the local structures of the resonating silicon atoms affect the value of this resonance shift.

In the framework of FAU type zeolites, each silicon atom is surrounded by three four-membered rings and one six-membered ring [37]. Based on NMR investigations of the aluminum ordering in zeolite Y [17, 96], the configurations given in Figure 7.9 exist. According to this scheme, silicon atoms with 3, 1, and 0 aluminum atoms in the first coordination sphere of T atoms are characterized by only one configuration in each case (Figures 7.9a, 7.9c, and 7.9d). In contrast, silicon atoms with two aluminum atoms in the first coordination sphere of T atoms are characterized by two different configurations: (i) Both Al atoms are located in the adjacent six-membered ring, such as in the Si(2Al)-I configuration, whereas in the other configuration (ii) one Al atom is located in the six-membered ring while another one is located in one of the positions of the four membered ring, such as in the Si(2Al)-II configuration (Figure 7.9b). In the local structure of the Si(3Al) silicon atoms, two aluminum atoms are located in the neighboring six-membered ring (Figure 7.9a). Also, the configuration Si(2Al)-I has two aluminum atoms in the adjacent six-membered ring (Figure 7.9b).

The strong dehydration-induced high-field shift of the ^{29}Si MAS NMR signal of the Si(3Al) silicon species of ca. 5 ppm indicates that two AlO_4 tetrahedra located in six-membered rings cause a significant variation of the local structure of neighboring silicon atoms. This change of the local structure is stronger than for the case with one AlO_4 tetrahedron in a six-membered ring (Figure 7.9c). In agreement with the experimental results, therefore, the ^{29}Si MAS NMR signal of Si(2Al) silicon species in non-hydrated zeolites H-Y is splitted into two signals: (i) for the configuration Si(2Al)-I, which is high-field shifted by ca. 5 ppm, and (ii) for the configuration Si(2Al)-II, which is high-field shifted by ca. 2 ppm only. The dehydration-induced high-field shift of the configuration Si(2Al)-II is the same as for Si(1Al) silicon species with one aluminum atom in the adjacent six-membered ring, while the resonance shift of the configuration Si(2Al)-I is the same as for Si(3Al) silicon species with

two aluminum atoms in the six-membered ring. Hence, the loop configuration and the aluminum ordering in the H-form of zeolites Y are the reasons for the different high-field shifts of the ^{29}Si MAS NMR signals of Si(nAl) silicon species upon dehydration of these materials.
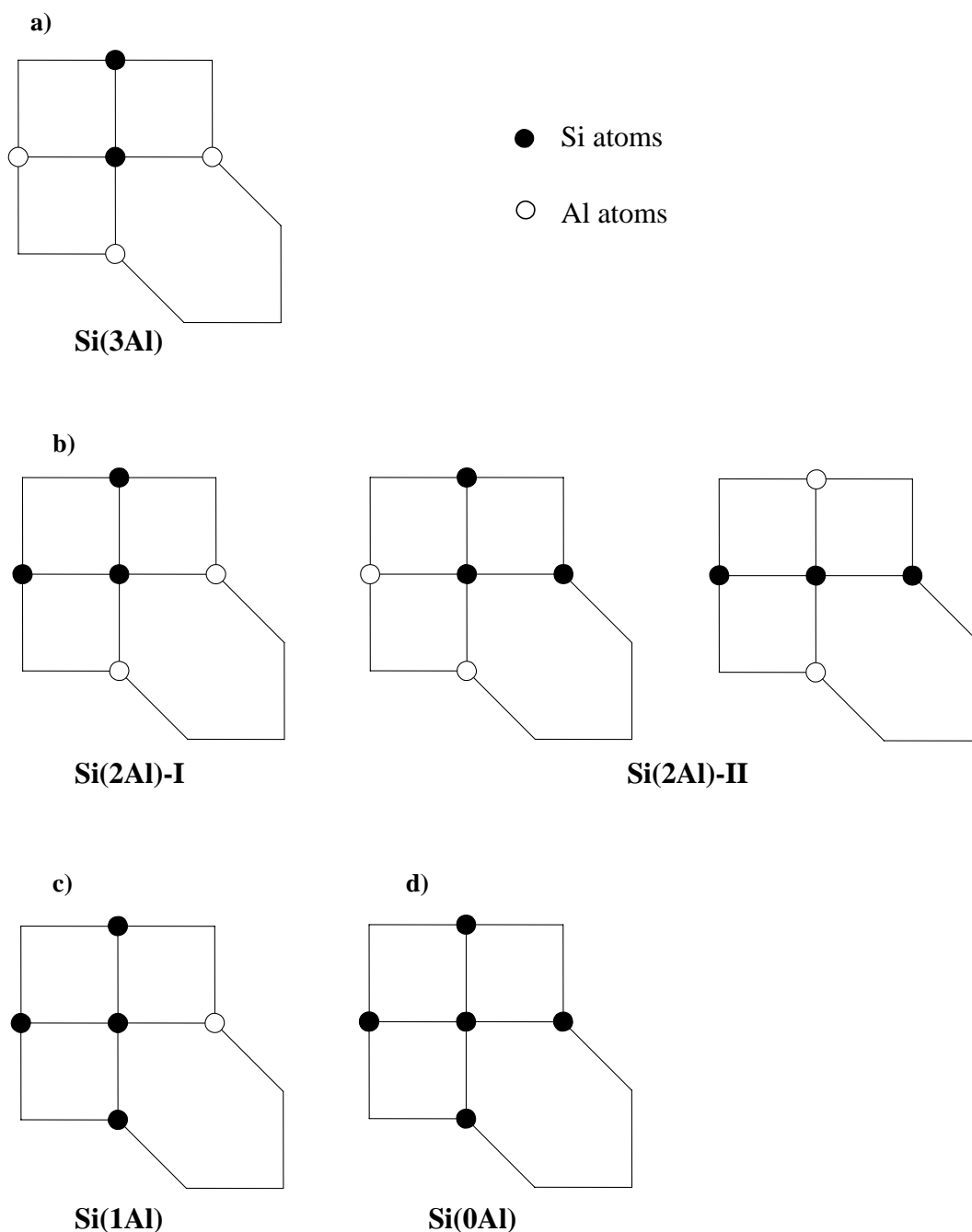
Figure 7.9 Loop configuration and aluminum ordering in the local structure of framework silicon atoms with 0 to 3 aluminum atoms in the first coordination sphere of T atoms in zeolites Y [17, 37, 96].

7.6   Conclusions

By a combination of different methods of solid-state NMR spectroscopy, the state of aluminum atoms in dealuminated and non-hydrated zeolites Y was investigated. ^{29}Si MAS NMR spectroscopy was utilized for a quantitative determination of the total amounts of aluminum atoms in the framework of non-hydrated zeolites Y. The amounts of threefold coordinated framework aluminum species were obtained in an indirect way, i.e., via an ammonia adsorption/desorption treatment of the non-hydrated materials and application of ^{1}H MAS NMR spectroscopy. The discrepancy between the amounts of tetrahedrally coordinated framework aluminum atoms, responsible for negative framework charges, and the amounts of charge-compensating residual sodium cations and bridging hydroxyl protons allowed the estimation of the mean cationic charge of extra-framework aluminum species. This mean cationic charge per extra-framework aluminum atom in non-hydrated zeolites Y was found to depend on the strength of dealumination by steaming.

In addition, the reasons of the resonance shifts and broadenings of the ^{29}Si MAS NMR signals of Si(nAl) silicon species in zeolites Y upon dehydration were investigated. To shed light on the origin of these effects, zeolites Na-Y partially exchanged with aluminum cations (Al,Na-Y) and zeolites H(x),Na-Y with different cation exchange degrees, x, were investigated by solid-state NMR spectroscopy. Depending on the dehydration temperature of zeolites Al,Na-Y, the formation of bridging OH groups via the mechanism of Hirschler and Plank [141, 142] or of extra-framework aluminum cations could be evidenced. In the former case, a high-field shift of the ^{29}Si MAS NMR signals of the Si(nAl) silicon atoms of up to 5 ppm was found, while in the latter case, a strong broadening of these signals occurred. This broadening was explained by ^{29}Si-^{27}Al couplings between framework silicon atoms and extra-framework aluminum cations. In the ^{29}Si MAS NMR spectra of non-hydrated zeolites H(x),Na-Y, a high-field shift of the Si(nAl) signals by 2 to 5 ppm was observed in comparison with the spectra of the hydrated materials. The value of this high-field shift was found to depend on the aluminum ordering in the local structure of the resonating framework silicon atoms. Two framework AlO$_4$ tetrahedra in the six-membered ring contributing to the local

structure of the resonating framework silicon atoms cause a stronger dehydration-induced high-field shift than one AlO_4 tetrahedron only. This is due to a larger structural flexibility of six-membered rings in comparison with four-membered rings containing the same number of AlO_4 tetrahedra. The above-mentioned finding helps to understand the variation of the ^{29}Si MAS NMR spectra of H-Y zeolites upon dehydration and rehydration.

8.   Number and Nature of Framework Aluminum Atoms in Non-hydrated Zeolites Y Studied by Adsorption of Probe Molecules

8.1   Introduction

The characterization of solid catalysts in a state comparable to their application in industrial processes requires the investigation of calcined and non-hydrated materials (discussed in Chapter 3 and 6). However, the dehydration-induced coordination change of the framework aluminum atoms in the vicinity of bridging hydroxyl protons in zeolite catalysts affects the ^{29}Si and ^{27}Al NMR parameters of silicon and aluminum atoms, respectively (see Chapter 7 and References [93, 94, 138, 148]). For non-hydrated zeolites H,Na-Y, a significant dehydration-induced high-field shift of Si(nAl) signals (n = 3, 2, 1) in the ^{29}Si MAS NMR spectra of the non-hydrated materials was found [138]. Due to the high-field shifts of Si(nAl) signals, the resolution of ^{29}Si MAS NMR spectra decreases considerably, therefore, the determination of the framework n_{Si}/n_{Al} ratio by ^{29}Si MAS NMR spectroscopy is complicated. In addition, a strong broadening of solid-state ^{27}Al NMR signals of non-hydrated materials induced by quadrupolar interactions was observed [93, 94, 148]. In moderate magnetic field, i.e. at B_0 = 9.4 T, this broadening of solid-state ^{27}Al NMR signals hinders the observation of aluminum atoms by the MAS technique, and makes it difficult to distinguish different ^{27}Al spin-echo NMR spectra signals [93, 94, 148]. Because of the reasons discussed in Chapter 6, probe molecules were adsorbed on the non-hydrated zeolites to reduce the quadrupolar interaction instead of water. Upon the adsorption of these probe molecules, a decrease of the quadrupolar interaction, but no influence on the aluminum species in the non-hydrated samples is achieved.

In the present work, the effect of the adsorption of ammonia (NH_3), pyridine (C_5H_5N), acetone (CH_3COCH_3) and acetonitrile (CH_3CN) on non-hydrated zeolites Y was studied by *in situ* and *ex situ* NMR spectroscopy. For comparison, water adsorption experiments were carried out. Depending on the properties of Brønsted acid sites and probe molecules, the formation of hydrogen bonds or a proton transfer from the catalyst to the probe molecules can

occur [143]. The proton affinities (*PA*) of water, acetonitrile, acetone, ammonia, and pyridine are 691, 779, 812, 854, and 930 kJ/mol, respectively [150]. The zeolite catalysts under study were the parent H-form zeolites Y and steamed materials. It is demonstrated that solid-state NMR spectroscopy of ammonia-loaded samples can be utilized as a standard tool for the quantitative characterization of the framework composition of zeolite catalysts in the non-hydrated state.

Non-hydrated zeolites H,Na-Y and deH,Na-Y/81.5 were prepared and activated as described in Section 5.2. The *in situ* adsorption experiments of water, ammonia, pyridine, acetone, and acetonitrile were performed via the injection equipment described in Section 5.3.4. The amounts of adsorbates were controlled by the flow velocity of the carrier gas or of the ammonia (Mass Flow Controller) and the flow duration. The equivalent number, *equiv.*, is the ratio of the amount of adsorbed molecules, n_{ad}, and the number of bridging OH groups acting as Brønsted acid sites (n_{OH}). In addition, *ex situ* adsorption experiments on non-hydrated zeolites H,Na-Y and deH,Na-Y/81.5 were performed with the loading of adsorbate on a vacuum line as described in Section 5.3.4.

The *in situ* experiments were performed on a Bruker MSL 400 spectrometer. ^{1}H and ^{27}Al MAS NMR experiments were recorded with a sample spinning rate of 10.0 kHz after a single-pulse excitation of 2.1 ($\pi/2$) and 0.61 ($< \pi/12$) μs and repetition times of 30 s and 500 μs, respectively. A fully hydrated zeolite NH$_4$-Y and a dehydrated (673 K) zeolite H-Y were used as the intensity standards of ^{27}Al and ^{1}H NMR spectroscopy. The *ex situ* ^{29}Si MAS NMR and ^{27}Al MQMAS NMR experiments were conducted on a Bruker MSL 400 spectrometer, Bruker AVANCE 400 and AVANCE 750 spectrometers, respectively. ^{29}Si MAS NMR spectra were recorded with a 7 mm MAS rotor system, a sample spinning rate of 3.5 kHz, and after a $\pi/2$ single-pulse excitation of 6.0 μs. Repetition times of 50 s for non-hydrated samples loaded with synthetic air and 10 s for rehydrated samples were used. DFS enhanced ^{27}Al MQMAS NMR spectra were obtained applying the split-t_1-whole echo pulse sequence with hard pulses of 3.3 μs and 13.7 μs, a soft pulse of 47 μs and a repetition time of 2 s (see in

Section 5.3.3). The Bruker softwares WINNMR, WINFIT, and XWINNMR were applied for the deconvolution and simulation of 1D NMR spectra and the transformation evaluation of 2D MQMAS spectra.

8.2   NMR Spectroscopic Investigations of Non-hydrated Zeolites upon Water Adsorption

8.2.1   *In situ* and *ex situ* MAS NMR Spectroscopic Investigations of Non-hydrated Zeolite H,Na-Y upon Water Adsorption

In situ MAS NMR spectroscopy was applied to study the influence of water on framework and extra-framework aluminum atoms. Figure 8.1a to 8.1f shows the *in situ* ^{1}H and ^{27}Al MAS NMR spectra of zeolite H,Na-Y loaded with different amounts of water. The equivalent of water is defined by *equiv.* $= n_{H2O}/n_{OH}$, where $n_{H2O} = (n_H - n_{OH})/2$. n_H is the total amount of protons in the *in situ* ^{1}H MAS NMR experiments, and n_{OH} is the amount of bridging OH groups in non-hydrated zeolites. Figure 8.1a shows the ^{1}H and ^{27}Al MAS NMR spectra of zeolite H,Na-Y before the *in situ* hydration experiments. Two signals of bridging OH groups at 3.8 and 4.6 ppm are observed in the ^{1}H MAS NMR spectrum. As given in Chapter 7, ca. 46.5 bridging OH groups per unit cell are detected. Upon the injection of water vapor, a signal occurs at 6.9 ppm and shifts to 5.0 ppm for higher loading. In addition, a decrease of the signals of bridging OH groups is observed. The signals in the range of 6.9 to 5.0 ppm are assigned to the hydroxonium ions, which are involved in a rapid chemical exchange with bridging OH groups [151, 152]. In recent investigations of hydrated zeolites H-Y by theoretical calculation methods [153], the formation of ion-pair complexes in the type of $ZO^--H^+(H_2O)_n$ was proposed. At *equiv.* > 1.4, a new signal at ca. 9.2 ppm is observed. This may be due to the protons in $Al(H_2O)_n^{3+}$ complexes [154, 155].

In the ^{27}Al MAS NMR spectrum of non-hydrated materials, a broad signal at ca. 55 ppm occurs, which belongs to tetrahedrally coordinated framework aluminum atoms compensated in their negative charge by residual Na$^+$ cations (**Al$^{IV}_{fr.}$**). The signal of
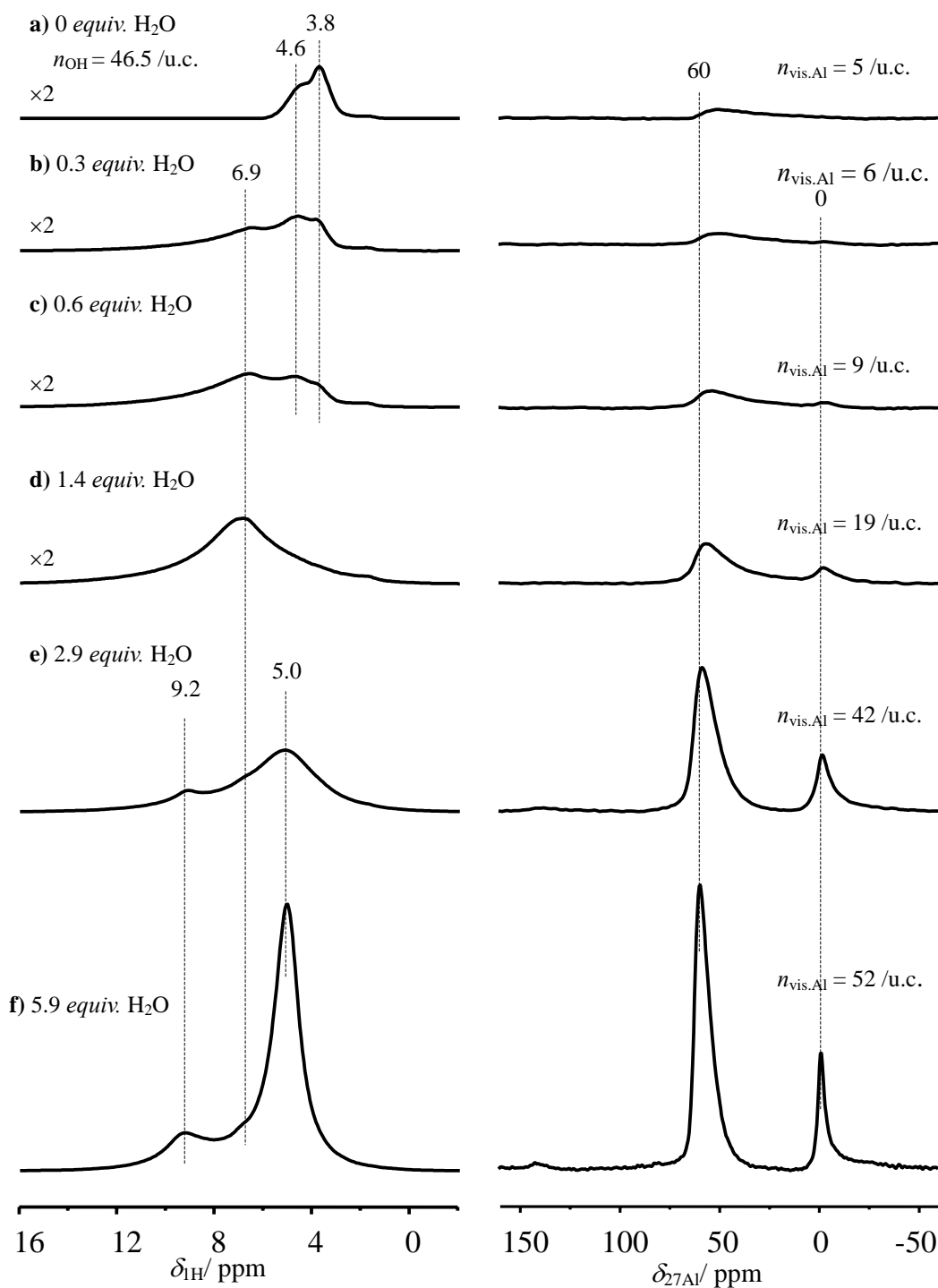
Figure 8.1 *In situ* ^{1}H (left) and ^{27}Al MAS NMR spectra (right) of non-hydrated zeolite H,Na-Y recorded at room temperature during the step by step hydration in a flow of nitrogen loaded with water.

tetrahedrally coordinated framework aluminum atoms ($\mathbf{Al^{IV}_{fr.}}$) becomes large and narrow upon adsorption of water. This is caused by the formation of $H^+(H_2O)_n$ complexes leading to a more symmetric local structure in the vicinity of the framework aluminum atoms in comparison with the aluminum atoms in the local structure of non-hydrated Brønsted acid sites [19]. In addition, a weak signal of octahedrally coordinated aluminum ($\mathbf{Al^{VI}_{fr.}}$) appears at ca. 0 ppm. This signal was also reported by Omegna *et.al.* [16]. In their model [16], some aluminum atoms coordinate to four framework oxygen atoms, one water molecule and one hydronium ion (H_3O^+). This assignment was supported by the occurrence of the ^{1}H MAS NMR signal of $Al(H_2O)_n^{3+}$ complexes in the spectra of samples upon adsorption of water and the constant framework n_{Si}/n_{Al} ratio of zeolites as determined by ^{29}Si MAS NMR spectroscopy (Chapter 7).

In the DFS enhanced ^{27}Al MQMAS NMR spectrum of rehydrated zeolite H,Na-Y (Figure 8.2a), a signal at 58 ppm with a second-order quadrupolar effect parameter of *SOQE* = 3.6 MHz (signal 1) and a signal at -2 ppm with *SOQE* = 2.4 MHz are observed. These signals are assigned to the above-mentioned $\mathbf{Al^{IV}_{fr.}}$ and $\mathbf{Al^{VI}_{fr.}}$ species occurring in the *in situ* ^{27}Al MAS NMR spectra. Their parameters and assignments are summarized in Table 8.1. These parameters agreed well with the results of ^{27}Al MQMAS NMR signals described in Chapter 6.

Table 8.1 Isotropic chemical shifts δ_{iso} and the second-order quadrupolar effect parameters *SOQE* of aluminum species in hydrated zeolites H,Na-Y (6 *equiv.*) and deH,Na-Y/81.5 (16 *equiv.*) determined by DFS enhanced ^{27}Al MQMAS NMR spectroscopy at B_0 = 9.4 T.

Sample	H,Na-Y	H,Na-Y	deH,Na-Y/81.5	deH,Na-Y/81.5	deH,Na-Y/81.5
Signal	1	2	1'	2'	3'
Assignment	$\mathbf{Al^{IV}_{fr.}}$	$\mathbf{Al^{VI}_{fr.}}$	$\mathbf{Al^{IV}_{fr.}}$	$\mathbf{Al^{IV}_{dis.}}$	$\mathbf{Al^{IV}_{fr.}}$ and $\mathbf{Al^{IV}_{ex.}}$
δ_{iso}/ ppm	58	-2	59	55	0
SOQE/ MHz	3.6	2.4	2.8	6.4	3.6
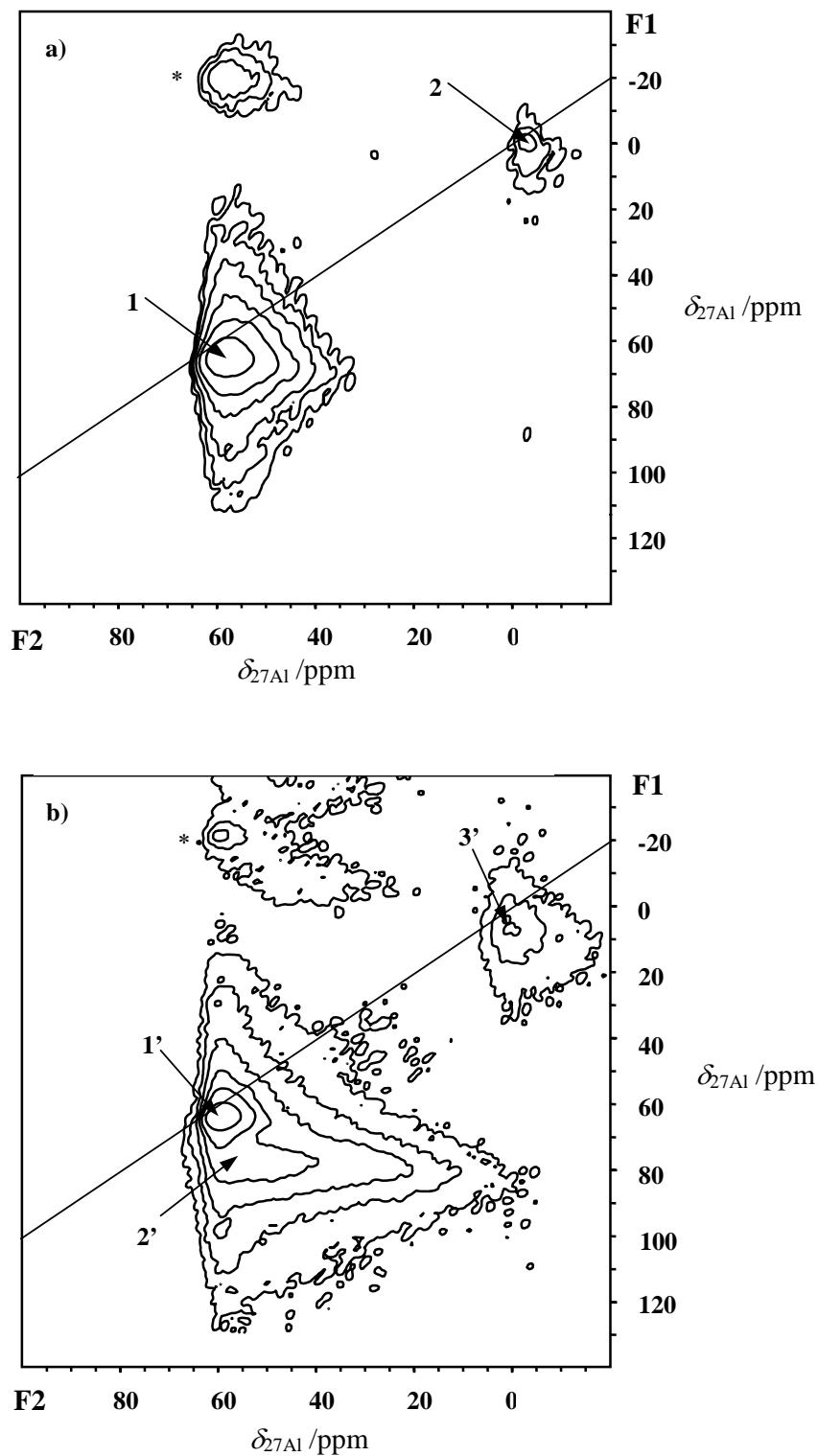
Figure 8.2 DFS enhanced ^{27}Al MQMAS NMR spectra of hydrated zeolites H,Na-Y (a) and deH,Na-Y/81.5 (b) recorded in a magnetic field of $B_0 = 9.4$ T. The parameters of these signals are summarized in Table 8.1.

Figure 8.3a shows the number of aluminum atoms in the *in situ* ^{27}Al MAS NMR spectra of zeolite H,Na-Y plotted as a function of the amount of adsorbed water molecules. Before the adsorption of water on zeolite H,Na-Y, ca. 5 tetrahedrally coordinated aluminum atoms per unit cell were observed in the spectrum, which agrees with the residual amount of Na$^+$ cations in zeolite H,Na-Y determined by atomic emission spectroscopy (AES-ICP, Perkin Elmer Plasma 400). At a loading of $0 < equiv. < 3$, the amount of detected aluminum atoms strongly increases (Figure 8.3a, dotted curve). However, no obvious influence on the amount of aluminum is observed at $equiv. > 3$. It should be noticed that ca. 52 aluminum atoms per unit cell were observed by ^{27}Al MAS NMR spectroscopy upon saturation with water is reached (Figure 8.3a, dotted curve). This value is close to the value of 52 aluminum atoms per unit cell determined by AES-ICP (Chapter 6).

To eliminate the effects of aluminum atoms compensated by Na$^+$ cations, the difference spectra of the *in situ* ^{27}Al MAS NMR spectra of zeolite H,Na-Y loaded with water (Figure 8.1b to 8.1f) and the ^{27}Al MAS NMR spectrum of non-hydrated and unloaded H,Na-Y (Figure 8.1a) is calculated. Using the parameters of aluminum species given in Table 8.1, these ^{27}Al MAS NMR difference spectra were decomposed, therefore, the number of each aluminum species are determined by their intensities. As shown by the solid curves in Figure 8.3a, 37 **Al$^{IV}_{fr.}$** atoms per unit cell and 9 **Al$^{VI}_{fr.}$** atoms per unit cell could be detected in the zeolite H,Na-Y upon the loading of water eventually. Generally, the framework n_{Si}/n_{Al} ratio can be calculated by the equation

$$n_{Si} / n_{Al} = (192 - n_{Al}^{fr.}) / n_{Al}^{fr.} \qquad\qquad (30)$$

where 192 is total number of T atoms in the zeolite (AES-ICP) and $n_{Al}^{fr.}$ is the number of aluminum atoms in the framework. However, the overlapping of the signals of $Al_{fr.}^{VI}$ species and octahedrally coordinated extra-framework aluminum makes the discussion of this value complicated. If it is assumed that all the octahedrally coordinated aluminum are at extra-framework position, the framework n_{Si}/n_{Al} ratio of 3.5 in zeolite hydrated zeolite

H,Na-Y is obtained. This value does not agree with the value of 2.8 obtained by ^{29}Si MAS NMR spectroscopy (Chapter 7).
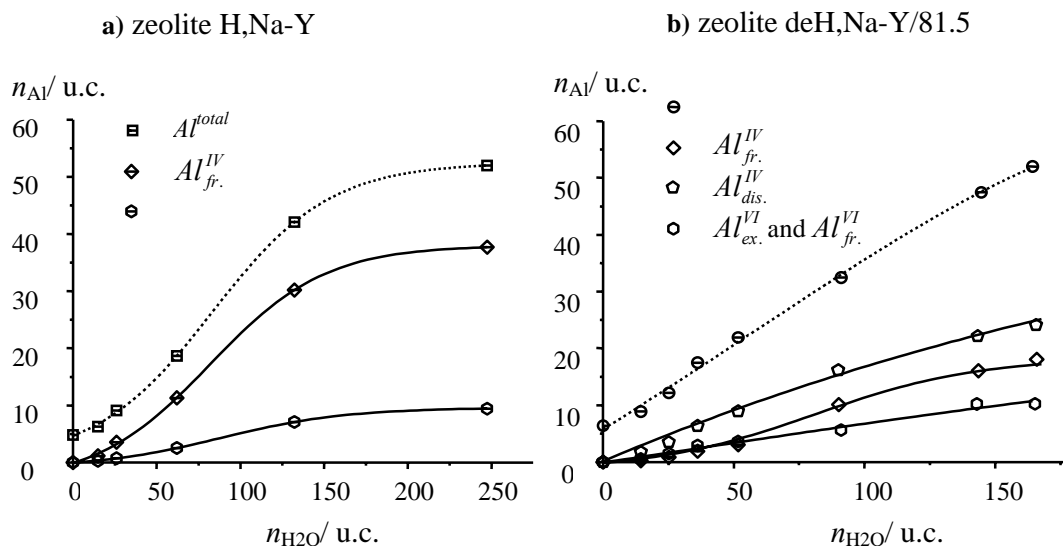
Figure 8.3 The amount of aluminum atoms observed in the *in situ* ^{27}Al MAS NMR spectra plotted as a function of the loading of water on zeolites H,Na-Y (a) and deH,Na-Y/81.5 (b). The dotted curves show the total amount of aluminum atoms. The amounts of different aluminum atoms upon adsorption of water are shown by solid curves.

8.2.2 *In situ* and *ex situ* MAS NMR Spectroscopic Investigations of Non-hydrated Zeolite deH,Na-Y/81.5 upon Water Adsorption

Figure 8.4 shows the *in situ* ^{1}H and ^{27}Al MAS NMR spectra of zeolite deH-Y/81.5 upon the adsorption of water. Bridging OH groups at 3.5 ppm, AlOH groups at 2.6 ppm, SiOH groups at 1.8 ppm, and AlOH groups at 0.6 ppm were observed in the ^{1}H MAS spectrum of zeolite deH-Y/81.5 before the adsorption of water. As described in Chapter 7, ca. 10.5 bridging OH groups per unit cell occur in non-hydrated zeolite deH-Y/81.5. Upon the loading of water molecules, the signal of water occurs in the range of 5.0 to 4.7 ppm (Figure 8.4a to 8.4f). In addition, a weak signal of Al(H$_2$O)$_n^{3+}$ complexes appears at 9.2 ppm for *equiv.* > 4.9. The assignments of these signals have been discussed in Section 8.2.1.
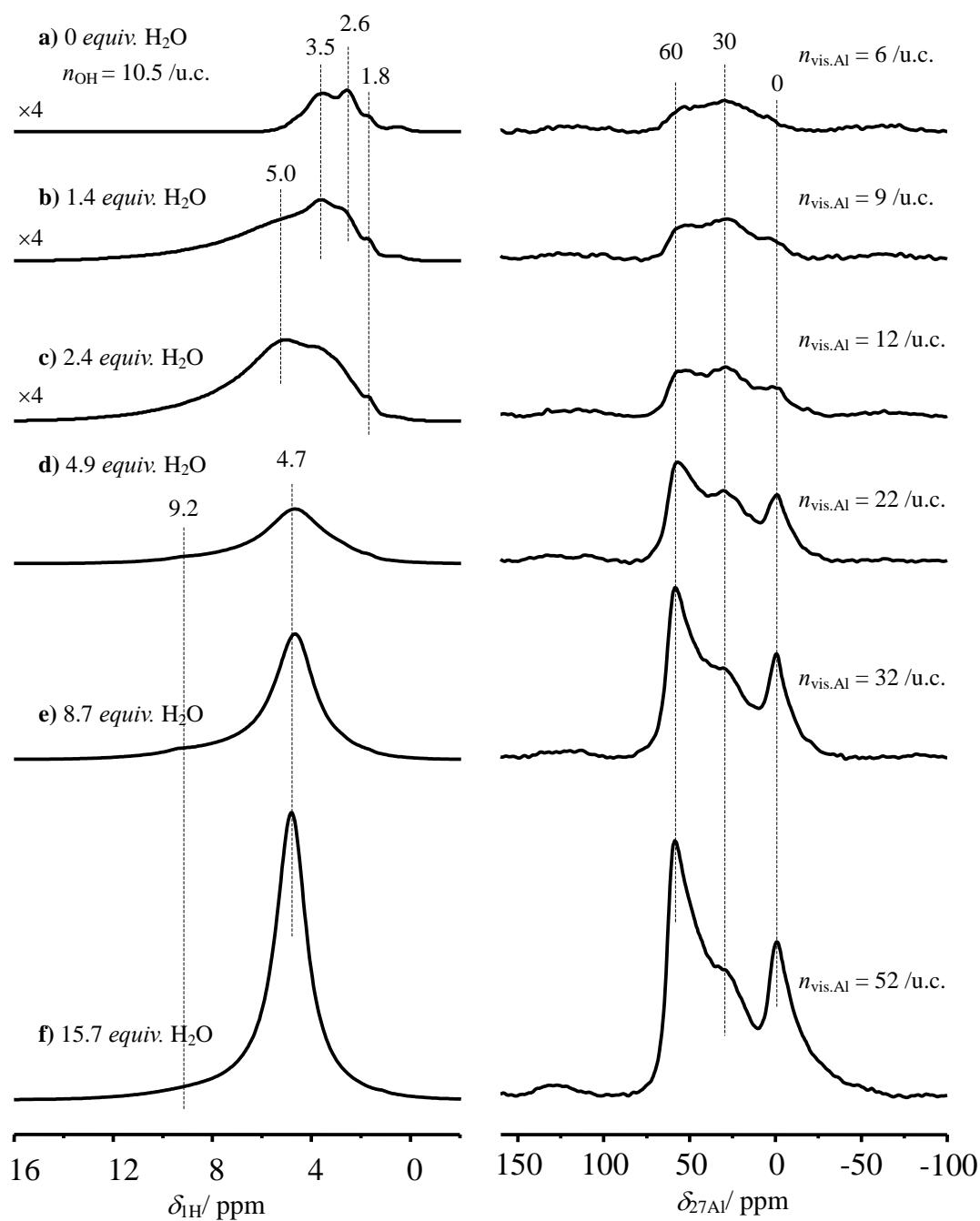
Figure 8.4 *In situ* ^{1}H (left) and ^{27}Al MAS NMR spectra (right) of non-hydrated zeolite deH,Na-Y/81.5 recorded at room temperature during the hydration in a flow of nitrogen loaded with water.

The *in situ* ^{27}Al MAS NMR spectra of zeolite deH-Y/81.5 obtained upon the loading of water are shown in Figure 8.4. To determine the quadrupole parameters of the aluminum

species, ^{27}Al MQMAS NMR experiments were carried out. In the DFS enhanced ^{27}Al MQMAS NMR spectrum of rehydrated zeolite H,Na-Y (Figure 8.2b), the signal 1', signal 2', and signal 3' can be observed. According to References [16, 100], the signals 1' to 3' are due to tetrahedrally coordinated framework aluminum atoms ($\mathbf{Al^{IV}_{fr.}}$) compensated in their negative charge by residual Na^+ cations or $H^+(H_2O)_n$ complexes, distorted tetrahedrally coordinated framework aluminum atoms ($\mathbf{Al^{IV}_{dis.}}$) compensated by aluminum cation, and octahedrally coordinated framework or extra-framework aluminum atoms ($\mathbf{Al^{VI}_{fr.}}$ and $\mathbf{Al^{VI}_{ex.}}$), respectively. The quadrupole parameters of these aluminum species are given in Table 8.1 and agree with these parameters in Chapter 6. Unfortunately, the different octahedrally coordinated aluminum species at framework or extra-framework positions could not be separated.

The total amount of aluminum atoms in zeolite deHNa-Y/81.5 as determined by *in situ* ^{27}Al MAS NMR spectroscopy increases linearly from ca. 6 to 52 aluminum atoms per unit cell as shown in Figure 8.2.b (dotted curve). The ^{27}Al MAS NMR difference spectra of zeolite deH,Na-Y upon adsorption of water were achieved by a similar way as the difference spectra of zeolite H,Na-Y in Section 8.2.1. Deconvolution of the spectra using the quadrupole parameters given in Table 8.1, indicates that up to 23 $\mathbf{Al^{IV}_{dis.}}$ atoms per unit cell, 16 $\mathbf{Al^{IV}_{fr.}}$ atoms per unit cell, and 12 $\mathbf{Al^{VI}_{fr.}}$ and $\mathbf{Al^{VI}_{ex.}}$ atoms per unit cell are affected by the water adsorption (Figure 8.2.b, solid curve). The framework n_{Si}/n_{Al} ratio of 3.8 calculated by Equation (30) does not agree with the value of 5.9 obtained by ^{29}Si MAS NMR spectroscopy (Chapter 7).

## 8.3 NMR Spectroscopic Investigations of Non-hydrated Zeolites upon Ammonia Adsorption

8.3.1 *In situ* and *ex situ* MAS NMR Spectroscopic Investigations of Non-hydrated Zeolite H,Na-Y upon Ammonia Adsorption

Figure 8.5, left, shows the *in situ* ^{1}H MAS NMR spectra of zeolite H,Na-Y recorded upon

loading with different amounts of ammonia (NH_3). The loading is given by *equiv.* = n_{NH3}/n_{OH} with n_{NH3} = (n_H-n_{OH})/3. For *equiv.* < 0.3, all ammonia molecules are protonated by Brønsted acid sites resulting in signals of ammonium ions at 7.6 and 6.4 ppm. For > 0.3 *equiv.*, different ^{1}H MAS NMR signals of ammonia and ammonium species are observed. Up to two signals appear at 5.7 to 3.3 ppm. According to Freude *et al.* [156] and Jacobs *et al.* [157], these ^{1}H MAS NMR signals were assigned to complexes of ammonia molecules and ammonium cations involved in a fast proton exchange (NH_3/NH_4^+). This assignment is supported by temperature-programmed desorption (TPD) and infrared spectroscopy (IR) of zeolite H-ZSM-5 upon ammonia adsorption at 293 K [158-160].

Figure 8.5, right, shows the ^{27}Al MAS NMR spectra of zeolite H,Na-Y loaded with the different amounts of ammonia. Upon adsorption of ammonia, a continuous increase of the signal of tetrahedrally coordinated framework aluminum atoms (**$Al^{VI}_{fr.}$**) can be observed. This is accompanied by an obvious decrease of the line width. The above-mentioned findings are due to the formation of ammonium ions and the deprotonation of the framework AlO_4 tetrahedra leading to a decrease of the quadrupolar interaction. The isotropic chemical shift δ_{iso} and the second-order quadrupolar effect parameter *SOQE* of this signal determined by DFS enhanced ^{27}Al MQMAS NMR spectrum (Figure 8.6a) are given in Table 8.2. In contrast to the spectrum of non-hydrated zeolite H,Na-Y recorded upon water adsorption, no signal of octahedrally coordinated aluminum occurs upon ammonia adsorption. It should be noticed that the *SOQE* value depends on the ammonia loadings and is 4.5 MHz for 1 *equiv.* and 3 MHz for 3 *equiv.*.

In Figure 8.7a, the total aluminum atoms observed by ^{27}Al MAS NMR spectroscopy are plotted as a function of the loading (dotted curve). The maximum number of aluminum atom reaches ca. 53 atoms per unit cell (Figure 8.7a, dotted curve). This number is close to the amount of 52 aluminum atoms per unit cell in the parent material determined by AES-ICP.
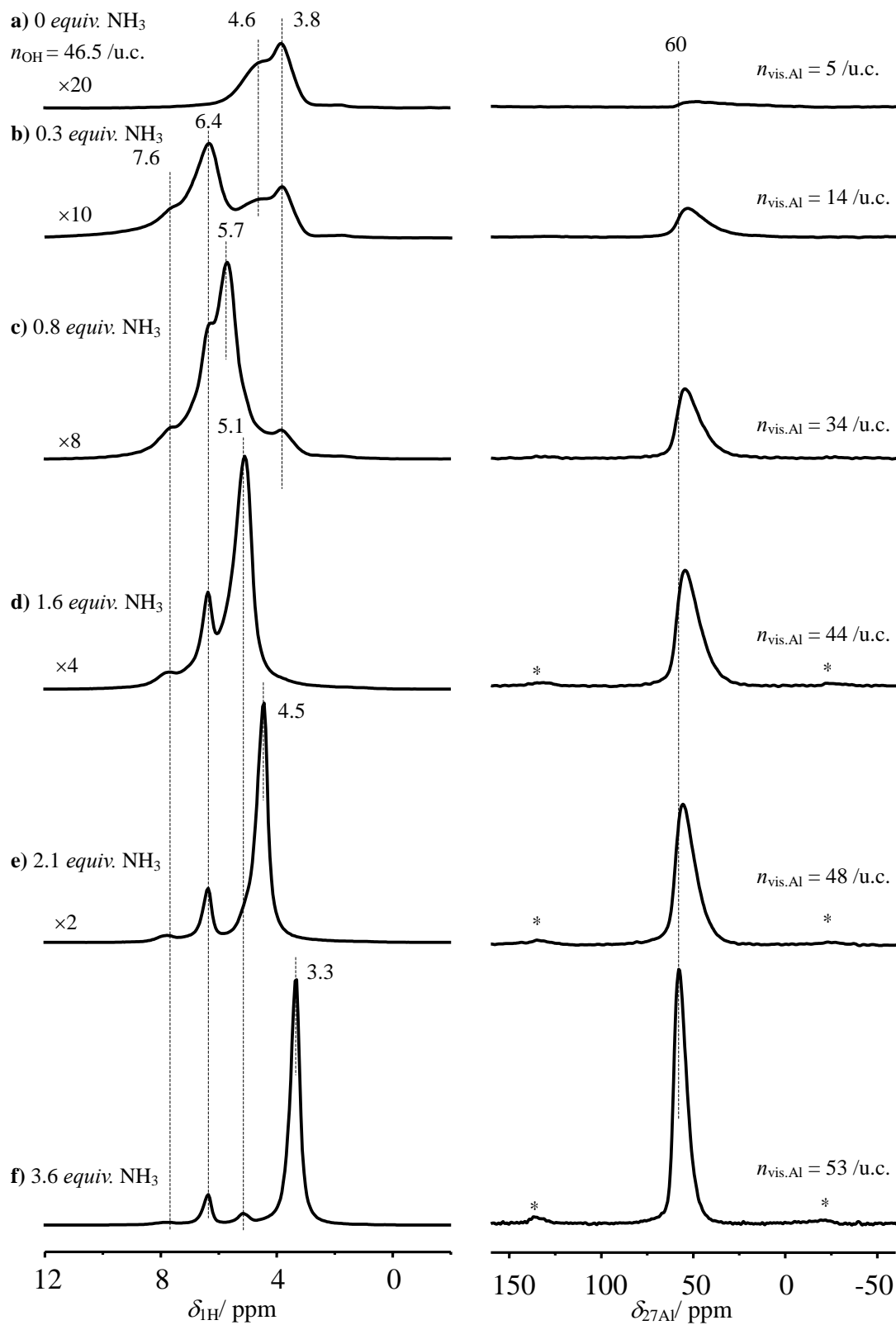
Figure 8.5 *In situ* ^{1}H (left) and ^{27}Al MAS NMR spectra (right) of non-hydrated zeolite H,Na-Y recorded at the room temperature upon adsorption of ammonia. Asterisks denote spinning sidebands.
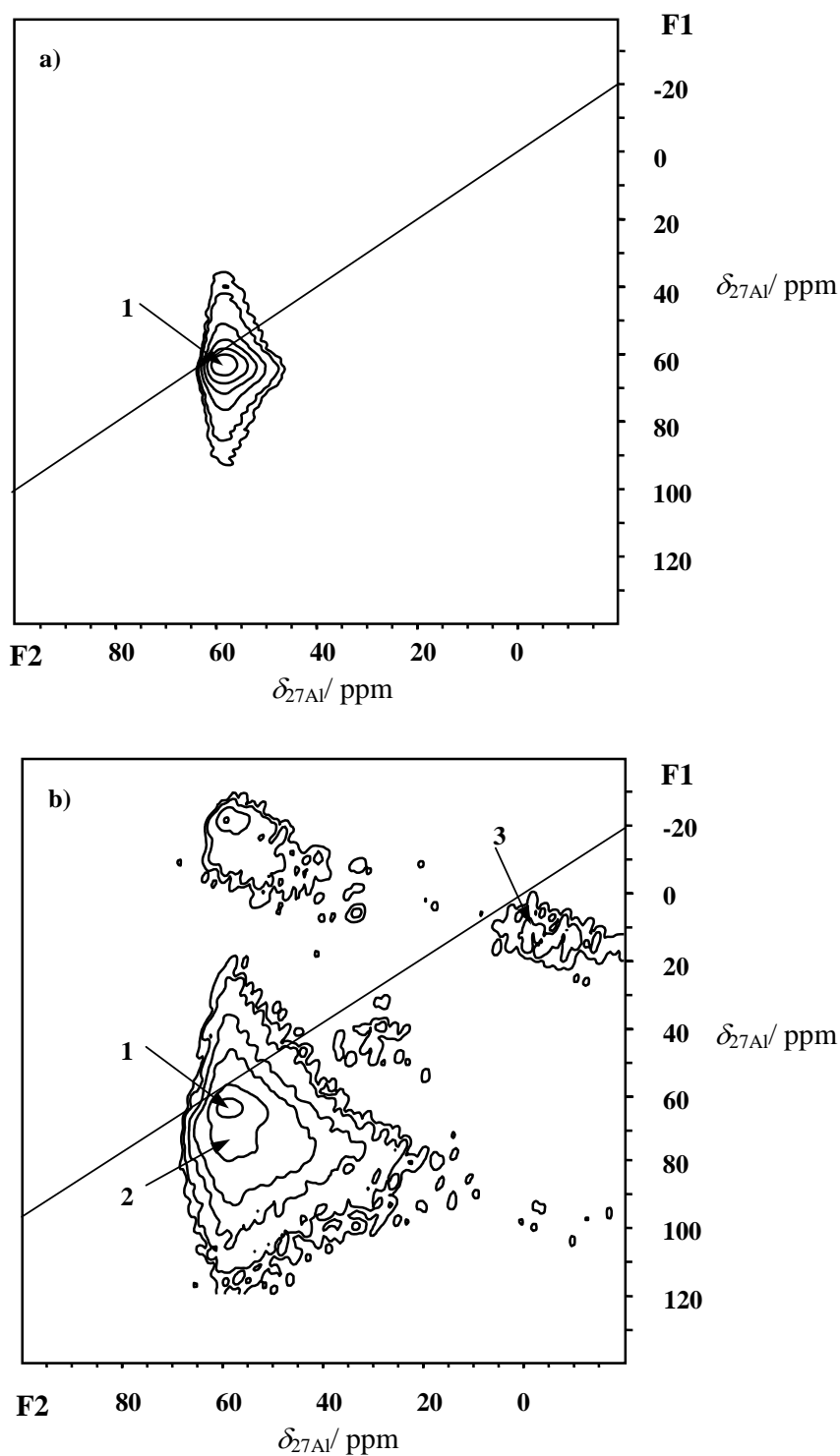
Figure 8.6 DFS enhanced ^{27}Al MQMAS NMR spectra of non-hydrated zeolites H,Na-Y loaded with ca. 3 *equiv.* ammonia (a) and deH,Na-Y/81.5 loaded with ca. 11 *equiv.* ammonia (b) and recorded at $B_0 = 9.4$ T. On both zeolites, the saturation of ammonia loading is reached. The parameters of these signals are summarized in Table 8.2.

Table 8.2 Isotropic chemical shifts δ_{iso} and the second-order quadrupolar effect parameters *SOQE* of aluminum species in zeolites H,Na-Y upon adsorption of ca. 3 *equiv.* ammonia and deH,Na-Y/81.5 upon adsorption of ca. 11 *equiv.* ammonia determined by DFS enhanced ^{27}Al MQMAS NMR spectroscopy at $B_0 = 9.4$ T.

Sample	H,Na-Y	deH,Na-Y/81.5	deH,Na-Y/81.5	deH,Na-Y/81.5
Signal	1	1	2	3
Assignment	$Al^{IV}_{fr.}$	$Al^{IV}_{fr.}$	$Al^{IV}_{dis.}$	$Al^{VI}_{ex.}$
δ_{iso}/ ppm	58	59	59	-3
SOQE/ MHz	3.0	3.1	5.2	3.1

a) zeolite H,Na-Y **b)** zeolite deH,Na-Y/81.5
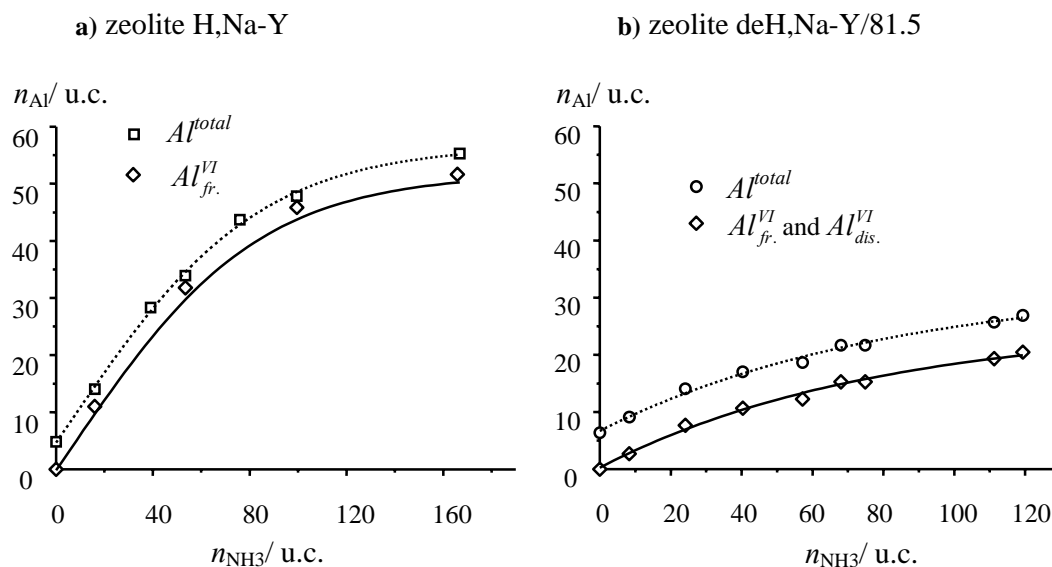
Figure 8.7 The amount of aluminum atoms observed in the *in situ* ^{27}Al MAS NMR spectra plotted as a function of the ammonia loadings on zeolites H,Na-Y (a) and deH,Na-Y/81.5 (b). The dotted curve shows the total amount of aluminum atoms. The amounts of aluminum atoms affected by ammonia adsorption are shown by solid curves.

According to Equation (30), the framework n_{Si}/n_{Al} ratio of 2.6 is obtained by ^{27}Al MAS NMR spectroscopy. The ^{27}Al MAS NMR difference spectra of zeolites H,Na-Y recorded upon adsorption of ammonia give the amount of aluminum atoms affected by ammonia as shown by the solid curve in Figure 8.7a. The amount of ammonia loading, which is determined by ^{1}H MAS NMR spectroscopy, indicates that ca. 3 ammonia molecules are

necessary to make one framework aluminum atom visible by ^{27}Al MAS NMR spectroscopy in the moderate magnetic fields.

Figure 8.8 shows the ^{29}Si MAS NMR spectra of non-hydrated zeolites H,Na-Y upon ammonia loading. Four signals of Si(nAl) species (n = 3, 2, 1, and 0) are well resolved in the ^{29}Si MAS NMR spectrum of zeolite H,Na-Y (Figure 8.8a). By the relative intensities of the Si(nAl) signals, the framework n_{Si}/n_{Al} ratio of 2.7 was calculated. This value agrees well with the framework n_{Si}/n_{Al} ratio of 2.6 obtained by ^{27}Al MAS NMR spectroscopy and the value of 2.7 determined by AES-ICP.

8.3.2   *In situ* and *ex situ* MAS NMR Spectroscopic Investigations of Non-hydrated Zeolite deH,Na-Y/81.5 upon Ammonia Adsorption

In Figure 8.9, the *in situ* ^{1}H and ^{27}Al MAS NMR spectra of zeolite deH,Na-Y/81.5 are recorded upon loading with different amounts of ammonia. As described in Chapter 7, 10.5 bridging OH groups per unit cell can be observed for the unloaded sample. With increasing ammonia loading, a ^{1}H MAS NMR signal occurs at 5.2 ppm and shifts to 2.7 ppm upon higher loadings. This signal is assigned to the NH_4^+/NH_3 complexes discussed in Section 8.3.1. In the ^{27}Al MAS NMR spectra of ammonia-loaded samples, a continuous increase of the signal of tetrahedrally coordinated framework aluminum atoms can be observed, while no signal of octahedrally coordinated framework aluminum atoms occurs.

Figure 8.6b shows the DFS enhanced ^{27}Al MQMAS NMR spectrum of zeolite deH,Na-Y upon loading of ammonia. Two signals of tetrahedrally coordinated framework aluminum and a very weak octahedrally coordinated framework aluminum atoms are separated. The quadrupole parameters obtained by ^{27}Al MQMAS spectroscopy are given in Table 8.2. Signals 1' to 3' are assigned to tetrahedrally coordinated framework aluminum atoms ($\mathbf{Al^{IV}_{fr.}}$) compensated by residual Na$^+$ cations or NH_4^+/NH_3 complexes, distorted tetrahedrally coordinated framework aluminum atoms ($\mathbf{Al^{IV}_{dis.}}$), and octahedrally coordinated extra-framework aluminum atoms ($\mathbf{Al^{VI}_{ex.}}$), respectively.
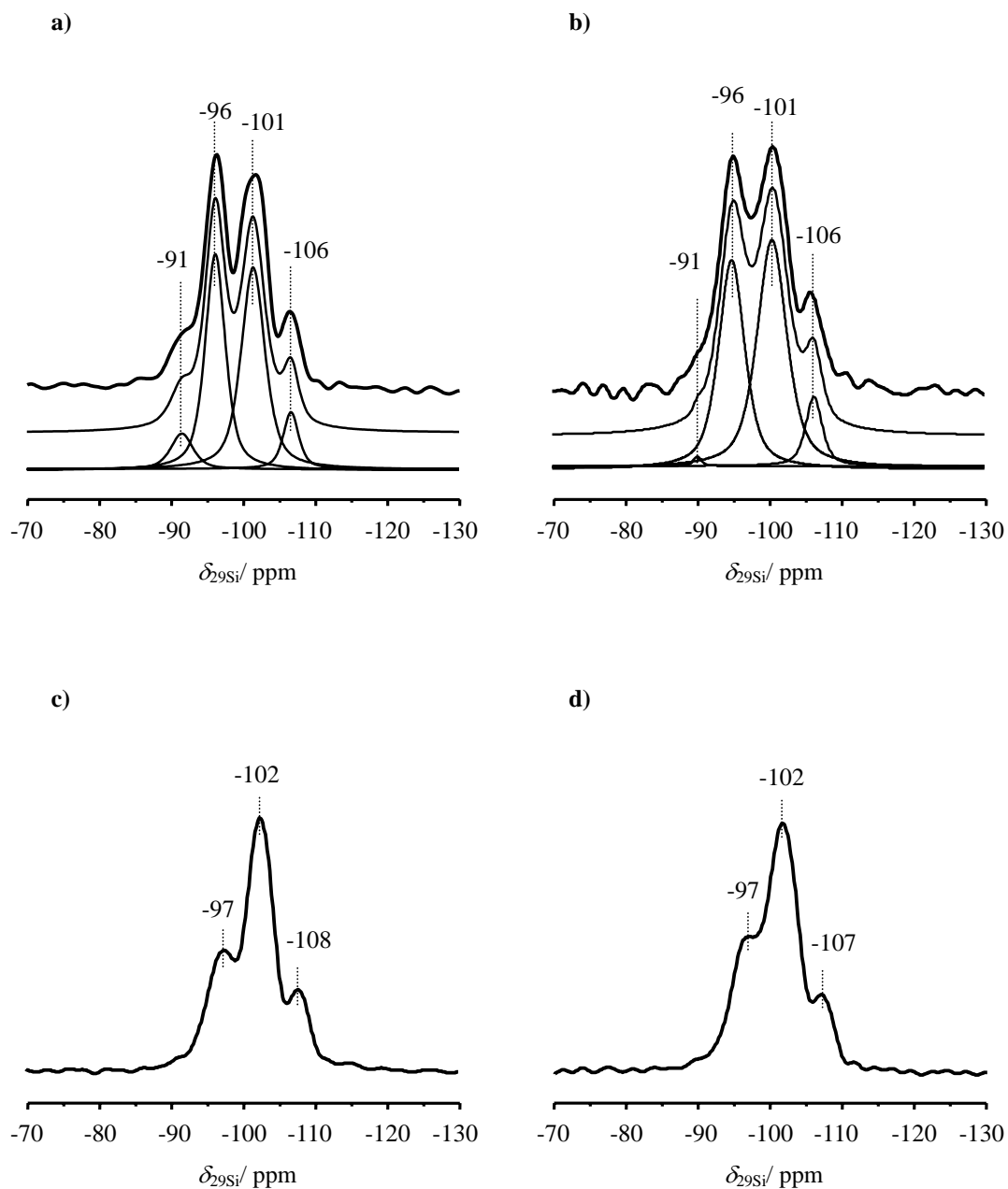
Figure 8.8 ^{29}Si MAS NMR spectra of non-hydrated zeolite H,Na-Y upon adsorption of ammonia (a), pyridine (b), acetonitrile (c), and acetone (d), respectively.
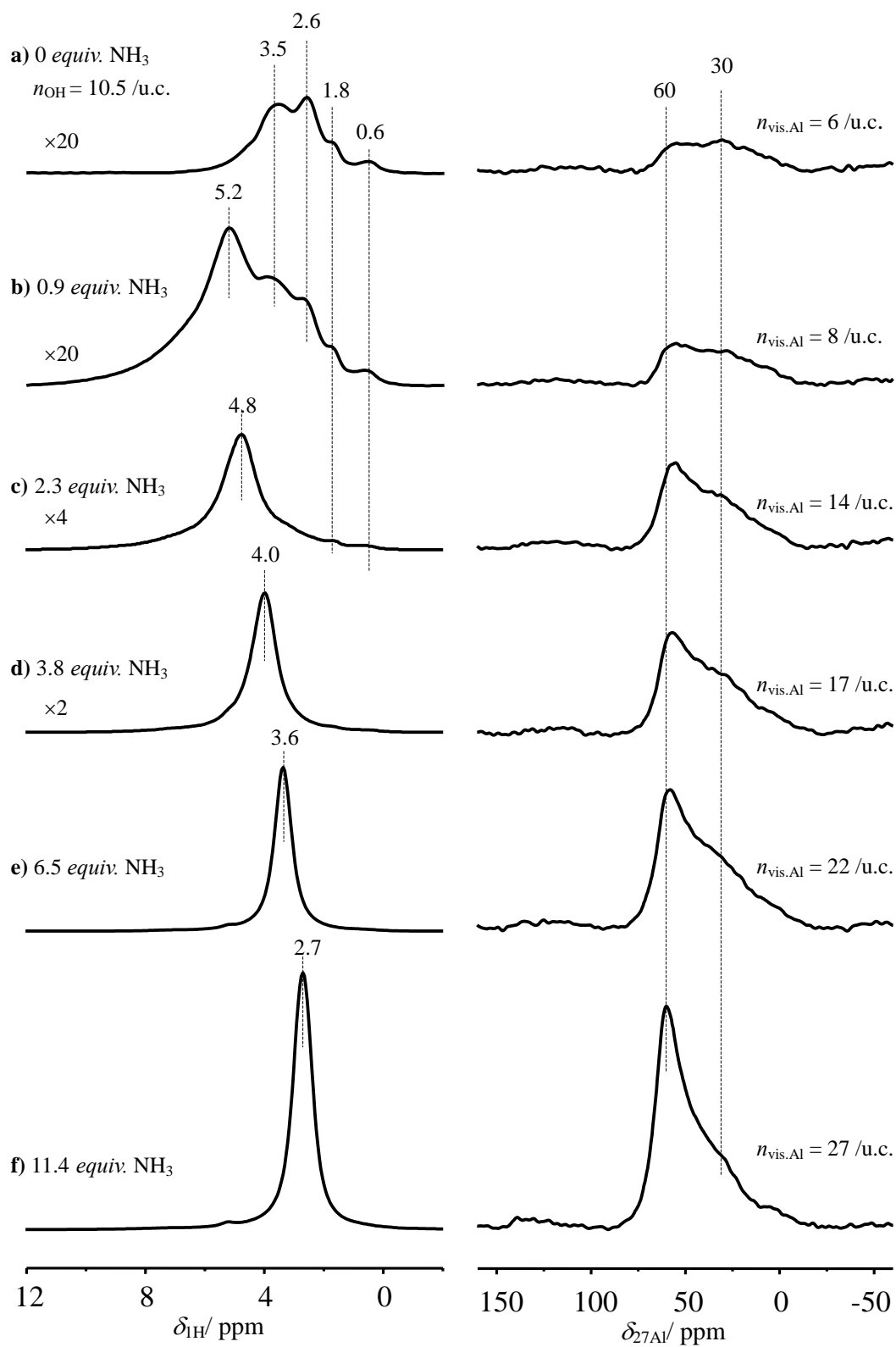
Figure 8.9 *In situ* ^{1}H (left) and ^{27}Al MAS NMR spectra (right) of non-hydrated zeolite deH,Na-Y/81.5 recorded at room temperature upon adsorption of ammonia.

In Figure 8.7b, the total amount of aluminum atoms, which are observed by *in situ* ^{27}Al MAS NMR spectroscopy, was plotted as a function of the ammonia loading (dotted line). The quantitative evaluation of the spectra indicates that ca. 27 aluminum atoms are visible by ^{27}Al MAS NMR spectroscopy after saturation by ammonia is reached. Since no $\mathbf{Al^{VI}_{fr.}}$ species is observed in the *in situ* ^{27}Al MAS NMR spectra, all the aluminum atoms (n_{Al}) are assumed to be $\mathbf{Al^{IV}_{fr.}}$ and $\mathbf{Al^{IV}_{dis.}}$. By Equation (30), a framework n_{Si}/n_{Al} ratio of 6.1 is obtained by ^{27}Al MAS NMR spectroscopy, which agrees with the value of 5.9 determined by ^{29}Si MAS NMR spectroscopy (Chapter 7). According to ^{1}H MAS NMR spectroscopy, ca. 120 ammonia molecules per unit cell must be loaded to make 22 aluminum atoms per unit cell visible in ^{27}Al MAS NMR spectra (Figure 8.7b solid line). Hence, ca. 5.5 ammonia molecules are required for 1 aluminum atom to reach a full decrease of the quadrupolar interaction in zeolite deH,Na-Y/81.5.

Since the hydration does not much influence the ^{29}Si MAS NMR spectrum of deH,Na-Y/81.5 (Chapter 7), the ^{29}Si MAS NMR spectrum of deH,Na-Y/81.5 upon ammonia adsorption is not discussed in the present work.

8.4 NMR Spectroscopic Investigations of Non-hydrated Zeolites upon Pyridine Adsorption

8.4.1 *In situ* and *ex situ* MAS NMR Spectroscopic Investigations of Non-hydrated Zeolite H,Na-Y upon Pyridine Adsorption

Figure 8.10, left, shows the *in situ* ^{1}H MAS NMR spectra of zeolite H,Na-Y loaded with different amounts of pyridine (C_5H_5N). The loading of pyridine was determined by ^{1}H MAS NMR spectroscopy and is given by *equiv.* $= n_{C5H5N}/n_{OH}$ with $n_{C5H5N} = (n_H - n_{OH})/5$, where n_H is the total number of hydrogen atoms, and n_{OH} is the number of bridging OH groups in zeolite H,Na-Y before pyridine adsorption. Upon starting the injection of pyridine, signals occur at 7.0 and 8.1 ppm due to ring protons of pyridine [161]. The signal of protons transferred from the zeolites to form pyridinium ions (PyrH[+]) is observed at ca. 16.5 ppm and has a line width

of ca. 4 ppm [143].
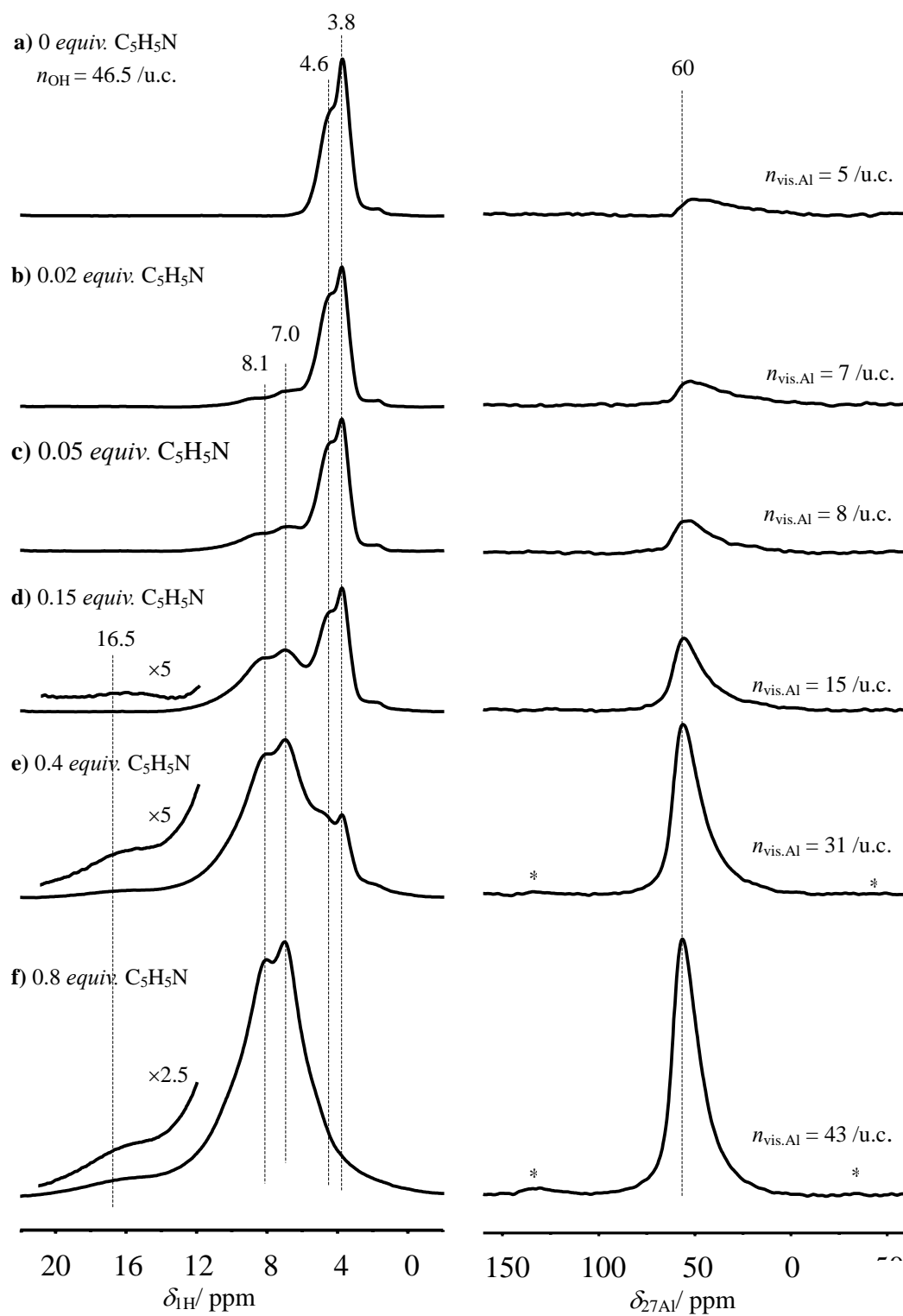
Figure 8.10 *In situ* ^{1}H (left) and ^{27}Al MAS NMR spectra (right) of non-hydrated zeolite H,Na-Y recorded at room temperature upon adsorption of pyridine.

The *in situ* ^{27}Al MAS NMR spectra of non-hydrated zeolite H,Na-Y in Figure 8.10, right, shows the effect of pyridine adsorption on the framework aluminum atoms. As discussed in Section 8.2.1, the ^{27}Al MAS NMR spectrum of the unloaded zeolite H,Na-Y shows a weak signal at ca. 55 ppm due to ca. 5 framework aluminum atoms per unit cell, which are compensated by residual extra-framework sodium cations. Upon loading of pyridine, a continuous increase of the signal of tetrahedrally coordinated framework aluminum can be observed, while no signal of octahedrally coordinated aluminum occurs. The reason lies in the formation of PyrH^{+} ions. This deprotonation of the framework recovers the symmetry of the distorted AlO$_4$ tetrahedra and creates the feasibility to detect framework aluminum atoms by ^{27}Al MAS NMR spectroscopy in the moderate magnetic fields. In order to obtain the quadrupole parameters of the aluminum species upon adsorption of pyridine, the DFS enhanced ^{27}Al MQMAS NMR spectrum shown in Figure 8.11a was recorded. Only one signal of tetrahedrally coordinated framework aluminum (signal 1) occurs in the ^{27}Al MQMAS spectrum of zeolite H,Na-Y. In Table 8.3, the quadrupole parameters obtained by ^{27}Al MQMAS NMR spectroscopy are given. These parameters support the above-mentioned assignment of signal 1.

The relationship between the amount of aluminum atoms visible in the *in situ* ^{27}Al MAS NMR spectra and the loading of pyridine is shown in Figure 8.12a. Upon adsorption of pyridine, the total amount of visible aluminum atoms increases linearly with the loading of pyridine (dotted line). Until the saturation is reached, ca. 43 aluminum atoms can be detected by ^{27}Al MAS NMR spectroscopy (dotted line). The ^{27}Al MAS NMR difference spectra give the numbers of pyridine-affected aluminum atoms as shown by the solid line in Figure 8.12a. It is interesting to note that 38 aluminum atoms per unit cell become visible by *in situ* ^{27}Al MAS NMR spectroscopy upon adsorption of 36 pyridine molecules. This finding indicates that 1 pyridine molecule is able to make 1 aluminum atom visible by ^{27}Al MAS NMR spectroscopy in moderate magnetic fields. In comparison with ca. 3 ammonia molecules necessary for 1 visible aluminum atom, it seems that pyridine is the better probe molecule for narrowing the ^{27}Al MAS NMR signal of the framework aluminum atoms. However, pyridine has an important disadvantage for this application. According to Equation (30), a framework
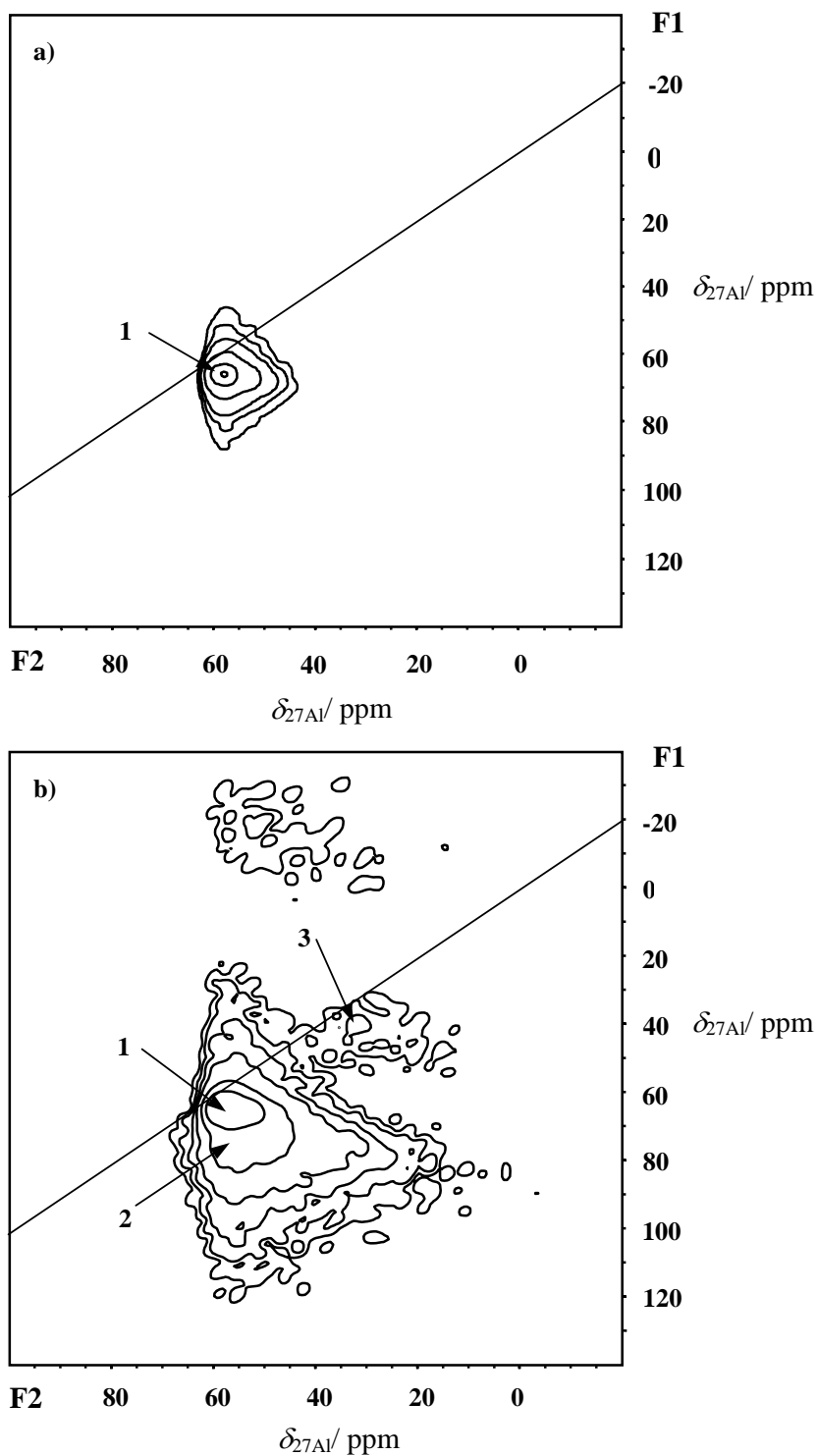
Figure 8.11 DFS enhanced ^{27}Al MQMAS NMR spectra of non-hydrated zeolites zeolite H,Na-Y (a) and zeolite deH,Na-Y (b) loaded with pyridine and recorded at $B_0 = 9.4$ T with the split-t_1-whole echo pulse sequence. On both zeolites, the saturation of pyridine loading is reached (< 1 *equiv.*). The parameters of these signals are summarized in Table 8.3.

n_{Si}/n_{Al} ratio of 3.5 is obtained by ^{27}Al MAS NMR spectroscopy of zeolite H,Na-Y loaded with pyridine. This value is far from the value of 2.7 determined by AES-ICP. This discrepancy might be due to the size of pyridine, which restricts the adsorption capacity for this molecule and hinders the detection of all framework aluminum atoms by ^{27}Al MAS NMR spectroscopy in moderate magnetic fields.

The ^{29}Si MAS NMR spectrum of zeolite H,Na-Y recorded upon the adsorption of pyridine is shown in Figure 8.8b. The framework n_{Si}/n_{Al} ratio of 3.0 was calculated according to the relative intensities of the signals of Si(nAl) species. This value is larger than the expected value of 2.7 determined by AES-ICP. The deviation is caused by the limitation in the pyridine adsorption capacity. In comparison with the ^{29}Si MAS NMR spectrum of non-hydrated zeolite H,Na-Y (Chapter 7 and Reference [138]), the ^{29}Si NMR signals of the silicon atoms in the local structure of Brønsted acid sites interacting with pyridine shift to lower field. As observed in the ^{29}Si MAS NMR spectrum of zeolite H,Na-Y loaded with ammonia, a reasonable resolution of ^{29}Si MAS NMR signals can be achieved upon pyridine adsorption. In the case of pyridine loaded sample, the ^{29}Si MAS NMR signals of silicon atoms in the local structure of the Brønsted acid sites, which do not interact with pyridine, are low-field shifted. These silicon sites are responsible for the deviation of the framework n_{Si}/n_{Al} ratio determined by ^{27}Al and ^{29}Si MAS NMR spectroscopy.

Table 8.3 Isotropic chemical shifts δ_{iso} and the second-order quadrupolar effect parameters *SOQE* of aluminum species in zeolites H,Na-Y and deH,Na-Y/81.5 determined upon adsorption of pyridine (< 1 *equiv.*) by DFS enhanced ^{27}Al MQMAS NMR spectroscopy at B_0 = 9.4 T.

Sample	H,Na-Y	deH,Na-Y/81.5	deH,Na-Y/81.5	deH,Na-Y/81.5
Signal	1	1	2	3
Assignment	$Al^{IV}_{fr.}$	$Al^{IV}_{fr.}$	$Al^{IV}_{dis.}$	$Al^{V}_{ex.}$
δ_{iso}/ ppm	58	57	56	33
SOQE/ MHz	3.8	4.0	5.8	5.2

a)   b)

n_{Al}/ u.c. n_{Al}/ u.c.
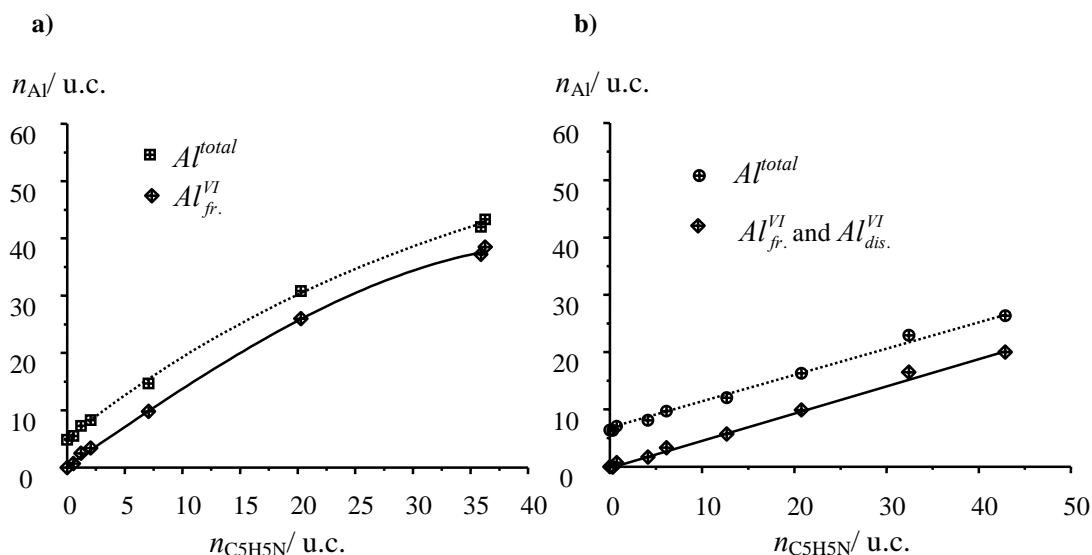
Figure 8.12 The amount of aluminum atoms observed in the *in situ* ^{27}Al MAS NMR spectra plotted as a function of the pyridine loadings on zeolites H,Na-Y (a) and deH,Na-Y/81.5 (b). The dotted curve shows the total amount of aluminum atoms. The amounts of aluminum atoms affected by pyridine adsorption are shown by solid curves.

8.4.2 *In situ* and *ex situ* MAS NMR Spectroscopic Investigations of Non-hydrated Zeolite deH,Na-Y/81.5 upon Pyridine Adsorption

Figure 8.13 shows the *in situ* ^{1}H and ^{27}Al MAS NMR spectra of zeolite deH,Na-Y/81.5 recorded upon different loadings of pyridine. ^{1}H MAS NMR signals occurring at 1.8, 2.6, and 3.5 ppm in the spectrum of unloaded zeolite deH,Na-Y/81.5 (Figure 8.13a) are assigned to SiOH, AlOH, and bridging OH groups, respectively (Chapter 7). Upon the injection of pyridine, ^{1}H MAS NMR signals appeared at 6.9, and 8.1 ppm, due to ring protons of pyridine and 14.1 ppm caused by pyridinium ions (PyrH[+]) [143, 161]. In the ^{27}Al MAS NMR spectra of the pyridine-loaded samples, again a continuous increase of the signal of tetrahedrally coordinated framework aluminum can be observed. No signal of octahedrally coordinated aluminum occurs.

The DFS enhanced [27]Al MQMAS spectrum of pyridine-loaded zeolite deH,Na-Y/81.5 is shown in Figure 8.10b. Two signals of tetrahedrally coordinated aluminum and a very weak signal of five-fold coordinated aluminum occur. The quadrupole parameters of these signals

are given in Table 8.3. According to these parameters, signals 1' to 3' are assigned to tetrahedrally coordinated framework aluminum atoms ($\mathbf{Al^{IV}_{fr.}}$)compensated by residual Na$^+$ cations or PyrH$^+$ complexes, distorted tetrahedrally coordinated framework aluminum atoms ($\mathbf{Al^{IV}_{dis.}}$), and five-fold coordinated extra-framework aluminum atoms ($\mathbf{Al^{V}_{ex.}}$), respectively.
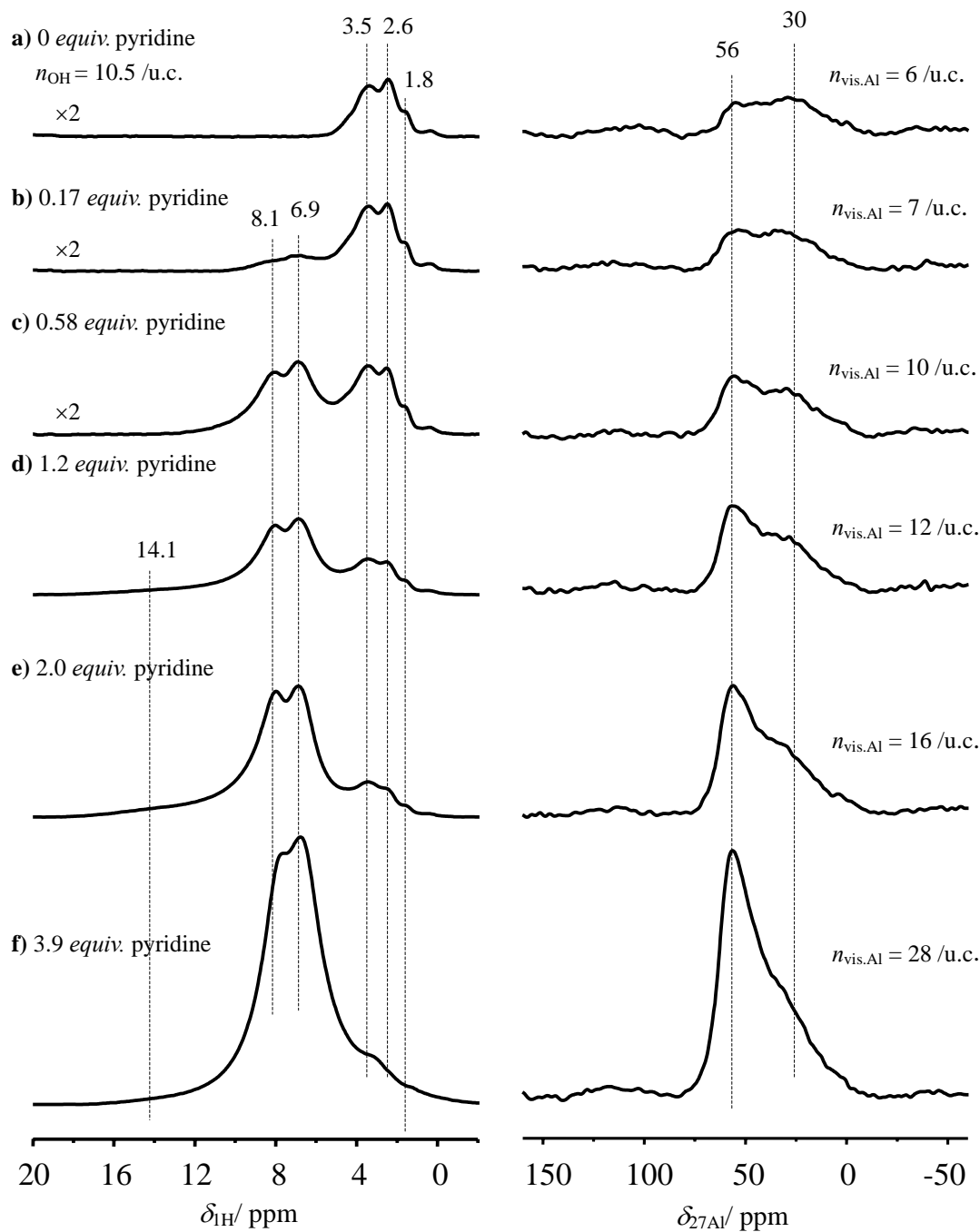
Figure 8.13 *In situ* ^{1}H (left) and ^{27}Al MAS NMR spectra (right) of non-hydrated zeolite deH,Na-Y/81.5 recorded at room temperature upon adsorption of pyridine.

Figure 8.12b shows the relationship between the amount of adsorbed pyridine and aluminum atoms affected by these probe molecules in zeolite deH,Na-Y/81.5. The maximum number of adsorbed pyridine molecules in zeolite deH,Na-Y is ca. 40 pyridine molecules per unit cell, which is close to 37 pyridine molecules per unit cell observed in zeolite H,Na-Y. This finding indicates that the pyridine adsorption capacity is the main reason of the deviation of the framework n_{Si}/n_{Al} ratios obtained by ^{27}Al and [27]Si MAS NMR spectroscopy discussed in Section 8.4.1. The numbers of pyridine-affected aluminum atoms obtained by the *in situ* ^{27}Al MAS NMR spectroscopy are shown in Figure 8.12b, solid line. It is important to note that the number of pyridine-affected aluminum atoms of zeolite deH,Na-Y/81.5 of 28 aluminum atoms per unit cell is close to the amount of framework aluminum of 27 aluminum atoms per unit cell as determined by ^{29}Si MAS NMR spectroscopy in Chapter 7. This indicates that most of aluminum atoms affected by pyridine are due to tetrahedrally coordinated framework aluminum atoms ($\mathbf{Al^{IV}_{fr.}}$ and $\mathbf{Al^{IV}_{dis.}}$), and the amount of five-fold coordinated $\mathbf{Al^{V}_{ex.}}$ species is very small. This agrees with the above-mentioned result of ^{27}Al MQMAS NMR spectroscopy.

8.5   NMR Spectroscopic Investigations of Non-hydrated Zeolites Y upon Acetonitrile and Acetone Adsorption

8.5.1   *In situ* and *ex situ* MAS NMR Spectroscopic Investigations of Non-hydrated Zeolite H,Na-Y upon Acetonitrile Adsorption

In Figure 8.14, the *in situ* ^{1}H and ^{27}Al MAS NMR spectra of zeolite H,Na-Y upon adsorption of acetonitrile (CH_3CN) are depicted. The equivalent number of acetonitrile is defined by *equiv.* $= n_{CNCH3}/n_{OH}$ with $n_{CNCH3} = (n_H - n_{OH})/3$, where n_H is the total number of hydrogen atoms detected by ^{1}H MAS NMR spectroscopy, and n_{OH} is the number of bridging OH groups in unloaded zeolite H,Na-Y. Upon loading of acetonitrile, two ^{1}H MAS NMR signals appear at 1.9 and 9.3 ppm. The appearance of these two signals is accompanied by a continuous decrease of the signals of bridging OH groups at 3.8 and 4.6 ppm. The two signals at 1.9 and 9.3 ppm are assigned to the protons in acetonitrile [161] and the hydroxyl protons of bridging

OH groups, which are bonded to acetonitrile [162], respectively.
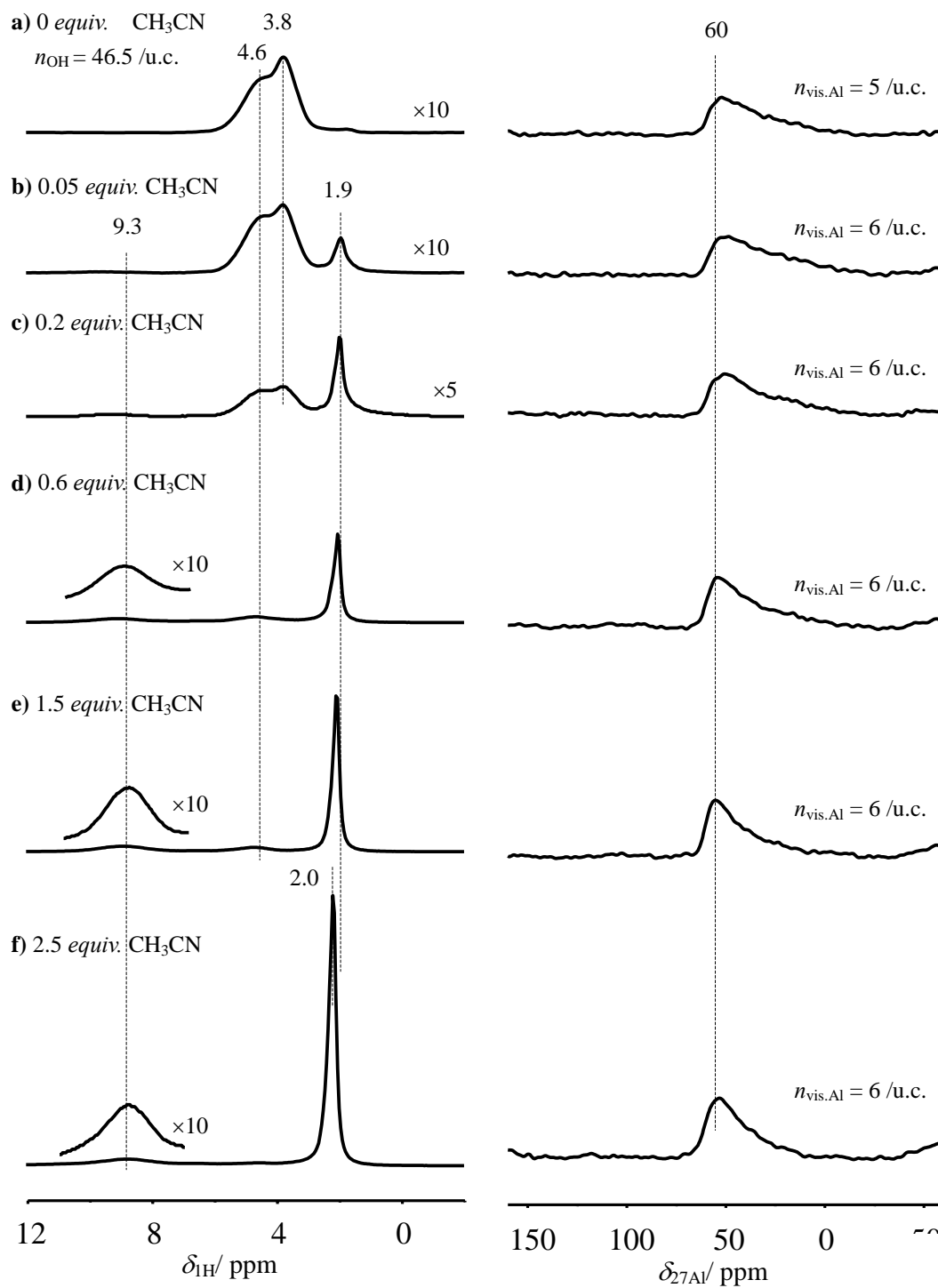
Figure 8.14 *In situ* ^{1}H (left) and ^{27}Al MAS NMR spectra (right) of non-hydrated zeolite H,Na-Y recorded at room temperature upon adsorption of acetonitrile.

In the ^{27}Al MAS NMR spectrum of unloaded zeolite H,Na-Y, a single signal of tetrahedrally coordinated framework aluminum atoms compensated by residual extra-framework sodium cations occurs at ca. 60 ppm. Upon the adsorption of acetonitrile, no significant changes are observed in the *in situ* ^{27}Al MAS NMR spectra (Figure 8.14, right). In Figure 8.15a, the numbers of aluminum atoms visible by ^{27}Al MAS NMR spectroscopy are plotted as a function of the acetonitrile loading. This quantitative evaluation shows that the number of aluminum atoms visible by ^{27}Al MAS NMR spectroscopy in the moderate magnetic fields keeps constant upon the loading of acetonitrile, even for the saturated sample. Therefore, no valuable information on the framework compositions can be provided by the ^{27}Al MAS NMR spectroscopy using the above-mentioned probe molecule.
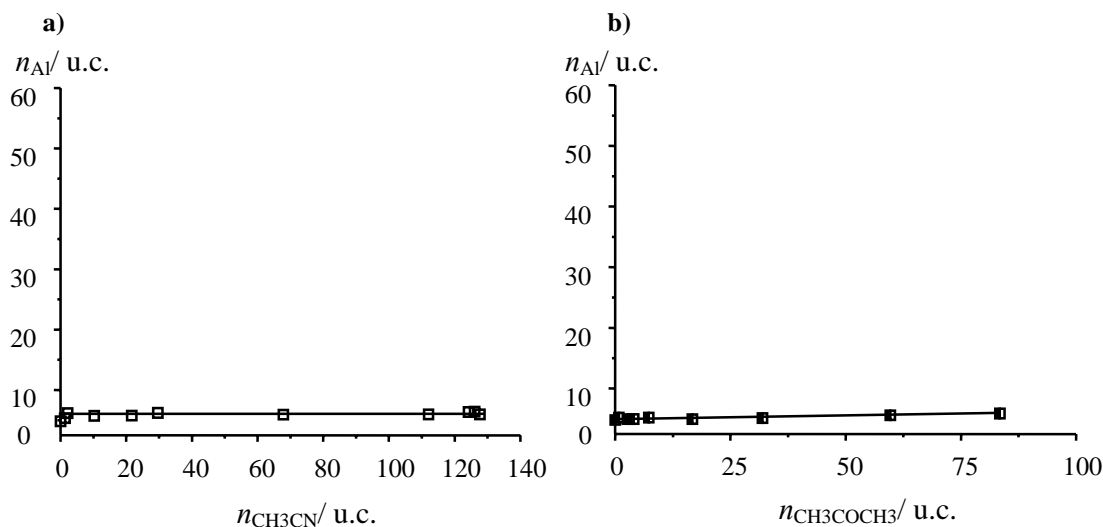

Figure 8.15 The totol amounts of aluminum atoms observed in the *in situ* ^{27}Al MAS NMR spectra plotted as a function of the acetonitrile (a) and acetone (b) loadings on zeolite H,Na-Y.

In order to investigate the influence of acetonitrile on aluminum species, higher magnetic fields are required. Figure 8.16a shows the DFS enhanced ^{27}Al MQMAS NMR spectroscopy of zeolite H,Na-Y upon adsorption of acetonitrile recorded at $B_0 = 17.6$ T. Four signals of different aluminum species are well resolved. The quadrupole parameters of these signals are summarized in Table 8.4. Signals 1 and 2 are assigned to the tetrahedrally coordinated framework aluminum compensated by residual extra-framework sodium cations
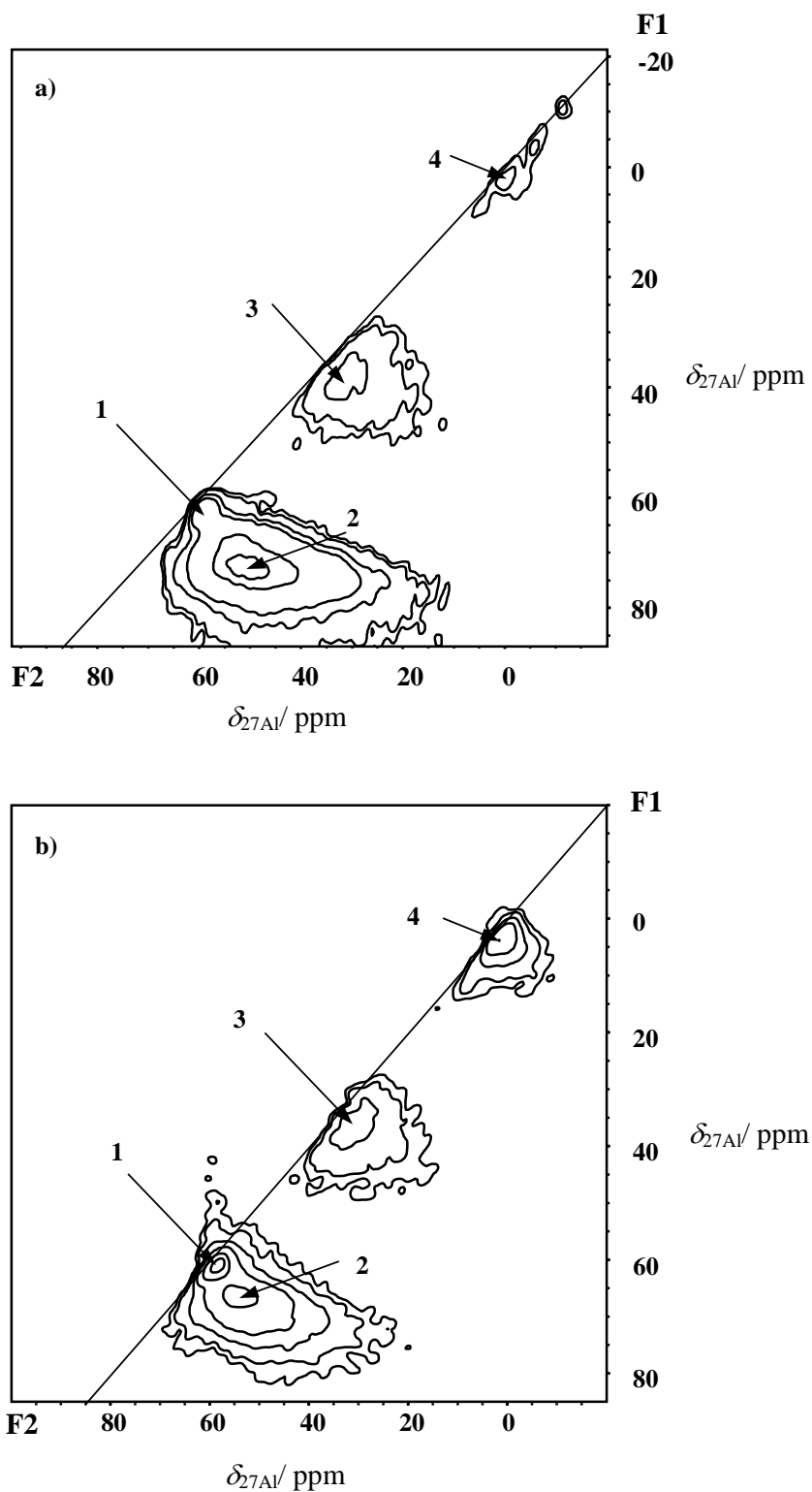
Figure 8.16 DFS enhanced ^{27}Al MQMAS NMR spectra of non-hydrated zeolite H,Na-Y loaded with ca. 2 *equiv.* acetonitrile (a) and ca. 2 *equiv.* acetone (b) recorded at $B_0 = 17.6$ T with the split-t_1-whole echo pulse sequence. In both of cases, the saturations are reached. The parameters of these signals are summarized in Table 8.4.
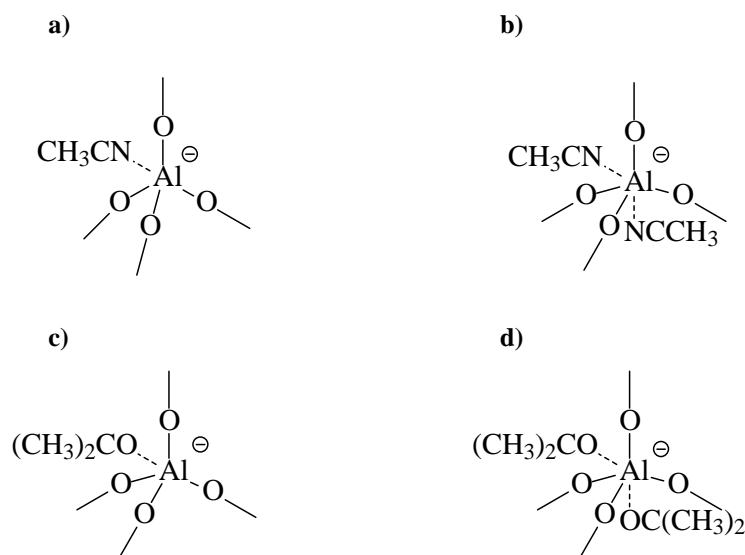
($\mathbf{Al^{IV}}$/Na^+) and in the local structure of Brønsted acid sites ($\mathbf{Al^{IV}}$/H^+). In comparison with the *SOQE* value of 16 MHz of $\mathbf{Al^{IV}}$/H^+ species in unloaded zeolite H,Na-Y [163], the *SOQE* value of signal 2 decreases to 12 MHz upon adsorption of acetonitrile, which is due to the effect of hydrogen bonds. In addition, two signals of five-fold coordinated and octahedrally coordinated aluminum species ($\mathbf{Al^{V}_{fr.}}$ and $\mathbf{Al^{VI}_{fr.}}$) occur in the DFS enhanced ^{27}Al MQMAS NMR spectrum of zeolite H,Na-Y upon acetonitrile loading. Because ca. 2 acetonitrile molecules per unit SiOHAl group were loaded, the signals of $\mathbf{Al^{V}_{fr.}}$ and $\mathbf{Al^{VI}_{fr.}}$ species may be caused by a coordination of nitrogen atoms in acetonitrile to framework aluminum atoms. Possible configurations are shown in Schemes 8.1a and 8.1b. Figure 8.17a shows the ^{27}Al MAS NMR spectrum of zeolite H,Na-Y loaded with acetonitrile, which was recorded at $B_0 =$ 17.4 T with a high spinning speed of 30 kHz. The simulation of the spectrum indicates that the content of $\mathbf{Al^{V}_{fr.}}$ and $\mathbf{Al^{VI}_{fr.}}$ species is ca. 5 % for each species.
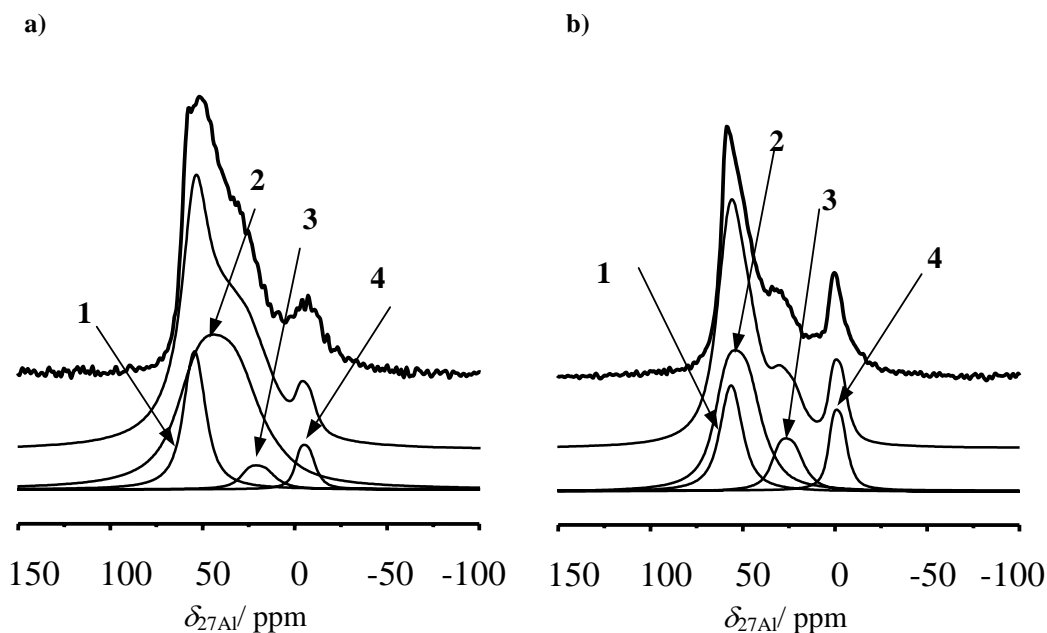
Figure 8.17 The ^{27}Al MAS NMR spectra of non-hydrated zeolite H,Na-Y upon adsorption of ca. 2 *equiv.* acetonitrile (a) and ca. 2 *equiv.* acetone (b) were recorded with spinning rate of 30 kHz at $B_0 =$ 17.6 T. The experimental spectra (top) are compared with the simulated spectra (bottom).

Table 8.4 Isotropic chemical shifts δ_{iso} and the second-order quadrupolar effect parameters *SOQE* of aluminum atoms in zeolites H,Na-Y determined upon adsorption of ca. 2 *equiv.* acetonitrile by DFS enhanced ^{27}Al MQMAS NMR spectroscopy at $B_0 = 17.6$ T.

Signal	1	2	3	4
Assignment	Al^{IV}/Na^+	Al^{IV}/H^+	$Al^V_{fr.}$	$Al^{VI}_{fr.}$
δ_{iso}/ ppm	60	65	30	0
SOQE/ MHz	5.1	12.0	7.6	3.6

Scheme 8.1

The ^{29}Si MAS NMR spectrum of zeolite H,Na-Y recorded upon acetonitrile loading is shown in Figure 8.8c. Three ^{29}Si MAS NMR signals occur at -97, -102, and -108 ppm. This spectrum is similar to the ^{29}Si MAS spectrum of unloaded zeolite H,Na-Y in Chapter 7 and Reference [138]. This indicates that the hydrogen bonds of acetonitrile with bridging OH groups don't suppress the low-field shift of ^{29}Si MAS NMR signals of Si(nAl) species in non-hydrated zeolite Y.

8.5.2   *In situ* and *ex situ* MAS NMR Spectroscopic Investigations of Non-hydrated Zeolite H,Na-Y upon Acetone Adsorption

Figure 8.18 shows the *in situ* ^{1}H and ^{27}Al MAS NMR spectra of zeolite H,Na-Y recorded upon adsorption of acetone (CH_3COCH_3). The equivalent number is given by *equiv.* = $n_{acetone}/n_{OH}$ with $n_{acetone} = (n_H-n_{OH})/6$, where n_H is the total number of hydrogen atoms detected by ^{1}H MAS NMR spectroscopy, and n_{OH} is the number of bridging OH groups in unloaded zeolite H,Na-Y. Two ^{1}H MAS NMR signals of bridging OH groups at 3.8 and 4.6 ppm are observed in the spectrum of the unloaded material (Figure 8.18a). Upon loading of acetone, the above-mentioned two signals shift to 12.0 ppm (Figure 8.18b to 8.18f), which indicates the formation of hydrogen bonds [164]. In addition, a ^{1}H MAS NMR signal occurs at 2.2 ppm due to methyl protons in the acetone molecules [161].

In the *in situ* ^{27}Al MAS NMR spectrum of unloaded zeolite H,Na-Y, a signal of tetrahedrally coordinated aluminum atoms compensated by the residual extra-framework sodium cations appears at ca. 60 ppm. As in the case of zeolite H,Na-Y recorded upon acetonitrile loading, no significant changes occur in the ^{27}Al MAS NMR spectra of zeolite H,Na-Y upon adsorption of acetone. The quantitative evaluation of the *in situ* ^{27}Al MAS NMR spectra shows that the number of aluminum atoms visible by ^{27}Al MAS NMR spectroscopy in moderate magnetic fields, only slightly increases from ca. 5 to ca. 7 atoms per unit cell after the maximum loading of acetone is reached (Figure 8.15b).

The DFS enhanced ^{27}Al MQMAS NMR spectrum of zeolite H,Na-Y recorded upon adsorption of acetone at $B_0 = 17.6$ T is shown in Figure 8.16b. Four aluminum species can be distinguished. The quadrupole parameters of each species are summarized in Table 8.5. Two signals at ca. 60 ppm, signals 1 and 2, are assigned to tetrahedrally coordinated framework aluminum atoms compensated by residual extra-framework sodium cations ($\mathbf{Al^{IV}}/Na^+$) and in the local structure of Brønsted acid sites ($\mathbf{Al^{IV}}/H^+$), respectively. For $\mathbf{Al^{IV}}/H^+$ species in zeolite H,Na-Y, the *SOQE* value declines from 16 to 9.4 MHz upon adsorption of acetone [163]. This is caused by the formation of hydrogen bonds of bridging OH groups with acetone molecules.
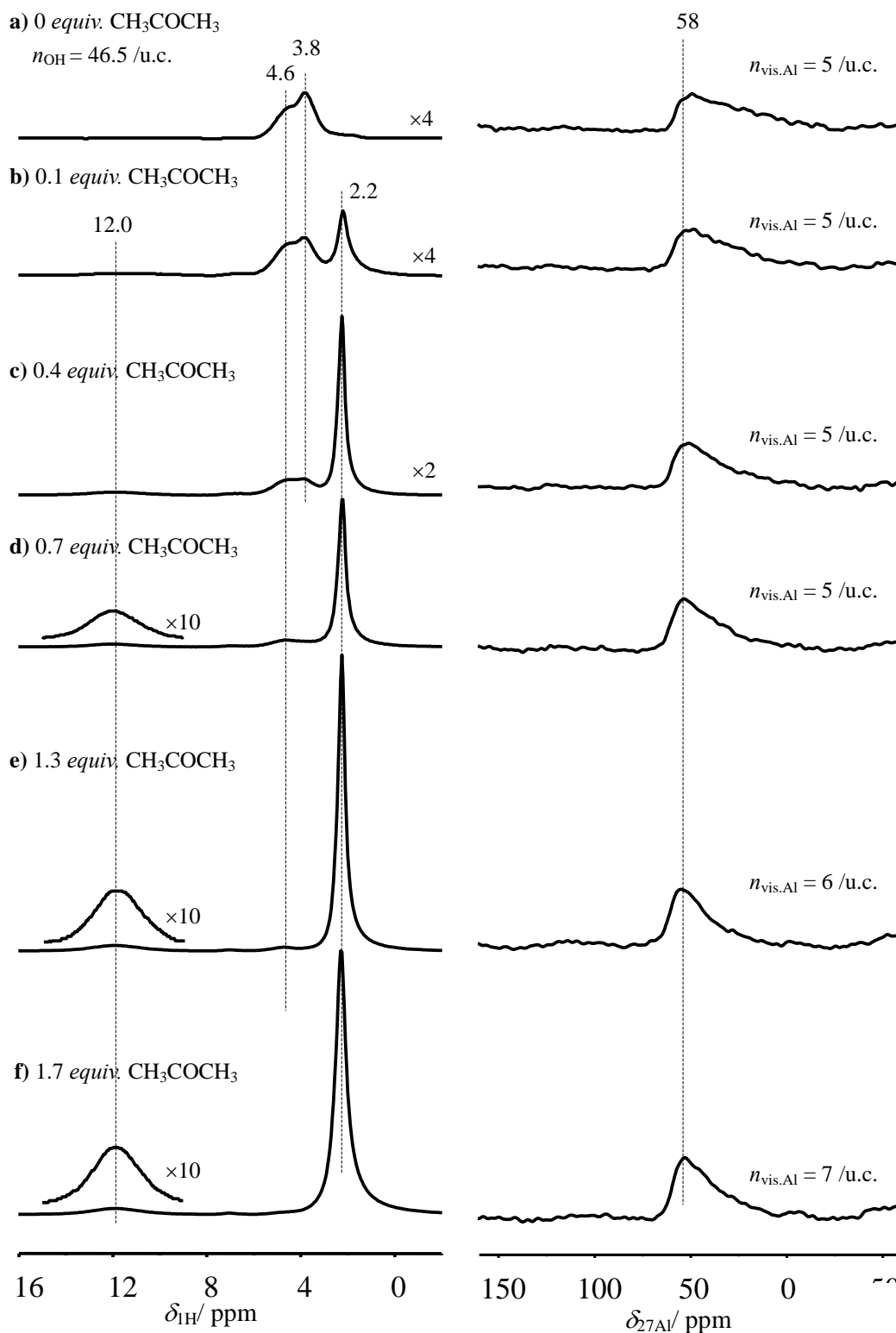
Figure 8.18 *In situ* ^{1}H (left) and ^{27}Al MAS NMR spectra (right) of non-hydrated zeolite H,Na-Y recorded at room temperature upon adsorption of acetone.

In addition, five-fold coordinated ($\mathbf{Al^{V}_{fr.}}$) and octahedrally coordinated aluminum species ($\mathbf{Al^{VI}_{fr.}}$) are observed. One possible explanation of the above-mentioned signals is that one or two acetone molecules directly coordinated to the framework aluminum (Schemes 8.1c and 8.1d). Another explanation is the formation of water molecules as reaction products of the aldol condensation [165, 166]. Also, these water molecules could coordinate to framework aluminum atoms. Using the quadrupole parameters given in Table 8.5, the ^{27}Al MAS NMR spectrum of acetone-loaded zeolite H,Na-Y recorded in a magnetic field of $B_0 = 17.6$ T was deconvoluted (Figure 8.17b). The relative intensities of signals 3 and 4 were found to be 13% and 12%, respectively.

Table 8.5 Isotropic chemical shifts δ_{iso} and quadrupolar coupling constants *SOQE* of aluminum species in zeolites H,Na-Y determined upon adsorption of ca. 2 *equiv.* acetone by DFS enhanced ^{27}Al MQMAS NMR spectroscopy at $B_0 = 17.6$ T.

Signal	1	2	3	4
Assignment	Al^{IV}/Na^+	Al^{IV}/H^+	$Al^{V}_{fr.}$	$Al^{VI}_{fr.}$
δ_{iso}/ ppm	61	66	35	4
SOQE/ MHz	5.1	9.4	7.6	4.9

The ^{29}Si MAS NMR spectrum of zeolite H,Na-Y recorded upon adsorption of acetone is shown in Figure 8.8d. The result is similar to that obtained for zeolite H,Na-Y loaded with acetonitrile (Figure 8.8c). Three ^{29}Si MAS NMR signals are observed at -97, -102, and -107 ppm. It is convinced that the formation of hydrogen bonds can not influence the local structure of Brønsted acid sites.

8.6 Effects of Probe Molecules on Framework Aluminum Atoms in Zeolites Y

In the present work, five probe molecules with different proton affinity *PA* values were used to investigate selectively the contents of framework aluminum atoms in non-hydrated zeolites by *in situ* and *ex situ* MAS NMR spectroscopy in a moderate magnetic field. Water molecules

strongly coordinated to framework aluminum atoms at defect sites, which cause the appearance of an ^{27}Al MAS NMR signal of octahedrally coordinated aluminum species at 0 ppm. Therefore, water adsorption on zeolites is not a suitable as standard method to investigate the number of framework aluminum atoms by ^{27}Al MAS NMR spectroscopy.

In the investigations of the non-hydrated materials upon adsorption of acetone (*PA* = 812 kJ/mol) and acetonitrile (*PA* = 779 kJ/mol), hydrogen bonds are formed between the probe molecules and Brønsted acid sites. However, these hydrogen bonds don't induce a significant change in the local structure of Brønsted acid sites, and can not make the framework aluminum atoms visible by ^{27}Al MAS NMR spectroscopy in moderate magnetic fields.

For the adsorption of pyridine and ammonia on non-hydrated zeolites, a proton transfer from the catalyst to the probe molecules (PyrH$^+$ or NH$_4^+$/NH$_3$) occurs, and no evidence for the formation of five-fold coordinated and octahedrally coordinated framework aluminum species is observed. More importantly, the framework aluminum atoms can be quantitatively detected by ^{27}Al MAS NMR spectroscopy in moderate magnetic fields. Furthermore, the variation of the local structure of Brønsted acid site due to the protonation leads to a well resolved Si(*n*Al) signals in the ^{29}Si MAS NMR spectra, allowing the calculation of the framework n_{Si}/n_{Al} ratio. However, the adsorption of pyridine is limited by the adsorption capacity of the microporous zeolite Y. Therefore, adsorption of ammonia is the better approach to determine selectively the amount of framework aluminum atom in non-hydrated zeolites by ^{27}Al MAS NMR spectroscopy.

It is interestingly to note that the base strength of probe molecules is reflected by the variation of the *SOQE* value of the framework aluminum atoms in the non-hydrated zeolites (Figure 8.19). As reported in Reference [163], the *SOQE* value of the framework aluminum atoms in the non-hydrated zeolites H-Y under dry nitrogen (*PA* value of nitrogen is 493.8 kJ/mol [150]) is ca. 16 MHz. It is well accepted that a very weak van der Waals interaction exists in this case. Therefore, no significant influence of nitrogen on the *SOQE* value occurs

(Figure 8.19, region I: Physical adsorption). With the increase of base strength of the probe molecules, such as acetonitrile or acetone, hydrogen bonds are formed between the Brønsted acid site and the probe molecules and lead to a decrease of the *SOQE* value (Figure 8.19, region II: Hydrogen bonds). In the case of probe molecules with larger *PA* value (> 850 kJ/mol), such as, ammonia or pyridine, a proton transfer from the Brønsted acid sites to the probe molecule occurs. In this case, the *SOQE* value is decreased to ca. 4 MHz (Figure 8.19, region III: Protonation). This finding can be explained by the formation of cationic species, such as, $PyrH^+$ and NH_4^+ cations, which is accompanied by a deprontonation of the local structure of Brønsted acid sites. Therefore, the different effects of these probe molecules on the zeolites framework become unobvious. The *PA* value of probe molecules protonated by zeolite H,Na-Y is ca. 850 kJ/mol, which is comparable to the values of 820 and 874 kJ/mol obtained by Bjørgen *et al.* [167] and Ehresmann *et al.* [11], respectively. It should be noted that the *PA* value of water is not shown in Figure 8.19, because water molecules agglomerate to clusters formed in the pores and cages of zeolites [155] and the *PA* value of isolated water molecules in the gas phase is not valid for a comparison with the *PA* values of the other probe molecules used in this study.
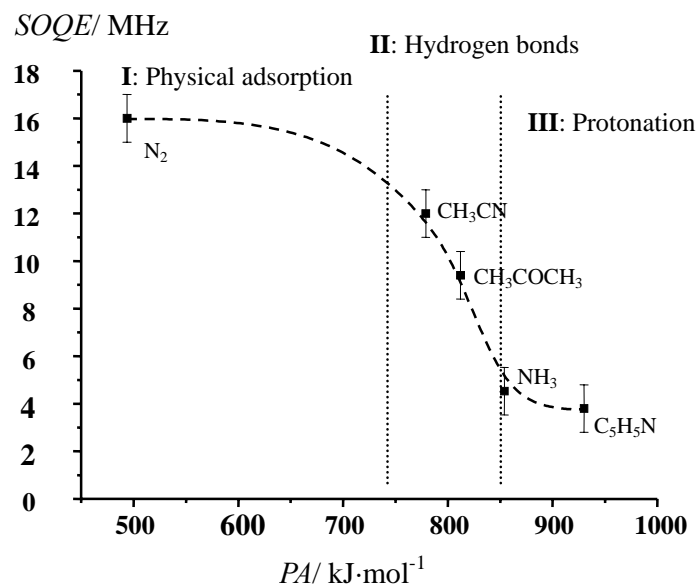
Figure 8.19 The second-order quadrupolar effect parameters *SOQE* of framework aluminum upon adsorption of probe molecules plotted as a function of the proton affinities *PA* values of these probe molecules.

8.7   Conclusions

Generally, the determination of the framework aluminum content of non-hydrated zeolite catalysts is hindered by high-field shifts of Si(nAl) signals in ^{29}Si MAS NMR spectroscopy and a strong broadening of the ^{27}Al MAS NMR signals of framework aluminum atoms in the vicinity of bridging hydroxyl protons. The rehydration of non-hydrated and steamed materials, however, is often accompanied by an uncontrolled hydrolysis of framework aluminum species and dehydroxylation. To overcome these problems, non-hydrated samples loaded with pyridine, ammonia, acetone, and acetonitrile were studied by *in situ* and *ex situ* NMR spectroscopy, respectively. Hydrogen bonds or a proton transfer from the Brønsted acid sites to the probe molecules were observed. It was found that a proton transfer from the Brønsted acid sites to the probe molecules is the key issue to make the framework aluminum atoms visible by ^{27}Al MAS NMR spectroscopy in moderate magnetic fields and to get well-resolved ^{29}Si MAS NMR spectra. The adsorption of ammonia on non-hydrated zeolite catalysts was found to be the best approach for determining the framework composition of these materials in the non-hydrated state.

9.   Extra-framework Aluminum Species in Non-hydrated Zeolites Y Studied by [27]Al Spin-echo, High-speed MAS, and MQMAS NMR Spectroscopy in Magnetic Fields of $B_0 = 9.4$ to 17.6 T

9.1   Introduction

In Chapter 8, the determination of framework aluminum contents in non-hydrated zeolites by solid-state ^{27}Al and ^{29}Si MAS NMR spectroscopy was described. The present Chapter focuses on the studies of different extra-framework aluminum species in non-hydrated zeolites.

A suitable approach for solid-state ^{27}Al NMR studies of non-hydrated zeolites is the spin-echo technique [93, 148, 168]. This approach allows the observation also of very broad signals. More modern techniques are high-speed MAS and MQMAS NMR spectroscopy in strong magnetic fields [94, 169, 170]. In ^{27}Al spin-echo NMR investigations of dealuminated and non-hydrated zeolites ZSM-5 and Y, two signals of aluminum species at framework and extra-framework positions could be distinguished [93, 148]. However, the strong overlap of the quadrupolar patterns hinders a quantitative evaluation of the spectra. As shown by solid-state ^{23}Na NMR studies of sodium cations in non-hydrated zeolites [169, 170, 171], experiments performed in different magnetic fields and applying modern 2D techniques can help to overcome this difficulty. Kentgens *et al.* [94] applied ^{27}Al MQMAS NMR spectroscopy combined with the double frequency-sweep (DFS) method for the study of aluminum species on weakly hydrated zeolite H-ZSM-5.

The assignment of solid-state ^{27}Al NMR signals in the present studies was supported by studies of parent zeolite H,Na-Y (Chapter 5), X-ray amorphous alumina (γ-Al$_2$O$_3$) and aluminum-exchanged zeolite Y (Al,Na-Y) as reference materials. The X-ray amorphous γ-Al$_2$O$_3$ with a specific surface area of $A = 150$ m^{2}g^{-1} is a product of Merck KGaA, Darmstadt, Germany. The preparation of zeolite Al,Na-Y is described in Section 7.1. It should be mentioned that all investigations were performed using samples in the non-hydrated state.

^{27}Al spin-echo NMR experiments were performed in magnetic fields of B_0 = 9.4 to 17.6 T on Bruker MSL 400 (9.4 T), Bruker AVANCE 600 (14.1 T), and Bruker AVANCE 750 (17.6 T) spectrometers. These investigations were carried out using 4 mm MAS NMR probes without sample spinning. The pulse sequence is described in Section 5.3.2. The number of scans was 4000-6000 at B_0 = 9.4 T, 1024 at B_0 = 14.1 T, and 640 at B_0 = 17.6 T. ^{27}Al high-speed MAS NMR experiments were performed at B_0 = 17.6 T using a 2.5 mm MAS NMR probe with a sample spinning frequency of ν_{rot} = 30 kHz, a single-pulse $\pi/12$ excitation with a pulse duration of 0.34 μs, and a repetition time of 2 s. DFS enhanced ^{27}Al MQMAS NMR spectra were obtained applying the split-t_1-whole echo pulse sequence with hard pulses of 3.3 μs and 13.7 μs, a soft pulse of 47 μs and a repetition time of 2 s (see also in Section 5.3.3). A 2.5 mm MAS NMR probe with an *rf* field of 120 kHz and a sample spinning frequency of ν_{rot} = 30 kHz were utilized. The Bruker softwares WINNMR, WINFIT, and XWINNMR were applied for the deconvolution and simulation of 1D NMR spectra and the transformation evaluation of 2D MQMAS spectra.

9.2 Solid-state ^{27}Al NMR Investigations of Non-hydrated Amorphous γ-Al$_2$O$_3$

Figure 9.1 shows the DFS enhanced ^{27}Al MQMAS NMR spectrum of non-hydrated amorphous γ-Al$_2$O$_3$ recorded at B_0 = 9.4 T. Two different aluminum species at isotropic chemical shifts of 68 and 12 ppm are distinguished. The spectroscopic parameters are summarized in Table 9.1. According to the above-mentioned isotropic chemical shift values, the low-field signal is assigned to tetrahedrally coordinated aluminum species (cluster **Al^{IV}**), while the high-field signal is caused by octahedrally coordinated aluminum species (cluster **Al^{VI}**). This finding agrees with the structure of γ-Al$_2$O$_3$ consisting of aluminum oxide clusters with a cubic packing of oxygen atoms, which form tetrahedral and octahedral holes filled with aluminum atoms [172].

Comparing the spectroscopic data given in Table 9.1 with those published for hydrated γ-Al$_2$O$_3$ [16], no change of the isotropic chemical shift of tetrahedrally and octahedrally

coordinated aluminum species upon dehydration was observed. However, an increase of the C_{QCC} value from ca. 4 MHz in the hydrated state to a value of 5.5 to 8.5 MHz occurs in result of dehydration.
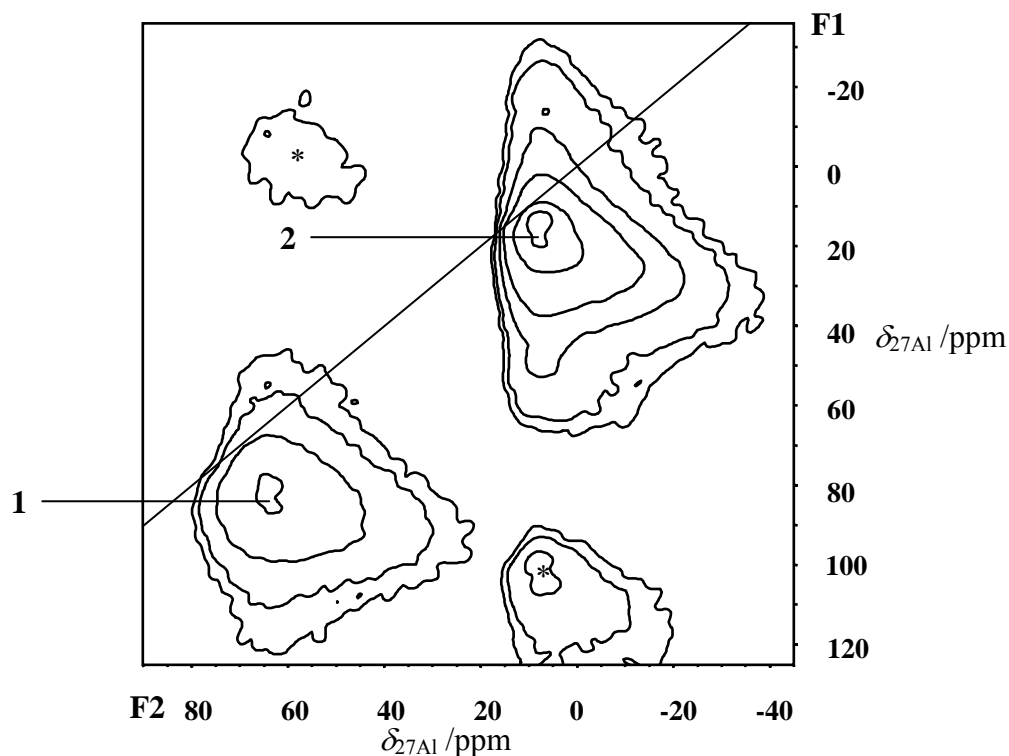

Figure 9.1 DFS enhanced ^{27}Al MQMAS NMR spectrum of non-hydrated γ-Al$_2$O$_3$ recorded at $B_0 = 9.4$ T with $\nu_{rot} = 30$ kHz and the split-t_1-whole echo pulse sequence.

Table 9.1 Isotropic chemical shifts δ_{iso}, quadrupolar coupling constants C_{QCC}, asymmetry parameters η_Q, and relative intensities I of aluminum species in non-hydrated γ-Al$_2$O$_3$ and non-hydrated zeolite Al,Na-Y determined by a simulation of the ^{27}Al spin-echo NMR and ^{27}Al high-speed MAS NMR spectra recorded in magnetic fields of $B_0 = 9.4$ to 17.6 T.

| Sample	γ-Al$_2$O$_3$	γ-Al$_2$O$_3$	Al,Na-Y	Al,Na-Y	Al,Na-Y
Signal	1	2	1	2	3
Assignment	cluster Al^{IV}	cluster Al^{VI}	Al^{IV}/Al^{x+}	Al^{IV}/Na$^+$	Al^{x+} cat.
δ_{iso} / ppm	68±5	12±5	70±10	60±5	35±5
C_{QCC} / MHz	8.5±0.5	5.5±0.5	14.5±1.0	5.5±0.5	6.0±0.5
η_Q	0.8	0.7	0.3	0.8	0.7
I / %	60	40	48	28	24

In order to obtain the amounts of different aluminum species, the ^{27}Al spin-echo NMR spectra of γ-Al$_2$O$_3$ were recorded at B_0 = 9.4, 14.1, and 17.6 T (Figure 9.2). With an increasing magnetic field, the resolution of ^{27}Al spin-echo NMR signals is significantly improved due to the decrease of the second-order quadrupolar broadening. The spectroscopic parameters obtained by DFS enhanced ^{27}Al MQMAS spectroscopy were used to simulate the ^{27}Al spin-echo NMR spectra. The relative intensities of tetrahedrally coordinated and octahedrally coordinated aluminum species in different magnetic fields are comparable. It is shown that 60% of aluminum atoms in non-hydrated γ-Al$_2$O$_3$ are present in tetrahedral coordination, while 40% of them are octahedrally coordinated (Table 9.1).
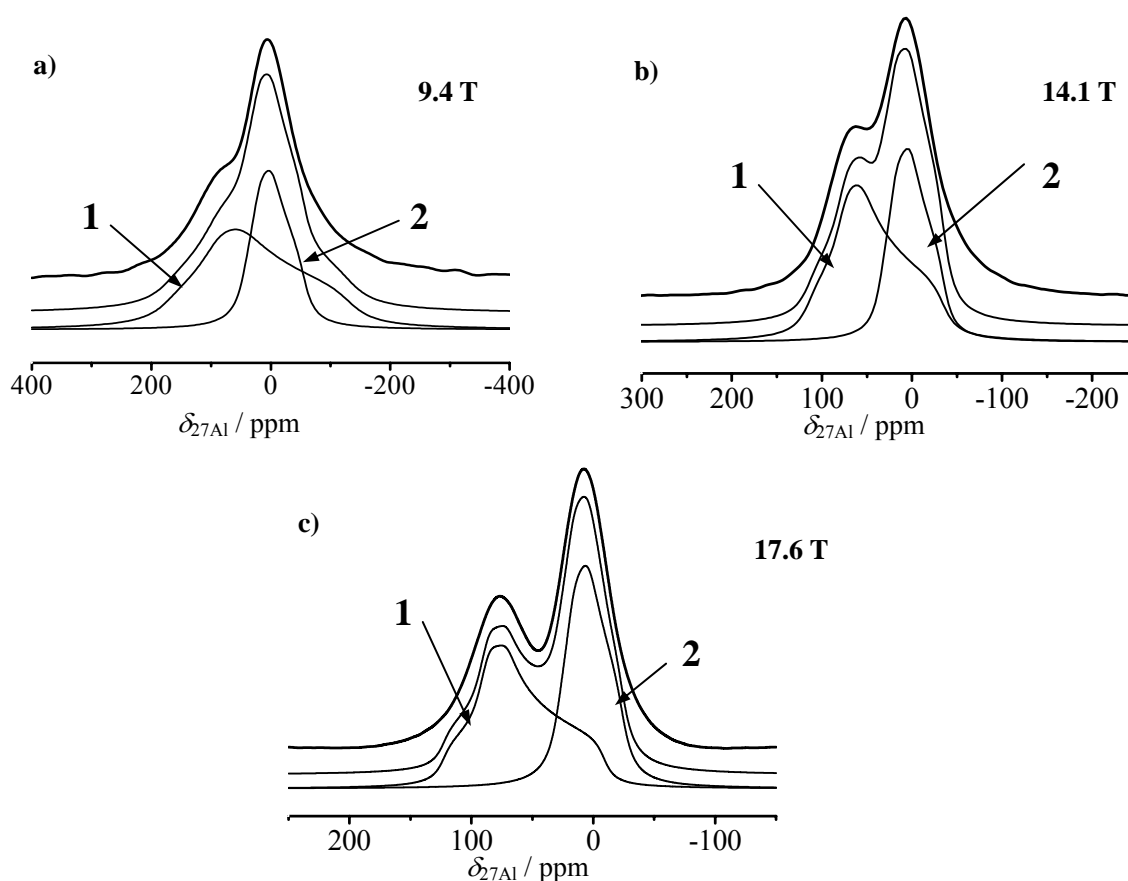
Figure 9.2 ^{27}Al spin-echo NMR spectra of non-hydrated γ-Al$_2$O$_3$ recorded at B_0 = 9.4 (a), 14.1 (b), and 17.6 T (c). The experimental spectra (top) are compared with the simulated spectra (bottom).

γ-Al$_2$O$_3$ is the low-temperature phase of solid aluminum oxides and consists of small clusters of ordered aluminum oxide being X-ray amorphous [172]. In the further work, therefore, the spectroscopic parameters of the cluster **Al^{IV}** and cluster **Al^{VI}** species,

summarized in Table 9.1, are utilized for the description of solid-state ^{27}Al NMR signals of neutral extra-framework aluminum oxide clusters in non-hydrated zeolites Y (Schemes 9.1a and 9.1b).


a) cluster **Al^{IV}**   b) cluster **Al^{VI}**   c) **Al^{IV}**/H$^+$

d) **Al^{IV}**/Na$^+$ e) **Al^{IV}**/Al^{x+} f) **Al^{x+}** cat.
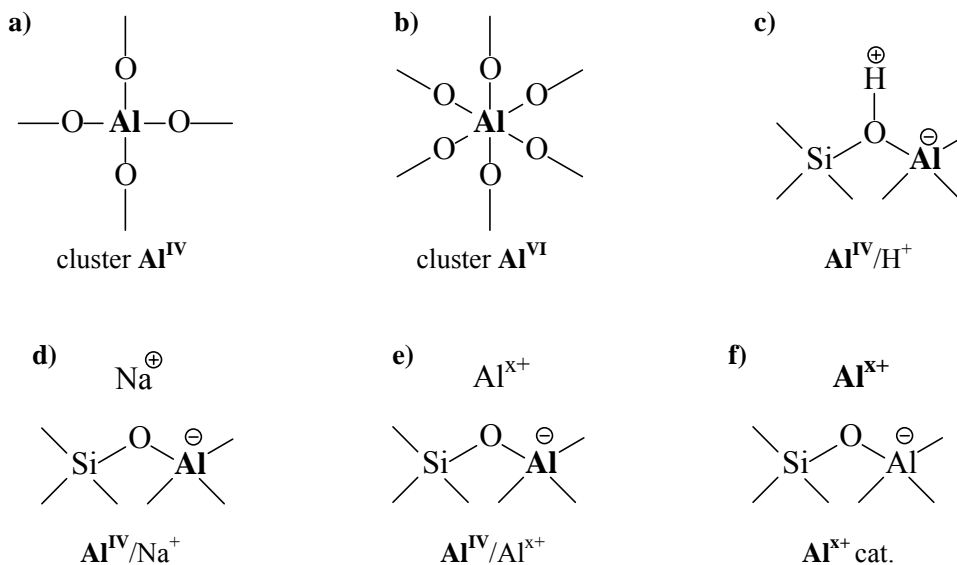
Scheme 9.1

9.3   Solid-state ^{27}Al NMR Investigations of Non-hydrated Zeolites Al,Na-Y

As shown in Section 7.4 and Reference [138], the occurrence of bridging OH groups, **Al^{IV}**/H$^+$, Scheme 9.1c can be neglected in zeolite Al,Na-Y, dehydrated at 723 K. Therefore, solid-state ^{27}Al NMR spectra of this sample consist of signals of framework aluminum atoms in the vicinity of extra-framework sodium cations (**Al^{IV}**/Na$^+$, Scheme 9.1d), framework aluminum atoms in the vicinity of extra-framework aluminum cations (**Al^{IV}**/Al^{x+}, Scheme 9.1e), and extra-framework aluminum cations themselves (**Al^{x+}** cat., Scheme 9.1f).
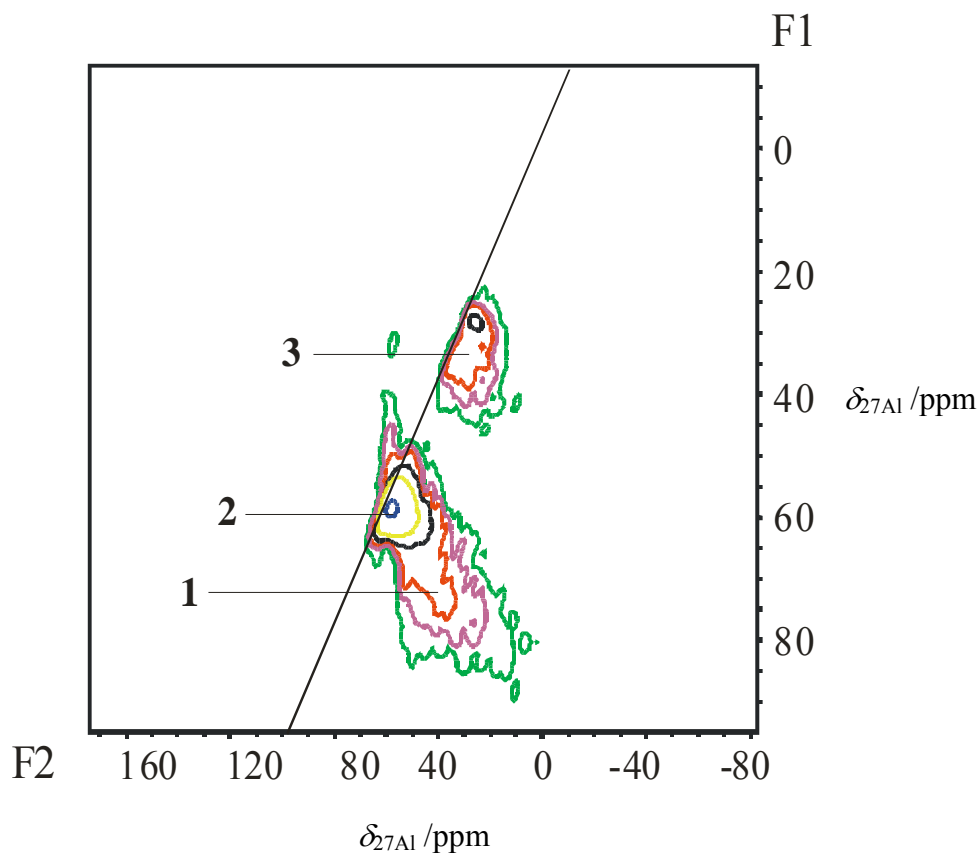
Figure 9.3 ^{27}Al MQMAS NMR spectrum of non-hydrated zeolite Al,Na-Y recorded at $B_0 =$ 17.6 T with $\nu_{rot} = 30$ kHz and the splite-t$_1$-whole echo pulse sequence.

Figure 9.3 shows the ^{27}Al MQMAS NMR spectrum of non-hydrated zeolite Al,Na-Y recorded at $B_0 = 17.6$ T. In this spectrum, three signals occur at isotropic chemical shifts of ca. 70 ppm (signal 1), 60 ppm (signal 2), and 35 ppm (signal 3) in the F1-dimension. Along the F2-dimension, these signals are shifted due to the second-order quadrupolar shift [103]. These second-order quadrupolar shifts amount to ca. 35 ppm for signal 1 and 5 ppm for signals 2 and 3 corresponding to *SOQE* values of ca. 15 MHz and 5.5 MHz, respectively. Because of limitations in the signal/noise ratio, no simulation of 1D slices obtained at the above-mentioned isotopic chemical shifts was performed.

In Figure 9.4, the ^{27}Al spin-echo NMR and ^{27}Al high-speed NMR spectra of non-hydrated zeolite Al,Na-Y recorded at $B_0 = 9.4$, 14.1, and 17.6 T are depicted. The

simulation of all these spectra was possibly assuming three signals with the isotropic chemical shifts and the *SOQE* value determined by MQMAS NMR spectroscopy. A summary of the spectroscopic parameters used for these simulations is given in Table 9.1.
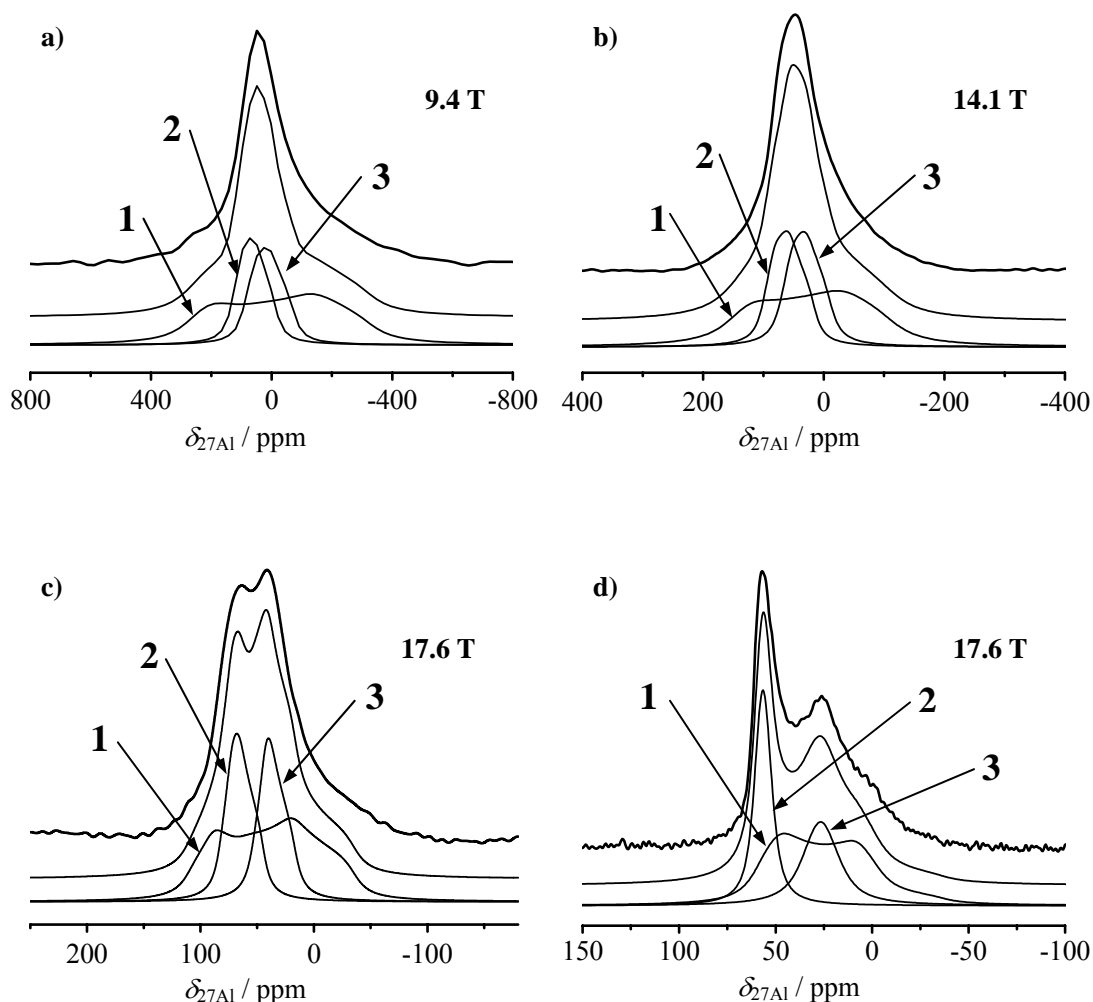
Figure 9.4 ^{27}Al spin-echo NMR spectra of non-hydrated zeolite Al,Na-Y recorded at $B_0 = 9.4$ (a), 14.1 (b), and 17.6 T (c). The spectrum in (d) was recorded with MAS ($\nu_{rot} = 30$ kHz) at $B_0 = 17.6$ T. The experimental spectra (top) are compared with the simulated spectra (bottom).

According to the chemical analysis of zeolite Al,Na-Y by AES, this material contains 70 aluminum atoms per unit cell. In this case, there are 16 framework aluminum atoms per unit cell compensated in their negative charge by extra-framework sodium cations (**Al^{IV}**/Na$^+$, Scheme 9.1d), 36 framework aluminum atoms per unit cell compensated by extra-framework aluminum cations (**Al^{IV}**/Al^{x+}, Scheme 9.1e), and 18 aluminum atoms per unit cell existing as

extra-framework cations ($\mathbf{Al^{x+}}$ cat., Scheme 9.1f). In the solid-state ^{27}Al NMR spectra of non-hydrated zeolite Al,Na-Y, signal 1 is the strongest component with a relative intensity of 48 % corresponding to 34 Al/u.c. Therefore, this signal was assigned to framework aluminum atoms compensated by extra-framework aluminum cations ($\mathbf{Al^{IV}/Al^{x+}}$). Signal 2 is typical for framework aluminum atoms compensated by extra-framework sodium cations ($\mathbf{Al^{IV}/Na^+}$) as observed in earlier studies [93, 148, 168]. Hence, signal 3 must be due to extra-framework aluminum cations ($\mathbf{Al^{x+}}$ cat.). The resonance position of signal 3 of 35 ppm could be an indication for a fivefold oxygen coordination of these species as suggested by Bhering *et al.* [72] for extra-framework $Al(OH)^{2+}$ species in result of quantum mechanical studies. The extra-framework aluminum species coordinate to framework oxygen atoms in the vicinity of framework aluminum atoms [72]. This coordination may be the reason for the strong quadrupolar broadening observed for signal 1 ($\mathbf{Al^{IV}/Al^{x+}}$: C_{QCC} = 14.5 MHz) in the spectra of non-hydrated zeolite Al,Na-Y.

9.4   Solid-state ^{27}Al NMR Investigations of Non-hydrated Zeolites H,Na-Y

Figure 9.5 shows the ^{27}Al MQMAS NMR spectrum of non-hydrated zeolite H,Na-Y recorded at B_0 = 17.6 T. This spectrum consists of at least two signals occurring at isotropic chemical shifts of ca. 75 ppm (signals 1') and 60 ppm (signal 2') in the F1-dimension. Along the F2-dimension, a second-order quadrupolar shift of ca. 40 ppm for signal 1' and 5 ppm for signal 2' was found. These second-order shifts correspond to *SOQE* values of ca. 16 MHz and 5.5 MHz, respectively. No simulation of 1D slices was performed because of limitations in the signal/noise ratio.

In Figure 9.6, the ^{27}Al spin-echo NMR and ^{27}Al high-speed NMR spectra of non-hydrated zeolite H,Na-Y recorded at B_0 = 9.4, 14.1, and 17.6 T are depicted. The simulation especially of the high-speed MAS NMR spectrum recorded at B_0 = 17.6 T requires three signals: Two quadrupolar patterns at ca. 70 ppm with C_{QCC} values of ca. 16 MHz (signal 1) and 14 MHz (signal 2) and a weak signal at ca. 60 ppm with a C_{QCC} value of ca. 5.5 MHz (signal 3). A summary of the spectroscopic parameters of these signals is given in Table 9.2.
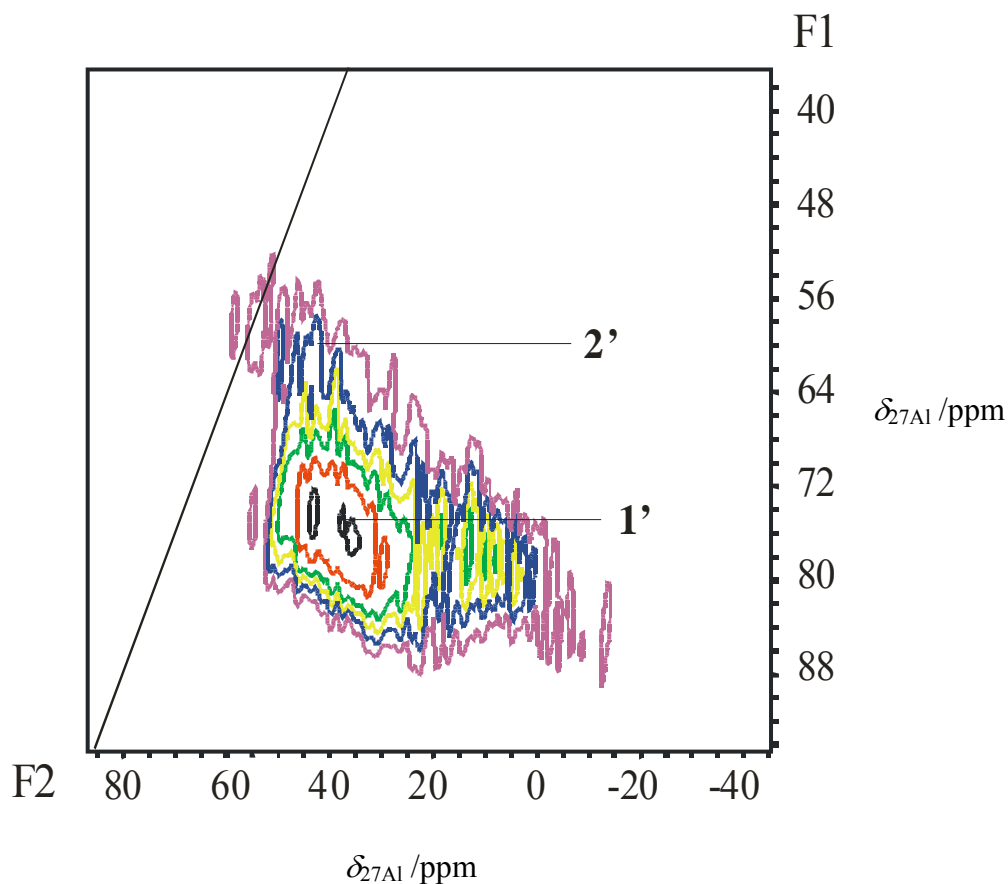
Figure 9.5 ^{27}Al MQMAS NMR spectrum of non-hydrated zeolite H,Na-Y recorded at B_0 = 17.6 T with ν_{rot} = 30 kHz and the split-t_1-whole echo pulse sequence.

Due to the low intensity and the spectroscopic parameters of signal 3, this component was assigned to framework aluminum atoms compensated by sodium cations ($\mathbf{Al^{IV}}$/Na$^+$, Scheme 9.1d) [93, 148, 168]. The strong quadrupolar broadenings of signals 1 and 2 indicate that these components are caused by framework aluminum atoms in the vicinity of bridging hydroxyl protons ($\mathbf{Al^{IV}}$/H$^+$, Scheme 9.1c). In earlier ^{27}Al spin-echo NMR studies of non-hydrated zeolites H-Y and H-ZSM-5, only one quadrupolar pattern similar to that of signals 1 and 2 was used to describe the signal of $\mathbf{Al^{IV}}$/H$^+$ species [93, 148, 168]. The simulation of the ^{27}Al high-speed MAS NMR spectrum of non-hydrated zeolite H,Na-Y/81.5, however, requires at least two patterns with similar isotropic chemical shifts but slightly different quadrupolar coupling constants. These two quadrupolar patterns may be due to

framework aluminum atoms in the vicinity of bridging hydroxyl protons (**Al^{IV}**/H$^+$) pointing into supercages and sodalite cages. This assumption is supported by the finding of similar relative intensities for signals 1 and 2 (see Table 2), since by ^{1}H MAS NMR spectroscopy of highly exchanged zeolites H,Na-Y an intensity ratio of ca. 1 : 1 was determined for bridging OH groups in supercages and sodalite cages [92, 148]. Because of the small difference between the quadrupolar coupling constants of signals 1 and 2, these two patterns occur as a single signal 1' in the ^{27}Al MQMAS spectrum in Figure 9.5.
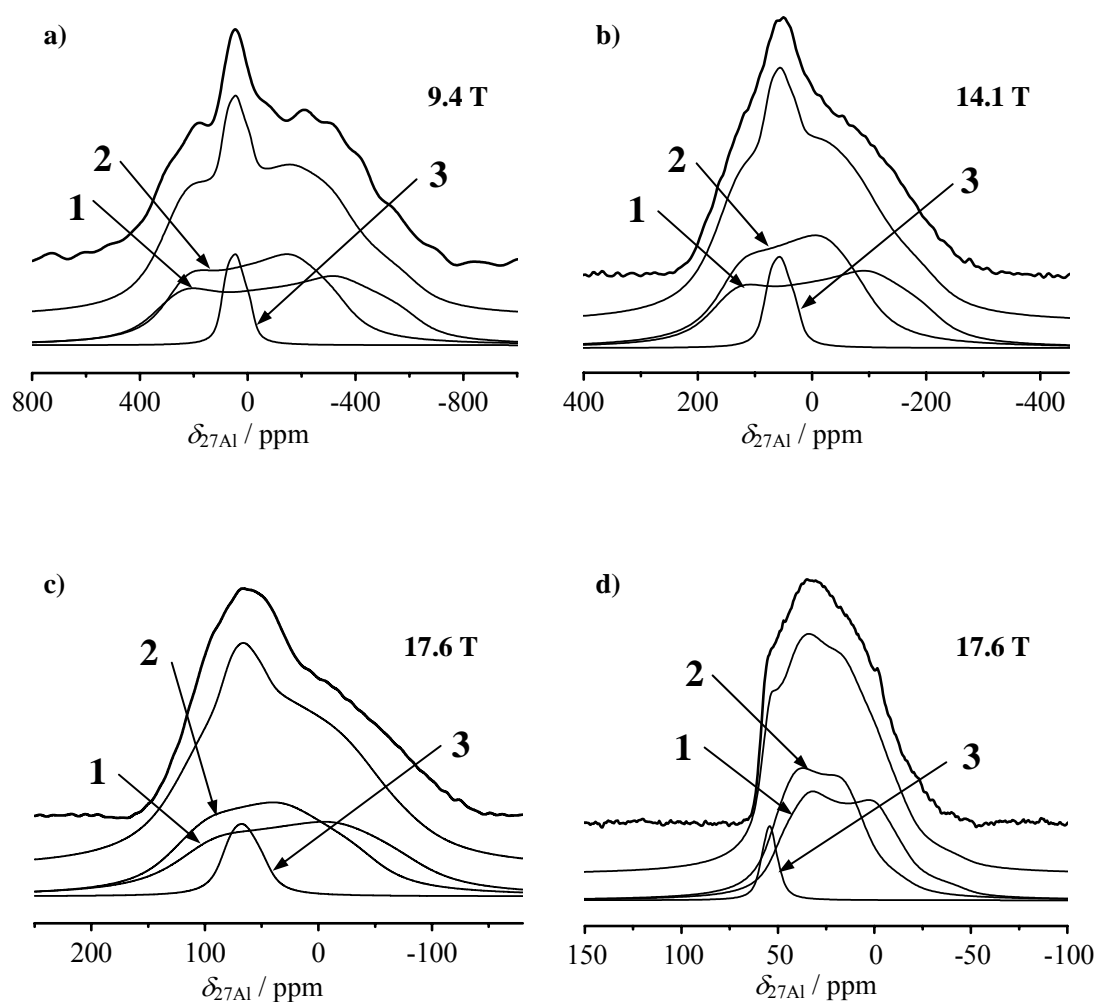
Figure 9.6 ^{27}Al spin-echo NMR spectra of non-hydrated zeolite H,Na-Y recorded at B_0 = 9.4 (a), 14.1 (b), and 17.6 T (c). The spectrum in (d) was recorded with MAS (ν_{rot} = 30 kHz) at B_0 = 17.6 T. The experimental spectra (top) are compared with the simulated spectra (bottom).

Table 9.2 Isotropic chemical shifts δ_{iso}, quadrupolar coupling constants C_{QCC}, asymmetry parameters η_Q, and relative intensities I of aluminum species in non-hydrated zeolite H,Na-Y determined by a simulation of the ^{27}Al spin-echo NMR and high-speed MAS NMR spectra recorded in magnetic fields of $B_0 = 9.4$ to 17.6 T.

Signal	1	2	3
Assignment	Al^{IV}/H^+	Al^{IV}/H^+	Al^{IV}/Na^+
δ_{iso} / ppm	70±10	70±10	60±5
C_{QCC} / MHz	16.0±0.5	14.0±0.5	5.5±0.5
η_Q	0.3	0.3	0.8
I / %	47	47	6

9.5 Solid-state ^{27}Al NMR Investigations of Non-hydrated Zeolite deH,Na-Y/81.5

Figure 9.7 shows the ^{27}Al MQMAS NMR spectrum of non-hydrated zeolite deH,Na-Y/81.5 recorded at $B_0 = 17.6$ T. This spectrum shows up to four signals occurring at isotropic chemical shifts of ca. 80 ppm (signal 1), 65 ppm (signal 2), 35 ppm (signal 3), and 10 ppm (signal 4) in the F1-dimension. Along the F2-dimension, second-order quadrupolar shifts of ca. 35 ppm for signal 1, 10 ppm for signal 2, and 5 ppm for signals 3 and 4 occur. These second-order quadrupolar shifts correspond to *SOQE* values of ca. 15 MHz, 8 MHz, and 5.5 MHz, respectively. No simulation of 1D slices was performed because of limitations in the signal/noise ratio.

The ^{27}Al spin-echo NMR and ^{27}Al high-speed NMR spectra of non-hydrated zeolite H,Na-Y/81.5 recorded at $B_0 = 9.4$, 14.1, and 17.6 T are depicted in Figure 9.8. In agreement with the signals found in the 2D ^{27}Al MQMAS spectrum in Figure 9.7, the simulation of the 1D spectra was performed assuming four signals at isotropic chemical shifts of 70, 65, 35, and 10 ppm with $C_{QCC} = 15.0$, 8.0, 7.5, and 5.0 MHz, respectively. A summary of the spectroscopic parameters of these signals 1 to 4 is given in Table 9.3.
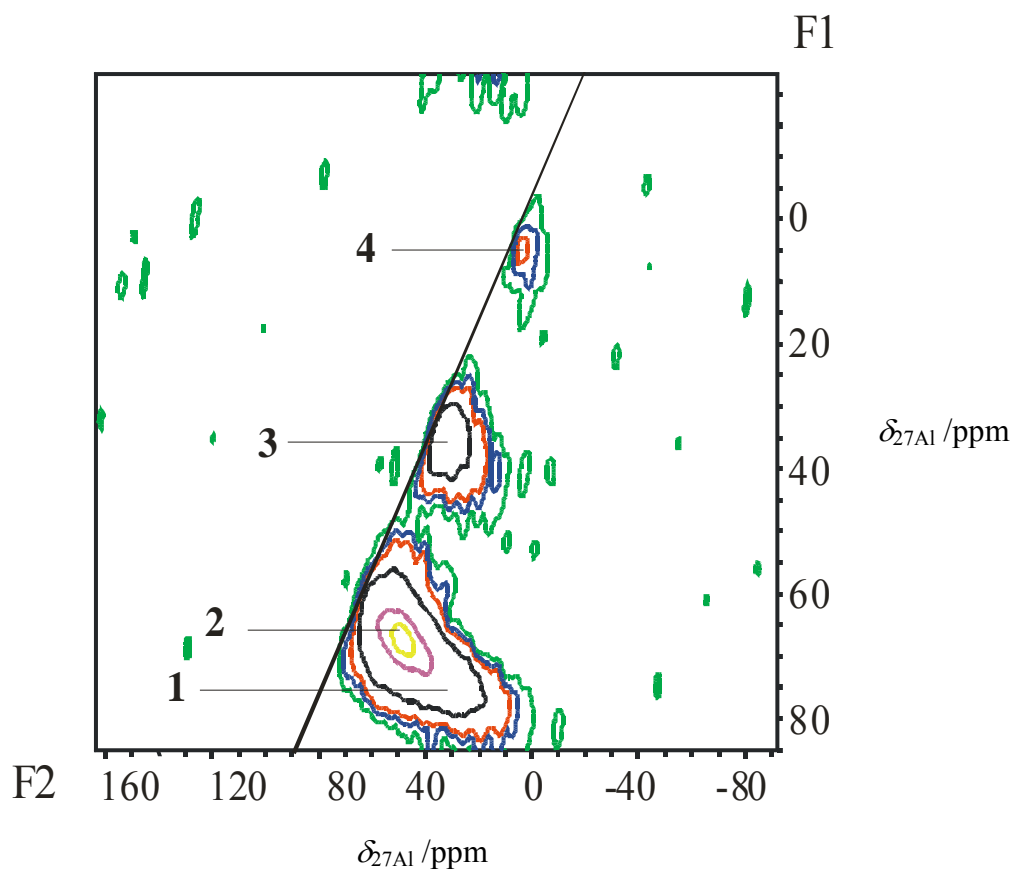
Figure 9.7 ^{27}Al MQMAS NMR spectrum of non-hydrated zeolite deH,Na-Y/81.5 recorded at $B_0 = 17.6$ T with $\nu_{rot} = 30$ kHz and the splite-t_1-whole echo pulse sequence.

For the assignment of signals 1 to 4 in the solid-state ^{27}Al NMR spectra of non-hydrated zeolite deH,Na-Y/81.5, the spectroscopic parameters and assignments of the signals obtained for non-hydrated γ-Al$_2$O$_3$, and zeolites Al,Na-Y and H,Na-Y were utilized. Considering the large C_{QCC} value and the isotropic chemical shift of signal 1 in the spectrum of non-hydrated zeolite deH,Na-Y/81.5, this component may be due to framework aluminum atoms in the vicinity of bridging hydroxyl protons (**Al^{IV}**/H$^+$) as well as framework aluminum atoms compensated by extra-framework aluminum cations (**Al^{IV}**/Al^{x+}). In the same manner, signal 2 was attributed to framework aluminum atoms compensated by extra-framework sodium cations (**Al^{IV}**/Na$^+$) as well as tetrahedrally coordinated aluminum atoms in neutral extra-framework aluminum oxide clusters (cluster **Al^{IV}**). Finally, signals 3 and 4 are caused by extra-framework aluminum cations (**Al^{x+}** cat.) and octahedrally coordinated aluminum

atoms in neutral extra-framework aluminum oxide clusters (cluster **Al^{VI}**), respectively. A summary of these signal assignments is given in Table 9.3, second line.
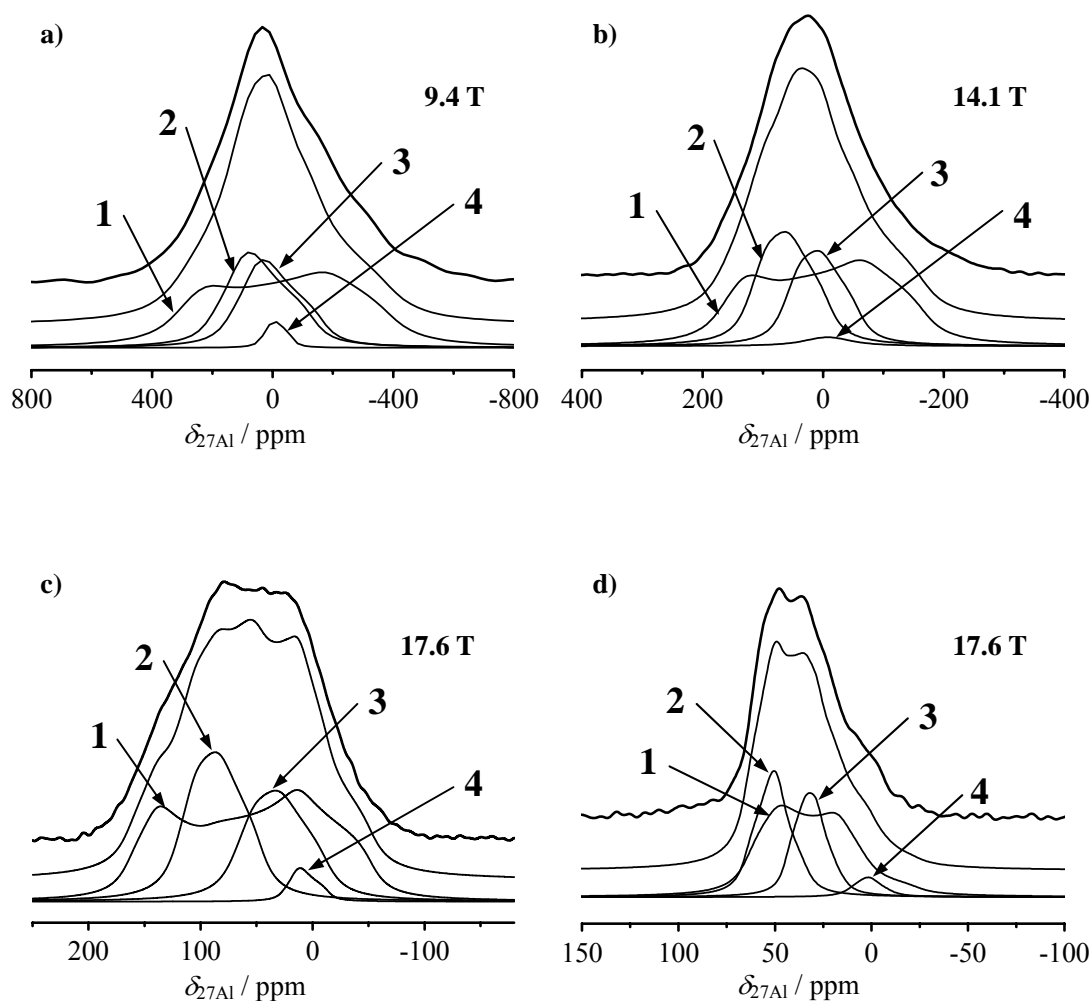
Figure 9.8 ^{27}Al spin-echo NMR spectra of non-hydrated zeolite deH,Na-Y/81.5 recorded at B_0 = 9.4 (a), 14.1 (b), and 17.6 T (c). The spectrum in (d) was recorded with MAS (v_{rot} = 30 kHz) at B_0 = 17.6 T. The experimental spectra (top) are compared with the simulated spectra (bottom).

9.6 Quantitative Discussion of Aluminum Species in Non-hydrated Zeolite deH,Na-Y/81.5

The chemical analysis of zeolite deH,Na-Y/81.5 by AES (52 Al/u.c., 3.6 Na$^+$/u.c.) and the relative intensities of the solid-state ^{27}Al NMR signals (last line in Table 9.3) allows a quantitative discussion of the distribution of aluminum species in this material in the

non-hydrated state. The relative intensity of signal 1 (48 %) corresponds to 25 Al/u.c. By ^{1}H MAS NMR it was determined that this zeolite catalyst exhibits 17 bridging OH groups per unit cell (**Al^{IV}/H$^+$**) (Chapter 7 and Reference [148]). Hence, 8 Al/u.c. occur as framework aluminum atoms compensated by extra-framework aluminum cations (**Al^{IV}/Al^{x+}**). The relative intensity of signal 2 (27 %) corresponds to 14 Al/u.c. By AES, the number of 3.6 sodium cations per unit cell (**Al^{IV}/Na$^+$**) was determined. Therefore, 10.4 Al/u.c. occur as tetrahedrally coordinated aluminum atoms in neutral extra-framework aluminum oxide clusters (cluster **Al^{IV}**). The relative intensities of signals 3 (21 %) and 4 (4 %) indicate the presence of 11 Al/u.c. as extra-framework aluminum cations (**Al^{x+} cat.**) and 2 Al/u.c. as octahedrally coordinated aluminum atoms in neutral extra-framework aluminum oxide clusters (cluster **Al^{VI}**).

Table 9.3 Isotropic chemical shifts δ_{iso}, quadrupolar coupling constants C_{QCC}, asymmetry parameters η_Q, and relative intensities I of aluminum species in non-hydrated zeolite deH,Na-Y/81.5 determined by a simulation of the ^{27}Al spin-echo NMR and high-speed MAS NMR spectra recorded in magnetic fields of $B_0 = 9.4$ to 17.6 T.

Signal	1	2	3	4
Assignment	**Al^{IV}/H$^+$**	**Al^{IV}/Na$^+$**	**Al^{x+} cat.**	cluster **Al^{VI}**
	Al^{IV}/Al^{x+}	cluster **Al^{IV}**		
δ_{iso} / ppm	70±10	65±5	35±5	10±5
C_{QCC} / MHz	15.0±1.0	8.0±0.5	7.5±0.5	5.0±0.5
η_Q	0.3	0.8	0.7	0.7
I / %	48	27	21	4

Based on the above-mentioned assignment of signals (see Table 9.3) and quantitative evaluation of signal intensities, the framework n_{Si}/n_{Al} ratio of non-hydrated zeolite deH,Na-Y/81.5 is available by solid-state ^{27}Al NMR spectroscopy. The total number of framework aluminum atoms is given by 25 Al/u.c. occurring as **Al^{IV}/H$^+$** and **Al^{IV}/Al^{x+}** species and 3.5 Al/u.c. occurring as **Al^{IV}/Na$^+$** species. In reasonable agreement with earlier ^{29}Si MAS

NMR studies, these values give a framework n_{Si}/n_{Al} ratio of 5.7.

Since 8 framework aluminum atoms per unit cell are compensated by extra-framework aluminum cations ($\mathbf{Al^{IV}}/Al^{x+}$) and ca. 23 Al/u.c. occur as extra-framework aluminum oxide clusters (cluster $\mathbf{Al^{IV}}$, cluster $\mathbf{Al^{VI}}$) and extra-framework aluminum cations ($\mathbf{Al^{x+}}$ cat.), a mean cationic charge per extra-framework aluminum atom of +0.35 follows. This value is in good agreement with the mean cationic charge of zeolite deH,Na-Y/81.5 determined recently by AES, ^{29}Si MAS NMR, and ^{1}H MAS NMR spectroscopy (in Chapter 7 and Reference [148]).

9.7   Conclusions

^{27}Al spin-echo, high-speed MAS, and MQMAS NMR spectroscopy performed in magnetic fields of B_0 = 9.4, 14.1, and 17.6 T were demonstrated to be useful tools for the characterization of framework and extra-framework aluminum species in non-hydrated zeolite catalysts. Non-hydrated γ-Al_2O_3 and aluminum-exchanged zeolite Y (Al,Na-Y) were investigated as reference materials for the assignment of solid-state ^{27}Al NMR signals. The spectra of non-hydrated γ-Al_2O_3 consist of signals of tetrahedrally and octahedrally coordinated aluminum atoms in clusters of aluminum oxide (cluster $\mathbf{Al^{IV}}$ and cluster $\mathbf{Al^{VI}}$, respectively). The spectra of non-hydrated zeolite Al,Na-Y are described by signals of tetrahedrally coordinated framework aluminum atoms compensated in their negative framework charges by extra-framework sodium cations ($\mathbf{Al^{IV}}/Na^+$), framework aluminum atoms compensated by extra-framework aluminum cations ($\mathbf{Al^{IV}}/Al^{x+}$), and extra-framework aluminum cations themselves ($\mathbf{Al^{n+}}$ cat.). The above-mentioned signals occur at characteristic resonance positions and/or exhibit characteristic quadrupolar coupling constants.

Solid-state ^{27}Al NMR investigations of non-hydrated zeolite H,Na-Y indicate that aluminum atoms in this material cause three different signals: Two quadrupolar patterns with slightly different quadrupolar coupling constants (C_{QCC} = 14-16 MHz) for framework aluminum atoms in the vicinity of bridging hydroxyl protons ($\mathbf{Al^{IV}}/H^+$) pointing into supercages and sodalite cages and a small pattern with a low quadrupolar coupling constant

(C_{QCC} = 5.5 MHz) for framework aluminum atoms compensated by extra-framework sodium cations ($\mathbf{Al^{IV}}$/Na$^+$).

The investigation of a steamed and non-hydrated zeolite deH,Na-Y/81.5 results in spectra consisting of at least four signals. The assignment of these signals was performed based on spectroscopic parameters of signals observed for non-hydrated γ-Al$_2$O$_3$ and zeolites Al,Na-Y and H,Na-Y. Two of the signals were explained by a superposition of the signals of framework $\mathbf{Al^{IV}}$/H$^+$ and $\mathbf{Al^{IV}}$/Al^{x+} species and by a superposition of signals of framework $\mathbf{Al^{IV}}$/Na$^+$ species and extra-framework cluster $\mathbf{Al^{IV}}$ species. The residual two signals are due to extra-framework $\mathbf{Al^{x+}}$ cations and extra-framework cluster $\mathbf{Al^{VI}}$ species. Based on the results of chemical analysis (AES) and the relative intensities obtained by solid-state ^{27}Al NMR spectroscopy of non-hydrated zeolite deH,Na-Y/81.5, the aluminum distribution in this material could be determined.

References

[1]   M. Hunger, Catal. Rev.-Sci. Eng. 39 (1997) 345-393.

[2]   D. Freude, M. Hunger, H. Pfeifer, Chem. Phys. Lett. 91 (1982) 307-310.

[3]   J. Klinowski, S. Ramdas, J.M. Thomas, C.A. Fyfe. J.S. Hartman, J. Chem. Soc., Faraday Trans. II, 78 (1982) 1025-1050.

[4]   V. Bosáček, D. Freude, T. Froehlich, H. Pfeifer, H. Schmiedel, J. Coll. Inter. Sci. 85 (1982) 502-507.

[5]   D. Freude, T. Froehlich, H. Pfeifer, H. Scheler, Zeolites 3 (1983) 171-173.

[6]   L.M. Bull, B. Bussemer, T. Anupold, A. Reinhold, A. Samoson, J. Sauer, A.K. Cheetham, R. Dupree, J. Am. Chem. Soc. 122 (2000) 4948-4958.

[7]   M. Hartmann, A.M. Prakash, L. Kevan, J. Chem. Soc., Faraday Trans. 94 (1998) 723-727.

[8]   M. Hunger, U. Schenk and A. Buchholz, J. Phys. Chem. B 104 (2000) 12230-12236.

[9]   M.W. Anderson, P.J. Barrie, J. Klinowski, J. Phys. Chem. 95 (1991) 235-239.

[10]   A. Buchholz, W. Wang, M. Xu, A. Arnold, M. Hunger, J. Phys. Chem. 108 (2004) 3107-3113.

[11]   J.O. Ehresmann, W. Wang, B. Herreros, D.P. Luigi, T.N. Venkatraman, W.G Song, J.B. Nicholas, J.F. Haw, J. Am. Chem. Soc. 124 (2002) 10868-10874.

[12]   C.A. Fyfe, J.L. Bretherton, L.Y. Lam, J. Chem. Soc., Chem. Commun. (2000) 1575-1576.

[13]   C.A. Fyfe, J.L. Bretherton, L.Y. Lam, J. Am. Chem. Soc. 123 (2001) 5285-5291.

[14]   B.H. Wouters, T. Chen, P.J. Grobet, J. Am. Chem. Soc. 120 (1998) 11419-11425.

[15]   B.H. Wouters, T. Chen, P.J. Grobet, J. Phys. Chem. B 105 (2001) 1135-1139.

[16]   A. Omegna, J.A. van Bokhoven, R. Prins, J. Phys. Chem. B 107 (2003) 8854-8860.

[17]   J. Klinowski, Chem. Rev. 91 (1991) 1459-1479.

[18]   J.A. van Bokhoven, Ad M.J. van der Eerden, D.C. Koningsberger, J. Am. Chem. Soc. 125 (2003) 7435-7442.

[19]   J.A. van Bokhoven, Ad M.J. van der Eerden, R. Prins, J. Am. Chem. Soc. 126 (2004) 4506-4507.

[20] D.S. Coombs, A. Alberti, T. Armbruster, G. Artioli, C. Colella, E. Galli, J.D. Grice, F. Liebau, J.A. Mandarino, H. Minato, E.H. Nickel, E. Passaglia, D.R. Peacor, S. Quartieri, R. Rinaldi, M. Ross, R.A. Sheppard, E. Tillmanns, G. Vezzalini, Can. Mineral. 35 (1997) 1571-1606.

[21] E.M. Flanigen, in: "Introduction to Zeolites Science and Practice", H. van Bekkum, E.M. Flanigen, P.A. Jacobs, J.C. Jansen (Eds.), Elsevier, Amsterdam, 2001, p. 11.

[22] L.W. Staples, Am. Mineral. 40 (11-2) (1955) 1095-1099.

[23] J.L. Guth, H. Kessler, in: "Catalysis and Zeolites – Fundamentals and Applications", J. Weitkamp, L. Puppe (Eds.), Springer-Verlag, Berlin, Heidelberg, New York, 1999, p. 1.

[24] S.T. Wilson, B.M. Lok, C.A. Messina, T.R. Cannan, E.M. Flanigen J. Am. Chem. Soc. 104 (1982) 1146-1147.

[25] A. Simmen, L.B. McCusker, C. Baerlocher, W.M. Meier, Zeolites 11 (1991) 654-661.

[26] J.M. Bennett, J.W. Richardson Jr., J.J. Pluth, J.V. Smith, Zeolites 7 (1987) 160-162.

[27] J.M. Bennett, J.P. Cohen, E.M. Flanigen, J.J. Pluth, J.V. Smith, ACS Sym. Ser. 218 (1983) 109-118.

[28] R. Millini, L. Montanari, G. Bellussi. Microporous Mater. 1 (1993) 9-15.

[29] R. Kumar, A. Thangaraj, R.N. Bhat, P. Ratnasamy, Zeolites 10 (1990) 85-89.

[30] M.A. Camblor, J. Pérez-Pariente, V. Fornés, Zeolites 12 (1992) 280-286.

[31] Eur Pat Appl 325053, 1989 (Inv. N.Y. Chen, S.M. McCullen).

[32] J. Kornatowski, B. Wichterlova, J. Jirkovsky, E. Löffler, W. Pilz, J. Chem. Soc., Faraday Trans. 92 (1996) 1067-1078.

[33] M.A. Camblor, M. Yoshikawa, S.I. Zones, M.E. Davis, in: "Synthesis of Porous Materials, Zeolites, Clays and Nanostructures", M.L. Occelli, H. Kessler (Eds.), Marcel Decker, New York, 1997, p. 243-261.

[34] C.O. Arean, Comments on Inorganic Chemistry 22 (2000) 241-273.

[35] C.T. Kresge, M.E. Leonowicz, W.J. Roth, J.C. Vartuli, J.S. Beck, Nature 359 (1992) 710-712.

[36] D.Y. Zhao, P.D. Yang, Q.S. Huo, B.F. Chmelka, G.D. Stucky, Curr. Opin. Solid State Mater. Sci. 3 (1998) 111-121.

[37]   a) C. Cascales, E. Gutierrez-Puebla, M. Iglesias, M.A. Monge and C. Ruiz-Valero, Angew. Chem. Int. Ed. 38 (1999), 2436-2439; b) A.K. Cheetham, G. Ferey and T. Loiseau, Angew. Chem. Int. Ed. 38 (1999) 3269-3292.

[38]   a) http://www.iza-structure.org/; b) C. Baerlocher, W.M. Meier, D.H. Olson (Eds.), "Atlas of Zeolite Framework Types", 5th, Elsevier, Amsterdam, 2001, 152.

[39]   A. Pfenninger, in: "Molecular Sieves 2 – Science and Technology", H.G. Karge, J. Weitkamp (Eds.), Springer, Berlin, Heidelberg, 1999, Vol. 2, p. 163.

[40]   W.G. Song, G.H. Li, V.H. Grassian, S.C. Larsen, Environmental Science & Technology 39 (5) (2005) 1214-1220.

[41]   Y. Sakurai, Y. Takahashi, T. Makino, Journal of Geochemical Exploration 64 (1998) 315-319.

[42]   T. Moller, R. Harjula, A. Paajanen, Separation Science and Technology 38 (2003) 2995-3007.

[43]   A.K. Zamanov, R.R. Aliev, V.A. Vyazkov. B.K. Nefedov, Chemistry and Technology of Fuels and Oils 27 (1991) 573-576.

[44]   H. Liu, G.D. Lei, W.M.H. Sachtler, Appl. Catal. A 146 (1996) 165-180.

[45]   C.J. Maiden, ChemTech 18 (1988) 38-41.

[46]   W. Wang, A. Buchholz, M. Seiler, M. Hunger, J. Am. Chem. Soc. 125 (2003) 15260-15267.

[47]   P.M.M. Blauwhoff, J.W. Gosselink, E.P. Kieffer, S.T. Sie, W.H.J. Stork, in: "Catalysis and Zeolites – Fundamentals and Applications", J. Weitkamp, L. Puppe (Eds.), Springer-Verlag, Berlin, Heidelberg, New York, 1999, p. 437.

[48]   J. Biswas, I.E. Maxwell, Appl. Catal. 58 (1990) 1-18.

[49]   J. Scherzer, Catal. Rev.- Sci. Eng. 31(3) (1989) 215-354.

[50]   F.G. Dwyer, P.J. Lewis, F.M. Schneider, Chem. Eng. 83 (1976) 90-91.

[51]   W. Hoelderich, M. Hesse, F. Naumann, Angew. Chem. Int. Ed. 27 (1988) 226-246.

[52]   http://www.iupac.org/.

[53]   G. Bergerhoff, W.H. Baur, W. Nowacki, N. Jb. Miner. Mh. (1958) 193-200.

[54]   W.H. Baur, Am. Mineral. 49 (1964) 697.

[55]   H.G. Karge, J. Weitkamp, "Molecular Sieves 3 – Science and Technology",

Springer-Verlag, Berlin, Heidelberg, 1998, p. 442.

[56] C.V. McDaniel, P.K. Maher, "Molecular Sieve Zeolites", Society of Chemical Industry, London, 1968, p.186.

[57] N.P. Rhodes, R. Rudham, J. Chem. Soc., Faraday Trans. 89 (1993) 2551-2557.

[58] M. Neuber, V. Dondur, H.G. Karge, L. Pacheco, S. Ernst, J. Weitkamp, in: "Innovation in Zeolite Materials Science", P.J. Grobet, W.J. Mortier, E.F. Vansant, G. Schulz-Ekloff (Eds.), Stud. Surf. Sci. Catal. Vol. 37, Elsevier, Amsterdam, 1987, p. 461.

[59] UK Pat 909 286, 1962 (Inv. D.W. Beck).

[60] UK Pat 972 831, 1964 (Inv. D.W. Beck).

[61] G.T. Kerr, J. Phys. Chem. 71 (1967) 4155-4156.

[62] G.T. Kerr, J. Catal. 15 (1969) 200-204.

[63] U. Lohse, M. Mildebrath, Z. Anorg. Allg. Chem. 476 (1981) 126-135.

[64] G.T. Kerr, in: "Molecular Sieves, Advances in Chemistry, Ser. 121". W.M. Meier, J.B. Uytterhoeven (Eds.), American Chemical Society, Washington, 1973, p. 219.

[65] G.H. Kuehl, J. Phys. Chem. Solids. 38 (1977) 1259-1263.

[66] G.T. Kerr, Zeolites 9 (1989) 350-351.

[67] D. Ma, F. Deng, R.Q. Fu, X.W. Han, X.H. Bao, J. Phys. Chem. B 105 (2001) 1770-1779.

[68] R.D. Shannon, K.H. Gardner, R.H. Staley, G. Bergeret, P. Gallezot, A. Auroux, J. Phys. Chem. 89 (1985) 4778-4788.

[69] M.J. Remy, D. Stanica, G. Poncelet, E.J.P. Feijen, P. Grobet, J.A. Martens, P.A. Jacobs, J. Phys. Chem. 100 (1996) 12440-12447.

[70] J. Scherzer, in: "Catalytic Materials: Relationship between Structure and Activity, " T.E. White, R.A. Della Betta, E.G. Derouane, R.T.K. Baker, (Eds.), ACS Symp. Ser. 248, Am. Chem. Soc., Washington D.C., 1984, p. 157.

[71] A. Gola, B. Rebours, E. Milazzo, J. Lynch, E. Benazzi, S. Lacombe, L. Delevoye, C. Fernandez, Microporous Mesoporous Mater. 40 (2000) 73-83.

[72] D.L. Bhering, A. Ramírez-Solís, C.J.A. Mota, J. Phys. Chem. B 107 (2003) 4342-4347.

[73] J.M. Ruiz, M.H. McAdon, J.M. Garcés, J. Phys. Chem. B 101 (1997) 1733-1744.

[74]   P. Lukinskas, D. Fǎrcaşiu, Appl. Catal. 209 (2001) 193-205.

[75]   G.M. Zhidomirov, A.L. Yakovlev, M.A. Milov, N.A. Kachurovskaya, I.V. Yudanov, Catal. Today 51 (1999) 379-410.

[76]   R.M. Lago, W.O. Haag, R.J. Mikovsky, D.H. Olson, S.D. Hellring, K.D. Schmitt, G.T. Kerr, in: "New Developement in Zeolites Science and Technoilogy", Y. Murakami, A. Iijima, J.P. Ward (Eds.), Stud. Surf. Sci. Catal. Vol. 28, Elsevier, Amsterdam, 1986, p. 677.

[77]   E. Brunner, H. Ernst, D. Freude, T. Fröhlich, M. Hunger, H. Pfeifer, in: " Zeolites: Facts, Figures, Future", P.A. Jacobs, R.A. van Santen (Eds.), Stud. Surf. Sci. Catal. Vol. 49, Elsevier, Amsterdam, 1989, p. 623.

[78]   H. Stach, J. Jaenchen, H.-G. Jerschkewitz, U. Lohse, B. Parlitz, M. Hunger, J. Phys. Chem. 96 (1992) 8480-8485.

[79]   D. Coster, A.L. Blumenfeld, J.J. Fripiat, J. Phys. Chem. B 98 (1994) 6201-6211.

[80]   Y. Isaev, J.J. Fripiat, J. Catal. 182 (1999) 257-263.

[81]   A. Corma, V. Fornés, F. Rey, Appl. Catal. 59 (1990) 267-274.

[82]   W.P.J.P. Jacobs, J.H.M.C. van Wolput, R.A. van Santen, Zeolites 13 (1993) 170-182.

[83]   E.M. Flanigen, H. Khatami, H.A. Szymanski, Adv. Chem. Ser. 10 (1971) 201-227.

[84]   J.H.C. van Hooff, J.W. Roelofsen, in: "Introduction to Zeolite Science and Practice", H. van Bekkum, E.M. Flanigen, J.C. Jansen (Eds.), Stud. Surf. Sci. Catal. Vol. 58, Elsevier, Amsterdam, 1991, p. 241.

[85]   P.A. Jacobs, J.B. Uytterhoeven, J. Chem. Soc., Faraday Trans. I 69 (1973) 359-372.

[86]   M. Hunger, J. Weitkamp, Angew. Chem. Int. Ed. 40 (2001) 2954-2971.

[87]   C. Pazè, A. Zecchina, S. Spera, A. Cosma, E. Merlo, G. Spanò, G. Girotti, Phys. Chem. Chem. Phys. 1 (1999) 2627-2629.

[88]   E.M. Flanigen, in: "Zeolite Chemistry and Catalysis", J.A. Rabo (Ed.), American Chemical Society, Washington D.C., 1976, p. 80.

[89]   A. Omegna, Dissertation, ETH Zurich, Swiss Federal Institute of Technology, 2003.

[90]   J.A. van Bokhoven, Ad M.J. van der Eerden, D.C. Koningsberger, in: "Impact of Zeolites and other Porous Materials on the New Technologies at the Beginning of the New Millennium", R. Aiello, F. Testa, G. Giordano (Eds.), Stud. Surf. Sci. Catal. Vol.

142, Elsevier, Amsterdam, 2002, p. 1885.

[91] A. Omegna, R. Prins, J.A. van Bokhoven, J. Phys. Chem. B 109 (2005) 9280-9283.

[92] M. Hunger, Catal. Rev.-Sci. Eng. 39 (1997) 345-393.

[93] D. Freude, H. Ernst, I. Wolf, Solid State Nucl. Magn. Reson. 3 (1994) 271-286.

[94] A.P.M. Kentgens, D. Iuga, M. Kalwei, H. Koller, J. Am. Chem. Soc. 123 (2001) 2925-2926.

[95] H.G. Karge, M. Hunger, H.K. Beyer, in: "Catalysis and Zeolites – Fundamentals and Applications", J. Weitkamp, L. Puppe (Eds.), Springer-Verlag, Berlin, Heidelberg, New York, 1999, p. 198.

[96] G. Engelhardt, D. Michel, in: "High-resolution Solid-state NMR of Silicates and Zeolites", Wiley & Sons, Chichester, New York, 1987, p. 130, 149, 154, 225, and 228.

[97] G. Engelhardt, U. Lohse, E. Lippmaa, M. Tarmak, M. Magi, Z. Anorg. Allg. Chem. 482 (1981) 49-64.

[98] J.M. Thomas, C.A. Fyfe, S. Ramdas, J. Klinowski, G.C. Gobbi, J. Phys. Chem. 86 (1982) 3061-3064.

[99] J.A. van Bokhoven, A.L. Roest, D.C. Koningsberger, J.T. Miller, G.H. Nachtegaal, A.P.M. Kentgens, J. Phys. Chem. B 104 (2000) 6743-6754.

[100] K.U. Gore, A. Abraham, S.G. Hegde, R. Kumar, J.P. Amoureux, S. Ganapathy, J. Phys. Chem. B 106 (2002) 6115-6120.

[101] A. Samoson, E. Lippmaa, Chem. Phys. Lett. 100 (1983) 205-208.

[102] P.P. Man, J. Klinowski, Chem. Phys. Lett. 147 (1988) 581-584.

[103] D. Freude, in: "Encylopedia of Anlytical Chemistry", R.A. Meyers (Ed.), Wiley, New York, Chichester, 2000, p. 12188.

[104] H. Ernst, D. Freude, H. Pfeifer, I. Wolf, in: "Zeolites and Related Microporous Materials: State of the Art 1994", J. Weitkamp, H.G. Karge, H. Pfeifer, W. Hoeldrich (Eds.), Stud. Surf. Sci. Catal. Vol. 84, Elsevier, Amsterdam, 1994, p. 381.

[105] L.B. Alemany, R.L. Callender, A.R. Barron, S. Steuernagel, D. Iuga, A.P.M. Kentgens, J. Phys. Chem. B 104 (2000) 11612-11616.

[106] M. Hunger, E. Brunner, in: " Molecular Sieves 4 – Science and Technology", H.G. Karge, J. Weitkamp (Eds.), Springer-Verlag, Berlin, Heidelberg, 2004, p. 201-293.

[107]   M.E. Rose (Ed.), "Elementary Theory of Angular Momentum", Wiley, New York, Chichester, 1957, p. 245.

[108]   A. Samoson, E. Lippmaa, A. Pines, Mol. Phys. 65 (1988) 1013-1018.

[109]   A. Samoson, E. Lippmaa, J. Magn. Reson. 84 (1989) 410-416.

[110]   A. Samoson, A. Pines, Rev. Sci. Instrum. 60 (1989) 3239-3241.

[111]   B.F. Chmelka, K.T. Mueller, A. Pines, J. Stebbins, Y. Wu, J.W. Zwanziger, Nature 339 (1989) 42-43.

[112]   K.T. Muller, B.Q. Sun, G.C. Chingas, J.W. Zwanziger, T. Terao, A. Pines, J. Magn. Reson. 86 (1990) 470-487.

[113]   J.W. Hennel, J. Klinowski, Topics in Current Chemistry 246 (2005) 1-14.

[114]   M.M. Maricq, J.S. Waugh, J. Chem. Phys. 70 (1979) 3300-3316.

[115]   J. Haase, E. Oldfield, J. Magn. Reson. A 104 (1993) 1-9.

[116]   J. Haase, E. Oldfield, J. Magn. Reson. A 101 (1993) 30-40.

[117]   A.C. Kunwar, G.L. Turner, E. Oldfield, J. Magn. Reson. 69 (1986) 124-127.

[118]   E.L. Hahn, Phys. Rev. 80 (1950) 580-594.

[119]   J. Rocha, C.M. Morais, C. Fernandez, Topics in Current Chemistry 246 (2004) 141-194.

[120]   A. Medek, J.S. Harwood, L. Frydman, J. Am. Chem. Soc. 117 (1995) 12779-12787.

[121]   C. Fernandez, J.P. Amoureux, Chem. Phys. Lett. 242 (1995) 449-454.

[122]   J.P. Amoureux, C. Fernandez, S. Steuernagel, J. Magn. Reson. A 123 (1996) 116-118.

[123]   J.S. Harwood, L. Frydman, J. Am. Chem. Soc. 117 (1995) 5367-5368.

[124]   S.P. Brown, S.J. Heyes, S. Wimperis, J. Magn. Reson. A 119 (1996) 280-284.

[125]   C. Fernandez, J.P. Amoureux, Solid State Nucl. Magn. Reson. 5 (1996) 315-321.

[126]   S.P. Brown, S. Wimperis, J. Magn. Reson. 124 (1997) 279-285.

[127]   D. Massiot, B. Touzo, D. Trumeau, J.P. Coutures, J. Virlet, P. Florian, P.J. Grandinetti, Solid State Nucl. Magn. Reson. 6 (1996) 73-83.

[128]   H. Schaefer, D. Iuga, R. Verhagen, A.P.M. Kentgens, J. Chem. Phys. 114(7) (2001) 3073-3091.

[129]   D. Iuga, H. Schaefer, R. Verhagen, A.P.M. Kentgens, J. Magn. Reson. 147 (2000) 192-209.

[130] M. Hunger, T. Horvath, J. Chem. Soc., Chem. Commun. (1995) 1423-1424.

[131] E. Bourgeat-Lami, P. Massiani, F. Di Renzo, P. Espiau, F. Fajula, Appl. Catal. 72 (1991) 139-152.

[132] G.L. Woolery, G.H. Kuehl, H.C. Timken, A.W. Chester, J.C. Vartuli, Zeolites 19 (1997) 288-296.

[133] P. Lentz, A.P. Carvalho, L. Delevoye, C. Fernandez, J.P. Amoureux, J.B. Nagy, Magnetic Resonance in Chemistry 37 (1999) S55-S62.

[134] D. Massiot, C. Bessada, J.P. Coutures, F. Taulelle, J. Magn. Reson. 90 (1990) 231-242.

[135] S. Altwasser, J. Jiao, S. Steuernagel, J. Weitkamp, M. Hunger, in: "Recent Advances in the Science and Technology of Zeolites and Related Materials", E. van Steen, L.H. Callanan, M. Claeys (Eds.), Stud. Surf. Sci. Catal. Vol. 154, Elsevier, Amsterdam, 2004, p. 3098.

[136] C. Fernandez, J.-P. Amoureux, J.M. Chezeau, L. Delmotte, H. Kessler, Microporous Mater. 6 (1996) 331-340.

[137] C.A. Fyfe, D.H. Brouwer, J. Am. Chem. Soc. 126 (2004) 1306-1307.

[138] J. Jiao, S.S. Ray, W. Wang, J. Weitkamp, M. Hunger, Z. Anorg. Allg. Chem. 631 (2005) 484-490.

[139] H. Koller, E.L. Meijer, R.A. van Santen, Solid State Nucl. Magn. Reson. 9 (1997) 165-175.

[140] R.W. Joyner, A.D. Smith, M. Stockenhuber, M.W.E. van den Berg, Phys. Chem. Chem. Phys. 6 (2004) 5435-5439.

[141] A.E. Hirschler, J. Catal. 2 (1963) 428-439.

[142] C.J. Plank, in: " Proc. 3rd Int. Congr. Catal. Vol. 1" W.M. Sachtler, G.C. Schuit, P. Zwietering (Eds.), North-Holland, Amsterdam, 1965, p. 727.

[143] M. Hunger, Solid State Nucl. Magn. Reson. 6 (1996) 1-29.

[144] M.T. Melchior, ACS Symp. Ser. 218 (1983) 243-265.

[145] M. Seiler, W. Wang, M. Hunger, J. Phys. Chem. B 105 (2001) 8143-8148.

[146] H. Ernst, D. Freude, I. Wolf, Chem. Phys. Lett. 212 (1993) 588-596.

[147] S. Ramdas, J. Klinowski, Nature 308 (1984) 521-523.

[148] J. Jiao, S. Altwasser, W. Wang, J. Weitkamp, M. Hunger, J. Phys. Chem. B 108 (2004)

14305-14310.

[149] J. Jiao, W. Wang, B. Sulikowski, J. Weitkamp, M. Hunger, Microporous Mesoporous Mater. 90 (2006) 246-250.

[150] a) http://webbook.nist.gov/chemistry; b) D.H. Aue, M.T. Bowers, in: "Gas Phase Ion Chemistry Vol. 2", M.T. Bowers (Ed.), Academic Press, New York, 1979, p. 1.

[151] A. Buchholz, W. Wang, A. Arnold, M. Xu, M. Hunger, Miroporous Mesoporous Mater. 57 (2003) 157-168.

[152] P. Batamack, C. Doremieux-Morin, R. Vincent, J. Fraissard, J. Phys. Chem. 97 (1993) 9779-9783.

[153] S. Jungsuttiwong, J. Limtrakul, T.N. Truong, J. Phys. Chem. B 109 (2005) 13342-13351.

[154] J.W. Akitt, J.M. Elders, X.L.R. Fontaine, J. Chem. Soc., Chem. Commun. (1986) 1047-1049.

[155] P. Batamack, R. Vincent, J. Fraissard, Catal. Today 28 (1996) 31-39.

[156] D. Freude, M. Hunger, H. Pfeifer, Z. Phys. Chem. (NF) 152 (1987) 171-182.

[157] W.P.J.H. Jacobs, J.W. Dehaan, L.J.M. Vandeven, R.A. van Santen, J. Phys. Chem. B 97 (1993) 10394-10402.

[158] F. Lónyi, J. Valyon, Miroporous Mesoporous Mater. 47 (2001) 293-301.

[159] A. Zecchina, L. Marchese, S. Bordiga, C. Pazè, E. Gianotti, J. Phys. Chem. B 101 (1997) 10128-10135.

[160] J.J. Fripiat, C. Van der Meersche, R. Touillaux, A. Jelli, J. Phys. Chem. 74 (1970) 382-393.

[161] H. Meier, in: "Spektroskopische Methoden in der organischen Chemie", M. Hesse, H. Meier, B. Zeeh (Eds.), Georg Thieme Verlag Stuttgart, New York, 1987, p.67-190.

[162] J.F. Haw, M.B. Hall, A.E. Alvarado-Swaisgood, E.J. Munson, Z. Lin, L.W. Beck, T. Howard, J. Am. Chem. Soc. 116 (1994) 7308-7318.

[163] J. Jiao, J. Kanellopoulos, W. Wang, S.S. Ray, H. Foester, D. Freude, M. Hunger, Phys. Chem. Chem. Phys. 7 (2005) 3221-3226.

[164] M. Xu, W. Wang, M. Hunger, J. Chem. Soc., Chem. Commun. (2003) 722-723.

[165] L.W. Beck, J.F. Haw, J. Phys. Chem. 99 (1995) 1076-1079.

[166] T. Xu, E.J. Munson, J. F. Haw, J. Am. Chem. Soc. 116 (1994) 1962-1972.

[167] M. Bjørgen, F. Bonino, B. Arstad, S. Kolboe, K. Lillerud, A. Zecchina, S. Bordiga, ChemPhysChem 6 (2005) 232-235.

[168] M. Hunger, T. Horvath, Ber. Bunsenges. Phys. Chem. 99 (1995) 1316-1320.

[169] M. Hunger, G. Engelhardt, H. Koller, J. Weitkamp, Solid State Nucl. Magn. Reson. 2 (1993) 111-120.

[170] M. Hunger, P. Sarv, A. Samoson, Solid State Nucl. Magn. Reson. 9 (1997) 115-120.

[171] S. Caldarelli, A. Buchholz, M. Hunger, J. Am. Chem. Soc. 123 (2001) 7118-7123.

[172] A.F. Hollemann, E. Wiberg, in: "Lehrbuch der Anorganischen Chemie", Walter de Gruyter (Ed.), Berlin, New York, 1995, p. 1081.

List of Publications

S. Altwasser, **J. Jiao**, S. Steuernagel, J. Weitkamp, M. Hunger, *Elucidating the dealumination mechanism of zeolite H-Y by solid-state NMR spectroscopy*, Studies in Surface Science and Catalysis 154 (2004) 3098-3105.

J. Jiao, S. Altwasser, W. Wang, J. Weitkamp, M. Hunger, *State of aluminum in dealuminated, non-hydrated zeolites Y investigated by multi-nuclear solid-state NMR spectroscopy*, Journal of Physical Chemistry B 108 (2004) 14305-14310.

J. Jiao, S.S. Ray, W. Wang, J. Weitkamp, M. Hunger, *Effect of dehydration on the local structure of framework silicon atoms in zeolites Y investigated by solid-state NMR spectroscopy,* Zeitschrift fur Anorganische und Allgemeine Chemie 631 (2005) 484-490.

W. Wang, **J. Jiao**, Y. Jiang, S.S. Ray, M. Hunger, *Formation and decomposition of surface ethoxy species on acidic zeolite Y*, ChemPhysChem 6 (2005) 1467-1469.

J. Jiao, J. Kanellopoulos, W. Wang, S.S. Ray, H. Foerster, D. Freude, M. Hunger, *Characterization of framework and extra-framework aluminum species in non-hydrated zeolites Y by ^{27}Al spin-echo, high-speed MAS, and MQMAS NMR spectroscopy in magnetic fields of B_0 = 9.4 to 17.6 T*, Physical Chemistry Chemical Physics, 7 (2005) 3221-3226.

J. Jiao, W. Wang, B. Sulikowski, J. Weitkamp, M. Hunger, *^{29}Si and ^{27}Al MAS NMR characterization of the framework composition of non-hydrated zeolite catalysts upon adsorption of ammonia*, Microporous and Mesoporous Materials, 90 (2006) 246-250.

J. Jiao, J. Kanellopoulos, W. Wang, J. Huang, V.R.R. Marthala, S.S. Ray, M. Hunger, *Effect of adsorbate molecules on the quadrupolar interaction of framework aluminum atoms in dehydrated zeolite H,Na-Y*, submitted.

Contributions at Conferences

J. Jiao, W. Wang, A. Buchholz, M. Hunger, *Investigation of the cationic state of extra-framework aluminum in hydrothermally treated zeolites H-Y by MAS NMR spectroscopy*, 16th German Zeolite Conference, March 3-5, 2004, Dresden, Germany, Poster presentation.

J. Jiao, W. Wang, M. Hunger, *Characterization of aluminum species in non-hydrated zeolites Y by ^{27}Al spin-echo NMR spectroscopy in different magnetic fields*, 17th German Zeolite Conference, March 2-4, 2005, Gieβen, Germany, Poster presentation

J. Jiao, J. Huang, W. Wang, M. Hunger, *Effects of probe molecules on the local structure of framework aluminum atoms in dehydrated zeolite catalysts studied by solid-state NMR spectroscopy*, 18th German Zeolite Conference, March 1-3, 2006, Hannover, Germany, Oral presentation.

Curriculum Vitae

Personal details:

Name:	Jian Jiao
Birth:	April 20, 1976, Sichuan, China
Family state:	single
Nationality:	Chinese

Education:

09/1994 – 07/1999 B. Sc. obtained in the department of Physical Chemistry, University of Science & Technology of China, Hefei, China

09/1999 – 12/2002 M. Sc. obtained in Dalian Institute of Chemical Physics, Chinese Academy of Sciences, Dalian, China, supervised by Prof. Dr. Xinhe Bao

05/2003– 04/2006 Ph. D. study in the Institute of Chemical Technology, University of Stuttgart, Stuttgart, Germany, supervised by Prof. Dr. Michael Hunger, subject: "Quantitative Characterization of Aluminum in Non-hydrated Zeolite Catalysts by Multi-nuclear Solid-state NMR Spectroscopy"